

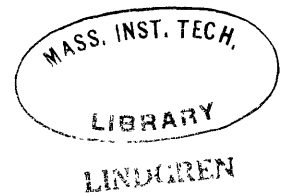
ON THE INTERPRETATION OF RESISTIVITY AND
INDUCED POLARIZATION FIELD MEASUREMENTS

by

PHILIP GEORGE HALLOF

S. B. , Massachusetts Institute of Technology
(1952)

SUBMITTED IN PARTIAL FULFILLMENT
OF THE REQUIREMENTS FOR THE
DEGREE OF DOCTOR OF
SCIENCE



at the

MASSACHUSETTS INSTITUTE OF
TECHNOLOGY

June, 1957

Signature of Author. *[Handwritten Signature]*
Department of Geology and Geophysics, 1957

Certified by.
[Handwritten Signature] Thesis Supervisor

Accepted by.
Chairman, Departmental Committee on Graduate Students

ON THE INTERPRETATION OF RESISTIVITY AND INDUCED POLARIZATION FIELD MEASUREMENTS

BY PHILIP G. HALLOF

"Submitted to the Department of Geology and Geophysics on April 15, 1957 in partial fulfillment of the requirements for the degree of Doctor of Science"

ABSTRACT

The solution of the equation for current conduction in a non-uniform medium suggests that the optimum information from surface measurements of the electrical properties of the ground can be obtained by localizing the sender, or applied current source, and the receiver, or potential measuring system, keeping one fixed in position while moving the other. The equation can be written as the usual Poisson's equation with two source terms. One source is the applied current source while the others are "induced" sources with their value proportional to the value of $[\nabla \ln \sigma \cdot \nabla \phi]$ at every point in the ground. Where σ is the conductivity function and ϕ is the electric potential.

Thus, the value of the induced sources changes as the location of the sender is changed. By making several potential measurements from one current location and then moving the current source the effect and location of the "induced" sources can to a certain degree be separated from that of the applied source.

Since the induced polarization effect changes the conductivity of a mineralized zone as the frequency of the current is changed, the idea of applied and induced sources can be applied to the interpretation of induced polarization measurements provided we realize that the induced sources on the outside of the ore body depend upon the frequency as well as the location of the applied source.

Field measurements are made along a line on the surface. Resistivity and induced polarization measurements are taken for every combination of sender and receiver position along the line. The results are then plotted on a two dimension plot using the locations of the sender and receiver as the two coordinates for each value obtained. These two dimensional arrays, when contoured, have characteristic shapes for various subsurface resistivity configurations. In particular, the results from lateral and vertical resistivity variations are easily recognized and their effects in the same area can be separated to a large degree.

The field results from known mineralized zones show, when plotted in this way, that the induced polarization effects have at least one order of magnitude more resolving power than the resistivity

measurements. However, in each of the cases studied, the resistivity contour maps did have some expression of the ore zone. This is largely a result of the method of plotting the data. If some method, such as the Wenner spread, where all four electrodes are moved at once, had been used, the resistivity results would have been even less conclusive or failed completely to indicate the mineralization. In most of the areas where the induced polarization measurements were a success, other geophysical methods have failed completely to outline the mineralization.

The two dimensional contour maps of the exact results from known resistivity cases are very useful in identifying characteristics of contour maps from field results. These results may be theoretical, as in the case of the results calculated in a medium of vertical layering; or experimental, as when the exact results from more complicated geometries are obtained by scale modelling. Some of the results from these exact cases are very similar to the contour maps of field results, and on this basis, an interpretation of the field results can be carried out.

The exact results from these known geometries are also useful for comparison purposes in the study of the approximate solution to the general solution for conduction in a non-uniform medium. The simplest theoretical solutions can be used to determine the true form of the approximate solution and the modelling results from the more complicated geometries can be used to determine the accuracy of the approximation.

Much more work on the accuracy of the approximate solution is warranted. If the approximation is accurate enough, the direct interpretation of resistivity, or induced polarization, results can be reduced to the solution of a system of linear equations. Thus, the approximate solution is the first step in determining the electrical properties and geometry of the ground directly from surface measurements.

TABLE OF CONTENTS

	<u>Page</u>
I. <u>INTRODUCTION</u>	
1.1 General Background	1
1.2 General Purposes of the Thesis Investigation	4
1.3 Organization of the Thesis	5
II. <u>THE PHYSICAL PROPERTIES TO BE CONSIDERED</u>	
IIA. <u>APPARENT RESISTIVITY AND INDUCED POLARIZATION EFFECTS</u>	
<hr/>	
2a.1 The Concept of Apparent Resistivity	9
2a.2 The Induced Polarization Phenomenon	10
IIB. <u>THE GENERAL RESISTIVITY PROBLEM</u>	
2b.1 General Discussion	15
2b.2 Equations of D. C. Conduction	15
2b.3 Methods of Solution	16
III. <u>METHOD USED IN PLOTTING RESISTIVITY AND INDUCED POLARIZATION DATA</u>	
<hr/>	
3.1 Reasons for Using this Method	22
3.2 Types of Senders and Receivers	22
3.3 Comparison with Usual Methods	24
3.4 The Two-Dimensional Plotting Method	25
3.5 The Effect of Vertical and Horizontal Resistivity Variations	28
3.6 Integration to Get the Potentials	34
IV. <u>FIELD RESULTS</u>	
4.1 General Discussion and Methods	41
4.2 Results from a Vertical Ore Body	43
4.3 Results from a Horizontal Ore Body	46
4.4 Resistivity and Induced Polarization Results from Vertical Interfaces	58
4.5 Conclusions	65
V. <u>FURTHER THEORETICAL TREATMENT</u>	
5.1 General Discussion	68
5.2 Vertical Interfaces	68
5.2a One Interface	71
5.2b Two Interfaces	78

TABLE OF CONTENTS (Cont'd)

	<u>Page</u>
V. <u>FURTHER THEORETICAL TREATMENT (Cont'd)</u>	
5.3 Usefulness of the Vertical Layering Solutions	94
5.4 Conduction in Anisotropic Layers	96
VI. <u>FURTHER EXACT RESULTS</u>	
6.1 The Need for Modelling Results	99
6.2 Methods and Procedures	103
6.3 Two Dimensional Modelling Results	114
6.4 Results from the Vertical Ore Body	118
6.5 Ore Body Dipping Toward the Sender	125
6.6 Ore Body Dipping Away from the Sender	130
6.7 The Horizontal Ore Body	135
6.8 Conclusions	153
VII. <u>INVESTIGATION OF THE APPROXIMATE CONDUCTION EQUATION</u>	
7.1 The Need for the Approximate Solution	155
7.2 The Approximate Solution	156
7.3 Solving the Inverse Problem	159
7.4 The Contrast Factor	162
VIII. <u>ACCURACY OF FIRST APPROXIMATION</u>	
8.1 Method of Attack	173
IX. <u>SUGGESTIONS FOR FURTHER WORK</u>	175
<u>APPENDIX A</u>	177
<u>APPENDIX B</u>	186
<u>APPENDIX C</u>	191
<u>ACKNOWLEDGEMENTS</u>	
<u>BIBLIOGRAPHY</u>	
<u>BIOGRAPHY OF AUTHOR</u>	

LIST OF TABLES

TABLE I	Representative Resistivity and Metal Factor Values from Field Work	<u>Page</u> 14
----------------	---	-------------------

LIST OF FIGURES

Fig. 1	Method of Plotting Data	27
Fig. 2	Field Map Mindamar Line P*	29
Fig. 3	Field Map Mindamar Line Y	31
Fig. 4	Field Map Mindamar Line Z	32
Fig. 5	Field Map Mindamar Line Q	32
Fig. 6	Field Map Mindamar Line P	33
Fig. 7	Demonstration of Integration Procedure	35
Fig. 8	Field Maps and Calculated Data from Dracut	39
Fig. 9	Field Maps Fredericktown Line A	48
Fig. 10	Field Maps Fredericktown Line C	50
Fig. 11	Field Maps Fredericktown Line B	52
Fig. 12	Field Maps Fredericktown Line Csh	53
Fig. 13	Field Maps, Fredericktown Lines A, B, C Integrated	55
Fig. 14	Field Maps Fredericktown Composite Map	57
Fig. 15	Field Maps Line A, W. First Part	61
Fig. 16	Field Maps Line W, A. Last Part	62
Fig. 17	Field Maps Line A, H. Last Part	63
Fig. 18	Coordinate System Used on Vertical Interface Solutions	70
Fig. 19	Source and Image Relationships for One Interface	70

LIST OF FIGURES (Cont'd)

		<u>Page</u>
Fig. 20	Coordinate System for One Interface	70
Fig. 21	One Interface, ρ_a Map from Potentials $\frac{\rho_2}{\rho_1} = 18/1$	74
Fig. 22	One Interface, ρ_a Map for Dipole Receiver $\rho_2/\rho_1 = 18/1$	74
Fig. 23	One Interface, ρ_a Map for Dipole Receiver $\rho_2/\rho_1 = 1/18$	74
Fig. 24	Coordinates for Two Interface Problem; Source in Region I	81
Fig. 25	Coordinates for Two Interface Problem; Source in Region II	81
Fig. 26	Plot of G (1.25;a)	89
Fig. 27	Vertical Dike, ρ_a Map from Potentials $\rho_2/\rho_0 = 1/18$	90
Fig. 28	Vertical Dike, ρ_a Map for Dipole Receiver $\rho_2/\rho_0 = 1/18$	90
Fig. 29	Vertical Dike, ρ_a Map from Potentials $\rho_2/\rho_0 = 18/1$	90
Fig. 30	Vertical Dike, ρ_a Map for Dipole Receiver $\rho_2/\rho_0 = 18/1$	90
Fig. 31	ρ_a Map of Conducting Hill	116
Fig. 32	Modelling Results Geometry A $\rho_1/\rho_0 = 1/25$	120
Fig. 33	Modelling Results Geometry A $\rho_1/\rho_0 = 1/40$	120
Fig. 34	Modelling Results Geometry B $\rho_1/\rho_0 = 1/25$	121
Fig. 35	Modelling Results Geometry B $\rho_1/\rho_0 = 1/40$	121

LIST OF FIGURES (Cont'd)

		<u>Page</u>
Fig. 36	Modelling Results Geometry A M. f. Map	123
Fig. 37	Modelling Results Geometry B M. f. Map	123
Fig. 38	Modelling Results Geometry C $\rho_1/\rho_0 = 1/25$	126
Fig. 39	Modelling Results Geometry C $\rho_1/\rho_0 = 1/70$	126
Fig. 40	Modelling Results Geometry D $\rho_1/\rho_0 = 1/25$	127
Fig. 41	Modelling Results Geometry D $\rho_1/\rho_0 = 1/70$	127
Fig. 42	Modelling Results Geometry C M. f. Map	129
Fig. 43	Modelling Results Geometry D M. f. Map	129
Fig. 44	Modelling Results Geometry E $\rho_1/\rho_0 = 1/25$	131
Fig. 45	Modelling Results Geometry E $\rho_1/\rho_0 = 1/70$	131
Fig. 46	Modelling Results Geometry F $\rho_1/\rho_0 = 1/25$	132
Fig. 47	Modelling Results Geometry F $\rho_1/\rho_0 = 1/70$	132
Fig. 48	Modelling Results Geometry E M. f. Map	133
Fig. 49	Modelling Results Geometry F M. f. Map	133
Fig. 50	Modelling results Geometry G $\rho_1/\rho_0 = 1/10.7$	136
Fig. 51	Modelling Results Geometry G $\rho_1/\rho_0 = 1/23$	136
Fig. 52	Modelling Results Geometry G $\rho_1/\rho_0 = 1/41$	137

LIST OF FIGURES (Cont'd)

		<u>Page</u>
Fig. 53	Modelling Results Geometry G $\rho_1/\rho_0 = 1/84$	137
Fig. 54	Modelling Results Geometry H $\rho_1/\rho_0 = 1/10.6$	138
Fig. 55	Modelling Results Geometry H $\rho_1/\rho_0 = 1/23$	138
Fig. 56	Modelling Results Geometry H $\rho_1/\rho_0 = 1/41$	139
Fig. 57	Modelling Results Geometry H $\rho_1/\rho_0 = 1/81.3$	139
Fig. 58	Modelling Results Geometry I $\rho_1/\rho_0 = 1/10.6$	140
Fig. 59	Modelling Results Geometry I $\rho_1/\rho_0 = 1/23.2$	140
Fig. 60	Modelling Results Geometry I $\rho_1/\rho_0 = 1/41$	141
Fig. 61	Modelling Results Geometry I $\rho_1/\rho_0 = 1/78$	141
Fig. 62	Modelling Results Geometry G M.f. Map; M.f. of Ore Body = 3700	142
Fig. 63	Modelling Results Geometry G M.f. Map; of Ore Body = 8990	142
Fig. 64	Modelling Results Geometry H M.f. Map; M.f. of Ore body = 3700	143
Fig. 65	Modelling Results Geometry H M.f. Map; M.f. of Ore Body = 8990	143
Fig. 66	Modelling Results Geometry I M.f. Map; M.f. of Ore Body = 3700	144
Fig. 67	Modelling Results Geometry I M.f. Map; M.f. of Ore Body = 8990	144

LIST OF FIGURES (Cont'd)

		<u>Page</u>
Fig. 68	Modelling Results , Geometry G, M. f. map; M. f. of Ore Body = 8110	145
Fig. 69	Modelling Results Geometry H, M. f. Map; M. f. of Ore Body = 7740	145
Fig. 70	Modelling Results Geometry I, M. f. Map; M. f. of Ore Body = 7400	146
Fig. 71	Curves for Contrast Factor on Sphere and Cylinder	165
Fig. 72	Coordinates to get $q_1(x)$	168
Fig. 73	Coordinates to get $q_2(x)$	168

I. INTRODUCTION

1.1 General Background

For many years, Prof. P. M. Hurley of the Department of Geology and Geophysics at M. I. T. has interested students in studying the electromagnetic methods of geophysical prospecting. In the past, several studies have been done under his leadership in this general field.

In particular, in the spring of 1953 he suggested that Mr. T. R. Madden, Mr. K. Vozoff and I use some funds that were available to investigate some particular problem in this field. At the time we were doing Ph. D work at M. I. T. , and were interested in electric prospecting in general. Mr. Madden and Mr. Vozoff both had a good deal of experience with the standard methods of resistivity surveying. At the suggestion of Prof. Hurley, and after some discussion and a survey of the literature, we decided to devote our efforts to studying induced polarization effects in the ground and their possible geophysical significance and use. Various groups had done some work in this field, but little had been published and we decided that some published information would be a contribution to the science.

All of the work up to that time had been done by studying the transients existing in the ground when a square pulse of current was applied. For reasons of economy and equipment portability, we decided to study the phenomenon in the frequency domain, i. e. , by using current signals of a single but variable frequency. We built and collected some

equipment and the first summer, that of 1953, was spent at the Mindamar Metals Corporation property at Stirling, Nova Scotia.

The work has continued since then with varying personnel and with support from various places. A great deal has been learned and a good deal of data have been collected. This information has or will appear in three Ph. D theses from M. I. T.

The first, by Dr. Vozoff, was submitted in June, 1956 and is a theoretical study of the equations governing electrical conduction in non-uniform media. He also used the high speed digital computer at M. I. T. to study the particular problem of conduction in a layered medium and developed a technique for going from the measured data to the constants of the ground.

The second, not yet finished, is a study by T. R. Madden of the physical and electrochemical phenomena that give rise to the induced polarization effects. The first results of Mr. Madden's investigations will be summarized later. His work shows that the induced polarization effect can be considered a bulk property of a mineralized zone just like the density or resistivity. This work has also made evident the kind of measurement that must be made to get the best resolution between mineralized and non-mineralized zones.

This is the starting point for this investigation. Knowing the effect we want to measure, in what way do we want to take the measurements? Also, since we can only make measurements on the earth's

surface, there remains the problem of interpretation. These problems are, of course, those of exploration geophysics in general.

It is only in a few special cases that this reverse interpretation problem can be done uniquely. Indeed, the cases in which the forward problem, i. e., calculating the effect on the surface for a given subsurface configuration, can be solved are quite limited. This is particularly true in those methods where an "applied" source is used to generate the field that is measured.

In gravity and magnetic explorations, the field to be measured originates with the anomalous region that is being searched for. In these methods, the effects on the surface from various different sizes and shapes of geometric configurations can be calculated. A few simple reverse problems can be solved exactly.

In the seismic and electrical methods much less can be done exactly, even with the forward problem. The science of seismology has gone far in solving the case of the layered medium but only recently has the effect of three-dimensional variations been investigated with any success.

The problem of horizontal layerings has also been thoroughly investigated in electrical prospecting methods and the forward and reverse problems solved. Only a few other special cases of the resistivity problem have been solved. In no other case, except the horizontally layered medium, is there a way of solving the reverse problem. The general

resistivity problem is an unsolved boundary value problem of great complexity. In his thesis, K. Vozoff has suggested an approximate solution to the reverse problem in the general case.

In the past the interpretation of resistivity data has been done by comparing field results with those cases where calculations could be made. On the basis of this "curve matching" inferences were drawn concerning the resistivity and geometric configuration of the subsurface. In the case of horizontal layering, these methods have proved to be quite reliable in most cases. However, in most cases, lateral variations exist that confuse the picture and make comparisons difficult.

1.2 General Purposes of the Thesis Investigation

The usual methods of taking resistivity measurements make the separation of the effects of lateral and vertical resistivity changes difficult, if not impossible. One problem to be considered is the study of resistivity effects and the development of a procedure that allows the most information possible to be gained from field data. Another problem to be considered is in which cases and to what degree the induced polarization measurements give more resolving power than resistivity measurements.

An additional purpose of this investigation is to provide exact resistivity and induced polarization data for specific configurations. Some of the information is provided by the solution of an additional theoretical case and some by scale modelling. These special cases

provide results that aid in the interpretation of the resistivity and induced polarization data from the field measurements. The exact results can also be used to check the accuracy of the first approximation.

1.3 Organization of the Thesis

The first part of the thesis is devoted to a discussion of the physical properties that we are interested in measuring, i. e. , the resistivity and induced polarization properties. We shall see that the induced polarization effect can be studied by studying how the resistivity, actually the impedance, of the subsurface changes as the frequency of the applied current is varied. For this reason, the interpretation of field measurements of the induced polarization effect is really a problem in interpreting resistivity data, or really changes in resistivity data. Therefore, a short discussion of the equation governing current flow in a medium of non-constant resistivity is included to give a basis upon which to begin.

The study of the general current flow equations suggests the idea of "induced sources" at surfaces of resistivity change. It is apparent, that in order to best locate these "induced sources", the apparent resistivity should be measured by completely separating the current source and potential measuring equipment and by changing either the location of the current source or the potential measurement, but one at a time. From this develops the method to be used in measuring and plotting the apparent resistivity and apparent induced polarization effect.

In order to demonstrate the advantages of the new method of plotting the results, several examples of field measurements are shown and discussed. These results, while demonstrating the superiority of the plotting method also show that in all the cases studied the induced polarization measurements give much more resolving power in the location of the mineralized zones. The field results are from:

- a) a massive Canadian Shield type deposit in Nova Scotia,
- b) a typical ore body in the southeastern Missouri Lead belt, and
- c) an enriched zone in one of the porphyry copper areas in southwestern United States.

Further interpretation of the results of the field work is carried out by comparing them with exact results from known geometries. First, the problem of resistivity measurements in a vertically layered earth is studied and the solution carried through to a useable form. Other exact results are obtained by using scale models of appropriate geometries. From these results, the possible importance of modelling in furnishing results to aid in interpretation is suggested.

The results of the modelling experiments, since they furnish exact results that can't be obtained by mathematical calculation, are also useful in studying the proposed approximate solution to the general resistivity problem. Some theoretical material is included to clarify

several points concerning the approximate solution. Finally, some of the exact results of the modelling are compared with approximate results calculated using the first approximation to the general solution. This work is not finished, further studies of the approximate solution are still being carried out with the aid of the digital computer.

This thesis then, as the title indicates, deals with the interpretation of field measurements of both resistivity and induced polarization. The resistivity, as we have seen, must be considered because we cannot say much about the induced polarization effects without analyzing at the same time the resistivity data.

For this reason, sections II and III are devoted to a brief discussion of the equations governing conduction and the method we use for presenting the field measurements. This method is new and is suggested by the form of the general equation. We are led directly to the field results in section IV and a discussion of the resistivity and metal factor over existing ore bodies and what the anomalies mean.

The next section, section V, deals with one of the few remaining problems that can be done exactly, that has not appeared completely solved in print. This is the problem of vertical layering and the calculation of potentials in this sort of geometry. Included also are the integrals used to evaluate the resistivity curves for this kind of geometry. Also briefly discussed is the problem of conduction in anisotropic layers.

Section VI of the thesis deals with the modelling work done to qualitatively assist in the interpretation of the field results, and section VII is a discussion of the first approximation of the equations governing conductions. These approximate relationships are much simpler to handle, and, as we shall see, present the possibility of doing the inverse resistivity problem in the general case. That is, going from the surface measurements to the resistivity configuration in the ground. Much of this has been covered in Dr. Vozoff's thesis and I will only refer to it; however, with the exact results of the modeling and the digital computer we have been able to test the approximate equation and the results are discussed.

II. THE PHYSICAL PROPERTIES TO BE CONSIDERED

IIA. APPARENT RESISTIVITY AND INDUCED POLARIZATION EFFECTS

2a.1 The Concept of Apparent Resistivity

The principles upon which resistivity measurements rest are too well known to need much repeating. Any book on applied geophysics discusses them thoroughly. If a current is caused to flow through the half space that is the surface of the ground, it will adjust itself, as in an electric circuit, so that a minimum of energy is expended. The current flow will tend to increase in regions of high conductivity and to decrease in areas where the resistivity is high.

Usually, current enters and leaves the ground through one set of electrodes and the potential differences between two other electrodes is measured. The interpretation consists of determining the pattern of current flow from the potential measurements and then to infer the location of zones of high and low conductivity in the ground. In general, the only surface available for taking measurements is the flat surface of the conducting half space, i. e. , the surface of the earth.

The results are usually reduced to the value of the "apparent resistivity" for any particular electrode configuration. The apparent resistivity is an abstract value that represents the constant value of resistivity that the half space would have to create the potential difference measured when current is applied. The apparent resistivity can be calculated for an electrode location if the values of voltage and current

are known. The calculated values of apparent resistivity are used, and misused, in varied ways. We shall go into the matter of interpretation later.

2a. 2 The Induced Polarization Phenomenon

The second subject to be covered in this investigation is the interpretation of induced polarization measurements. The nature and cause of the induced polarization effect has been studied by T. R. Madden of M. I. T. His findings will soon be available in his Ph. D thesis. Mr. Madden's work has also suggested the kind of measurement that should be made in order to get the best resolution from the induced polarization effects as we measure them on the surface.

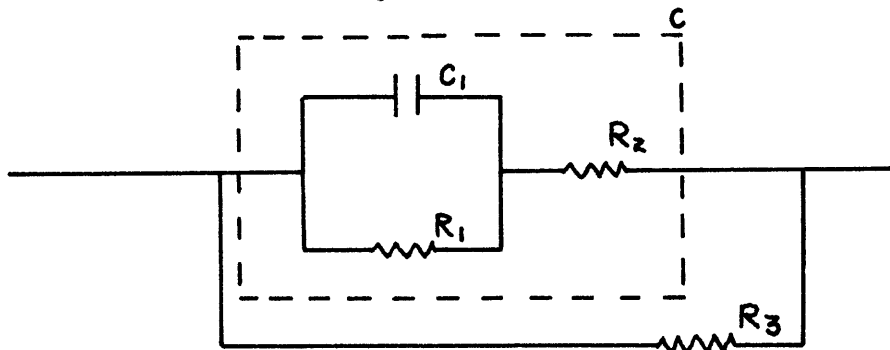
Mr. Madden's complete thesis will be available soon, and rather than try to paraphrase some of his important conclusions, I'm going to include several paragraphs from a preliminary report in which he describes the induced polarization effect.

"Induced polarization as a geophysical measurement refers to the blocking action or polarization of a metallic or electronic conductor in a medium of ionic conduction. This blocking, which depends on the chemical energies necessary to allow the ions to give up or receive electrons from the metal surface, represents an electrical resistance, for 1Cm^2 of surface, equivalent to perhaps as many as 20 cm of pore conduction path. The ions in solution outside the metal surface can approach very closely to that surface (within atomic dimensions) so

that appreciable capacitive coupling can take place across the solid-solution interface. The capacitance amounts to around $20 \mu\text{f}$ per cm^2 , so that even at frequencies as low as 1 cps the capacitive coupling takes over from the resistive coupling across the interface".

"At D. C. or very low frequencies (period of seconds) the surface impedance is so high that with moderately-sized metallic minerals, the electric currents would rather go around the mineral than buck the surface impedance. At higher frequencies the capacitive impedance decreases enough to allow more and more electrical paths involving the metallic minerals to be opened up. Thus the overall impedance of the rock as an electrical element shows a decrease with frequency. The spectrum is smoothed out over quite a range from tens of seconds to milliseconds, so that even though the total change of impedance may be several-fold, there is practically no phase shift associated with the impedance. The magnitude of the effects depends a great deal on the details of the pore geometry and the positioning of the metallic minerals with respect to these pore spaces, and the best approach is probably an empirical one!"

"The question of what should be measured is an important one and one which we feel has often been improperly answered. A rough circuit of the rock impedance could be drawn as:



Where C_1 and R_1 represent the surface impedance of the metallic minerals; R_2 represents the resistance of the pore paths blocked off by the metallic minerals; and R_3 represents the pore paths around the minerals. The presence of R_3 is very important in the overall effects that are measured. If one measured impedance, the role of R_3 is obvious, but it is also involved if the voltages set up by the discharge of C_1 are measured. For instrumental reasons, we measure the rock impedance as a function of frequency. (Pulse analysis or current decay measurements, the measurements in the time domain, give the same information)."

"The interpretation of field measurements will involve the resistivity picture as the rest of the ground is electrically connected to any mineralized zone, so that we feel that thinking of the induced polarization as impedance effects puts one on the right footing to deal with the field interpretation problem. Our frequency spectrum is a rather sketchy one, involving only two frequencies; one is the low end of the spectrum, and one well up into the high end. (.1 - .05 and 10 cps) so that C_1 comes in as a relatively high impedance at the low frequency and as a low impedance at the high frequency. To offset the influence of R_3 , which can be very great if the rock has suffered any post-mineralization shearing, we divide the % difference between the D. C. and A. C. impedance by the D. C. impedance. If the electrical paths involving the metallic minerals has the impedance $Z(\omega)$, then the total impedance is:

$$\frac{Z \times R_3}{Z + R_3}$$

$$\text{Thus } \frac{Z(o) \times R_3}{Z(o) + R_3} - \frac{Z(\omega) \times R_3}{Z(\omega) + R_3} = \frac{Z(o) - Z(\omega)}{Z(o) \times Z(\omega)}$$

$$\frac{Z(o) \times R_3}{Z(o) + R_3} \times \frac{Z(\omega) \times R_3}{Z(\omega) \times R_3}$$

"Besides putting shear paths into R_3 , most of the pore paths around the metallic minerals can also be placed in this category. In a crude way, therefore, $z(\omega)$ represents only the impedance of the electrical paths involving the metallic minerals. If, as we have already stated, and as laboratory sample substantiated, $Z(o) \gg Z(\omega)$ then this factor which we call the "metal factor" $\approx 1/Z(\omega)$. In our measurements we only have $\omega = 60$. The metal factor is proportional to the conductivity of those paths involving metallic minerals. At 10 cps, $Z(\omega) \gg R_2$ unless the pore paths between the metallic minerals are very short. As the mineralization becomes more extensive, more paths will involve metallic minerals, and these paths will become shorter. Therefore, a very large variation of metal factors is possible".

The metal factor as described above is then the quantity that we measure in the field. As Mr. Madden states above, the variations in the m. f. are very large. In Table 1 are tabulated values compared with representative resistivity values. The apparent metal factor in field work is calculated using the apparent resistivity for the station

at the two frequencies. Units of resistivity throughout our work have been in ohm feet, and the metal factors are calculated using resistivities in these units.

TABLE I

**REPRESENTATIVE RESISTIVITY AND METAL FACTOR VALUES
FROM FIELD WORK**

$\rho/2\pi$ in ohm-feet		Metal factors	
Valley fill (in S. W.)	5-100	granitic rocks (acid)	< 1
Enriched porphyry copper ore	5-10	basalts (basic with magnetite)	1-10
Glacial till (wet)	100-300	finely disseminated sulphides	10-100
Limestone areas	200-500	disseminated sulphides	100-1000
Altered igneous rocks (in S. W.)	200-700	enriched porphyrys	1000-10,000
Sheared or altered igneous	300-1000	massive sulphides	> 10,000
Igneous areas (unaltered)	1000-5000	up to 100,000 and perhaps higher	

We have then two important properties of the metal factor which make it a better parameter to measure than resistivity. One is that it has a wider range of natural values than resistivity and the other is that by its very nature it tends to eliminate the effect of parallel conducting paths such as shear zones. We will see later that it has even more advantages.

IIb. THE GENERAL RESISTIVITY PROBLEM

2b.1 General Discussion

We have seen that although the induced polarization effect has its origin at metal-solution interfaces within the rock aggregate, it may be looked at as a bulk property of the rock, like its density or resistivity. Indeed, the easiest way to look at it is that the resistivity of the metal bearing rock changes with frequency. The magnitude and rate of the change are dependent upon the amount of metal present as well as many other factors such as particle size, location, etc.

Since this is a problem in resistivity it might be well for us to first consider the problem of interpreting current flow in the ground.

2b.2 Equations of D. C. Conduction

We need consider the equations of D. C. conduction only, because at the frequencies, distances and conductivities we will be using none of the coupling or radiation effects are important. That is, even though we are going to make an A. C. resistivity measurement, the current flow lines will be the same as for D. C. conduction, in the absence of metallic conductors. The induced polarization, since it changes the resistivity of some blocks of rock, will alter the current flow lines. This is the effect we are trying to find.

We can get our equations by assuming no time dependence in Maxwell's Electromagnetic Equations. In that case, we have, for the

Electric vector \vec{E} that we know

$$\nabla \times \vec{E} = 0 \text{ and the conduction equation}$$

$$\vec{J} = \sigma \vec{E} \text{ for isotropic media.}$$

Now, since \vec{E} is curl free it can be represented as the negative gradient of a scalar

$$\vec{E} = -\nabla \phi$$

We also know, because of current conservation that the divergence of the current is zero everywhere except where current is applied, i. e.

$$\nabla \cdot \vec{J} = q(r) \delta(r)$$

if we consider the case where the current is applied at $r = 0$.

The relationships may be combined to give

$$\nabla \cdot \sigma \nabla \phi = -q \delta(r)$$

or

$$\sigma \nabla^2 \phi + \nabla \sigma \cdot \nabla \phi = -q \delta(r)$$

or finally

$$\nabla^2 \phi + \nabla \left[\ln \sigma \right] \cdot \nabla \phi = -\frac{q}{\sigma} \delta(r)$$

This then is the equation that governs the flow of current in the general isotropic medium with non-constant σ . As we shall see, its solution in this form is very difficult.

2b.3 Methods of Solution

The method of studying the solutions of resistivity problems in the past has been to divide the geometry being considered into regions

in which σ was constant. In this case $\nabla \left[\ln \sigma \right]$ is zero in each region and Poisson's equation is then valid in each region, i. e.

$$\nabla^2 \phi = - \frac{\gamma}{\sigma} \delta(r)$$

This equation along with the closely related Laplace equation is perhaps the most studied of mathematical physics and many examples have been solved. The boundary conditions are that at the boundary of regions of different conductivities the potential ϕ and the normal current flow must be continuous.

One method used in solutions is the method of images. This method is a special case of the method of Green's Functions in which the boundary is given the properties of a reflector and the potential in a region is looked upon as being due to current sources in that region and their images in the boundaries. This method is applicable in all cases where plane boundaries are present, but if more than one reflector is present a series of images is needed and the infinite series is often poorly convergent. Nevertheless, some problems have been solved in this manner. (Logn, 1954; Unz, 1953) and many others have used images to solve the problem of horizontal, vertical and dipping beds.

The more general method, which gives the same answer in a different form, is that of harmonic solutions, or, as it is more commonly called in mathematical physics, the method of eigenfunctions. If in the system we are considering the boundaries of the regions of

constant conductivity coincide with constant coordinates of some orthogonal, curvi-linear coordinate system the method of eigenfunctions can be used. Solutions to Laplace's equation are known and tabulated for most of the simple coordinate systems. The expressions for the potential in the homogeneous regions are then matched at the boundary and we have the solution we desire; except that it is very seldom in a closed or simple form.

This method has been used in many resistivity problems where the necessary conditions are present. It was first done for horizontal layers (Hummel, 1932; Stefanescu et al 1930; Tagg, 1930). (Mooney, 1954) has a long bibliography dealing with the horizontal layering problem. Recently, the vertical and dipping layers have been considered (Logn, 1954; Maeda, 1955) using eigenfunctions. Various problems of buried spheres and spheroids have also been done in varying degrees. (Clark, 1956; Cook et al 1954; Seigel, 1952; Van Nostrand, 1953).

Rather than simplifying the problem by showing that one of the above is a better way of doing the problems, I am going to further complicate the picture by adding a third way of looking at the problem. If we write our general equation in the form

$$\nabla^2 \phi = - \left[\frac{\rho}{\sigma} \delta(r) + \nabla (\ln \sigma) \cdot \nabla \phi \right]$$

it looks a good deal more familiar and we consider the term $\nabla (\ln \sigma) \cdot \nabla \phi$ to be an additional source term. We can write the formal solution in

the form of the well known solution to Poisson's equation. (Morse and Feshback, 1953, Chapter X).

$$\phi(r) = \frac{1}{4\pi} \iiint_{V'} \frac{\frac{\psi(r) \delta(r)}{\sigma(r)} + \nabla r' \ln \sigma(r) \cdot \nabla r' \phi(r')}{R} dV'$$

or

$$\phi(r) = \frac{1}{4\pi} \iiint \frac{\psi(r') \delta(r') dV'}{\sigma(r') R} + \frac{1}{4\pi} \iiint \frac{\nabla' \ln \sigma(r') \cdot \nabla' \phi(r')}{R} dV'$$

where $R = |r - r'|$ is the distance between the point of observation and the point of integration. Using the properties of the delta function

$$\phi(r) = \frac{1}{4\pi r} \frac{\psi}{\sigma(r)_{r=0}} + \frac{1}{4\pi} \iiint \frac{\nabla' \ln \sigma(r') \cdot \nabla' \phi(r')}{|r - r'|} dV'$$

and we see that the first term is just the potential from our applied current source and that it falls off as $(\frac{1}{r})$ as it should.

What are the terms in the integral? This term shows that we must add to this applied source term similar $(\frac{1}{r})$ potentials that have as their point of source those points where $\overline{\nabla \ln \sigma}$ has a non-zero value, or, places where σ has a non-constant value. The strength of each of these "induced" sources is proportional to the rate of change of σ at that point and to the $\overline{\nabla \phi}$ or the electric vector \overline{E} at that point (and to their relative vector directions).

For a small localized resistivity anomaly, such as an ore body in normal country rock, the $\overline{\nabla \ln \sigma}$ will be zero everywhere except at the outside of the ore body. Here we will have induced sources all of which

will contribute to the measured potentials on the surface. If we were to subtract off the $(\frac{1}{r})$ term from our applied source, we would be left with the potentials from the induced sources. This then is very similar to gravity or other potential problems. The source of the potentials measured on the surface is located at the places where the physical properties of the rock change.

As mentioned previously the strength of the induced sources is dependent on several factors. One is the magnitude of the term $\overline{\nabla \ln \sigma}$, this depends upon the resistivity contrast between the country rock and the ore body. The strength of the sources also depends upon the magnitude of E at the point where $\overline{\nabla \ln \sigma} \neq 0$. One important factor here will be the distance from the applied source, but since the current flow lines will be altered by the presence of the conductor, other things must be considered also. Finally, the angle between the electric vector E and $\overline{\nabla \ln \sigma}$ will influence the source strength. The question of the strength of these sources is then a difficult one; this is the reason that only the simplest resistivity problems have been solved theoretically.

The general attack on this problem has been discussed by Vozoff (1956) and we will return to it later. It is enough now to realize that the induced sources are located at the points in the earth where the resistivity values change.

Before leaving this section, a few words should be said about

the induced polarization effect. If the resistivity of the metal bearing region changes as we use different frequencies, then the induced sources at the edge of this region will be different for different frequency sources. From the appearance of the equation it seems that the change of induced source strength as the size of $\overline{\nabla \ln \sigma}$ changes at a point is quite complicated; nevertheless, we know that a change will occur and that the potentials from the induced sources, when measured, will also change as the frequency of the applied current is varied. It is this change in measured potentials that we will identify with the induced polarization effect.

III. METHOD USED IN PLOTTING RESISTIVITY AND INDUCED POLARIZATION DATA

3.1 Reasons for Using This Method

The integral equation, which suggests the idea of 'induced sources' gives a clue to how best to gather resistivity data in the field. The size of the induced source is dependent upon the location of the applied current source and, of course, the measured potential depends upon the relative location of the applied current, the induced sources and the point of measurement. In order to try to separate the effects of applied and induced sources it would be best to use localized, separated senders and receivers. That is, apply the current at some particular point on the surface and measure the potential at other points.

3.2 Types of Senders and Receivers

When current is applied at some point on the ground and we speak of the potential at some other point we mean the potential with respect to infinity. This potential, being a solution of Laplace's equation is quite smooth and regular in nature. Moreover, small regions of resistivity change will not alter the value of the potential very much even if they are very near the point of measurement. This kind of measurement in the field requires two remote, or infinite, electrodes since we must also remove current from the ground somewhere. For this reason, the potential measurement is very seldom made in the field.

If the second current electrode is removed to infinity and potential differences between two adjacent points are measured we are essentially measuring the first derivative of the potential from a current source. This kind of arrangement I will call the pole-dipole configuration. In all the measurements made using this configuration, the length of the dipole was kept constant while its separation from the pole was varied. Since the slope of the potential curve is much more sensitive to small changes in resistivity this kind of measurement is more sensitive to surface variations in resistivity and in the field gives more irregular results.

If the current is applied at two closely spaced points and the potential difference is measured at two other adjacent points, we have a measurement of the second derivative of the potential from a pole current source. This is the "eltran" or dipole-dipole configuration and measurements of potentials in the ground using this spread are even more irregular than the first derivatives. In practice the length of both dipoles is held constant and their separation varied.

The fact that potentials are smoother than their derivatives is used widely in the interpretation of gravity data where second derivative maps are used to accentuate small anomalous regions on the gravity map.

The potentials, or their derivatives, are seldom used as such in interpreting resistivity data. Almost always, the potentials measured

are normalized with respect to the distance from the current source, by multiplying by the appropriate geometric factor. This transforms the potentials into apparent resistivities. This is the resistivity that the half space would have to have to give you a certain potential reading when a known current is applied. The geometric factor can be computed for any electrode configuration.

3.3 Comparison with Usual Methods

Many papers published lately are concerned with new configurations and geometries in the apparent hope that some new electrode geometry will solve the problem of resistivity interpretation. These new geometries mix up the sender and receiver locations and make the separations of the effect of the induced sources more difficult. (Carpenter, 1955 and 1956; Crumrine, 1950).

I believe that the trend should be in the other direction, to make simpler measurements but more of them. Most of the measurements described in the literature are based on the Wenner spread or some variation of it like the Lee partitioning spread. Using these spreads two different kinds of measurements are made. These are depth profiling and lateral profiling. In the former, variations of resistivity with depth are investigated by expanding the scale of the electrode geometry, and in the latter, horizontal variations of resistivity are investigated by moving the whole set of electrodes along the ground keeping the scale the same.

In both procedures all four electrodes are moved at the same time. Also, the current electrodes are widely separated with the potential measuring electrodes between them. This makes it impossible to determine what factor might be responsible for the difference between two successive readings. By localizing the sender and receiver and by moving them one at a time we can begin, as we shall see, to separate the effects of lateral and vertical resistivity variations. Also, the pole-dipole and dipole-dipole configurations have the advantage of needing only a short length of wire to take the potential reading and this reduces any possible A. C. pick-up in the wire.

3.4 The Two-Dimensional Plotting Method

As in most resistivity methods all of the readings were taken along a straight line on the surface of the ground. Usually, equidistant stations were measured ahead of time to serve as electrode locations. Most of the early work was done with the dipole-dipole spread while later the pole-dipole configuration was used.

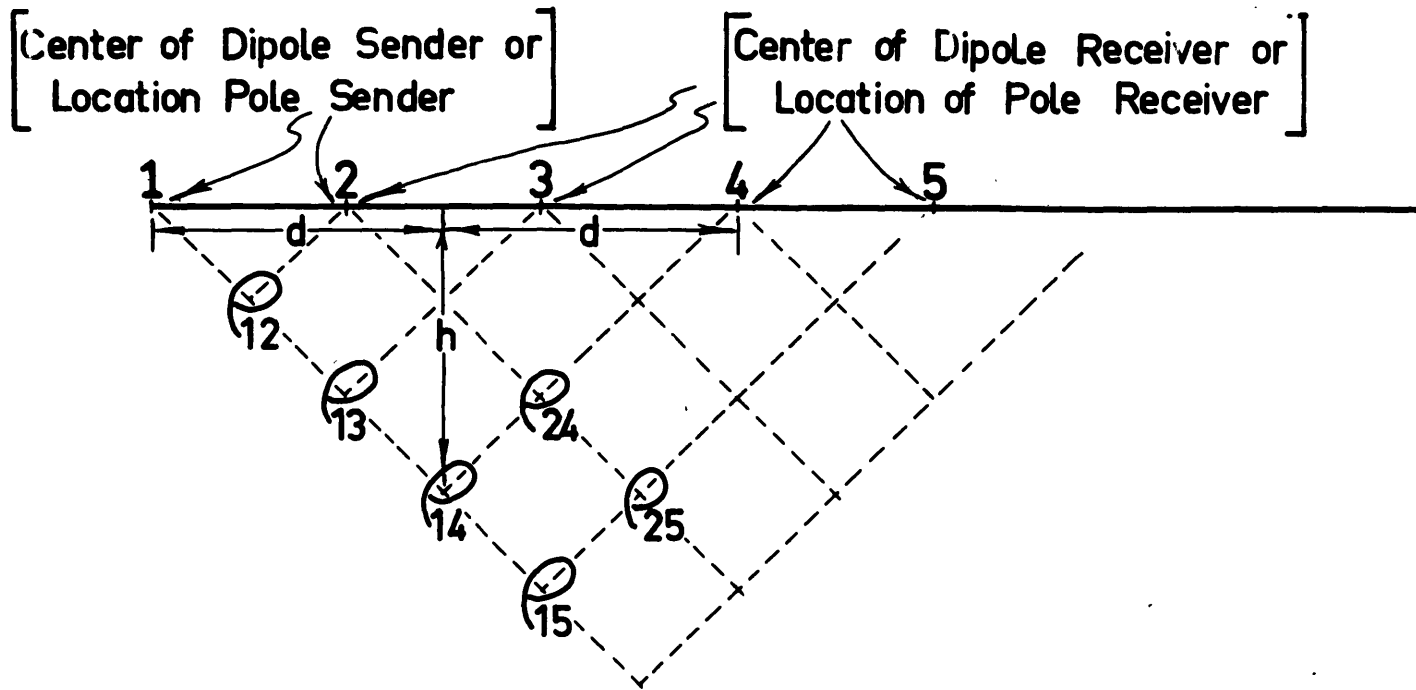
In order to get the maximum possible information about the resistivity in the ground, we then measured the apparent resistivity and the apparent metal factor for every possible sender-receiver combination along the line. In practice the sender was located and the potential measurements were made at all other stations. The sender was then moved forward one station and the procedure repeated.

The data is then plotted on a two dimensional map using the

midpoint between the centers of the sender and receiver and their separation as coordinates. Consider Fig. 1, the value (ρ_{14}) is the value of the apparent resistivity when the center of the sender is at station 1 and the center of the receiver is at station 4. The value (ρ_{14}) is plotted at the intersection of 45° lines from the sender and receiver along the line. When all of the (ρ_a) values are plotted in this way we have a two-dimensional array of data as opposed to the one-dimensional curve that is usually plotted. A 45° line of data in this array is equivalent to the data from an expanding Wenner spread, while any horizontal line of data is for the same electrode separation and is equivalent to a horizontal profile. However, by displaying the data in this way we are better able to keep track of variations of both.

The array of data is then contoured, usually using logarithmic contours because the variations are large. We then have what amounts to a two-dimensional mapping of the resistivities below the resistivity line into the apparent resistivity map. It should not be regarded as a section map because even for horizontal layering the separation is equal to the depth of the region affecting the current only in very special cases. (Vozoff, 1956; Mooney and Wetzel, 1955). The separation of the electrodes does in some way determine the depth being sampled, though, and in this way we have the mapping.

As I mentioned above, the apparent metal factors were calculated at each station and then they were plotted in the same way. When plotting



EXPLANATION OF DATA PLOTTING

Fig.1 .

the field data it was found helpful if both the resistivity and the induced polarization maps could be examined at the same time. Therefore, in most of the field investigations the results were plotted on composite maps. The apparent resistivity values were mapped above the center line and the apparent metal factors were plotted below the line. In this way we have in one map a complete picture of the electrical properties of the ground. As pointed out by Mr. Madden and as evidenced by all of our field work, both kinds of data are necessary to be able to say anything about the importance of the induced polarization effect. Moreover, the very nature of the kind of induced polarization measurement we make necessitates the measuring of apparent resistivities so the data are available. The measured D. C. apparent resistivity is used for the apparent resistivity maps.

3.5 The Effect of Vertical and Horizontal Resistivity Variations

If the only variation of the ground resistivity is with depth, the measured apparent resistivities will depend only on the separation between sender and receiver and the contours on the map will be horizontal. In Fig. 2 are the results from a survey on the property of Mindamar Metals Corporation at Stirling, Nova Scotia. The basement was overlaid by about 100 feet of conductive glacial till. Since the basement was more or less uniform in rock type this was an ideal two layer geometry. The measurements were made using a dipole-dipole configuration with 100 foot spacing. The hill started to thin at station 13 and this is reflected

MINDAMAR
LINE P*

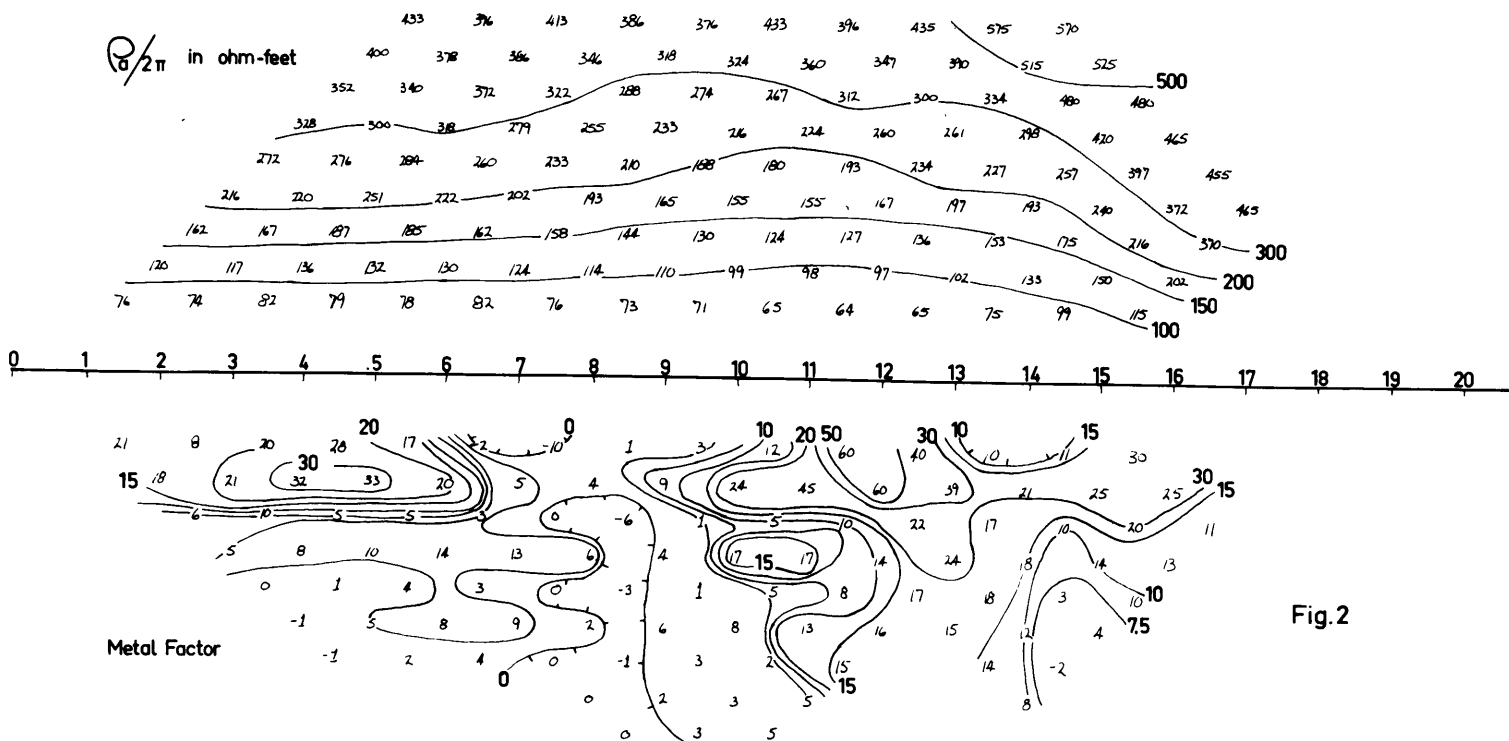


Fig.2

in the resistivity map by the fact that higher apparent resistivities were measured for shorter spreads. The contours start to bend toward the surface. The metal factor map for this line shows no patterns except for two small closures for shallow spreads.

If the resistivity of ground varies laterally along the line we would expect the apparent resistivities to change as the sender or receiver move across these variations. This situation would give rise to 45° contours on the map. In Fig. 3 is a map from an area where several lateral changes were present. It was made using a dipole-dipole configuration with 200 foot spacing.

Station 6 was on top of a hill of conductive glacial till about 100 feet thick. The till thinned quickly so that station 18 was in a marshy area with bedrock only 4 feet down. There were a few outcrops along the line and a few places where the marshy land was deeper. This gave rise to wide variations in the surface resistivities along the line and the resistivity map is dominated by 45° contours. The map also shows that the M_f's were relatively insensitive to the resistivity variations. They remained small all along the line.

Fig. 4 is another line from the same area. This line was at right angles to a group of vertical formations and shear zones. Because of the shear zones and the change of rock type the lateral variations of resistivity were large, and again, we see that the apparent resistivity contours are mostly at 45° directions. Once again, the metal factors measured varied much less than the resistivities.

MINDAMAR

LINE Y

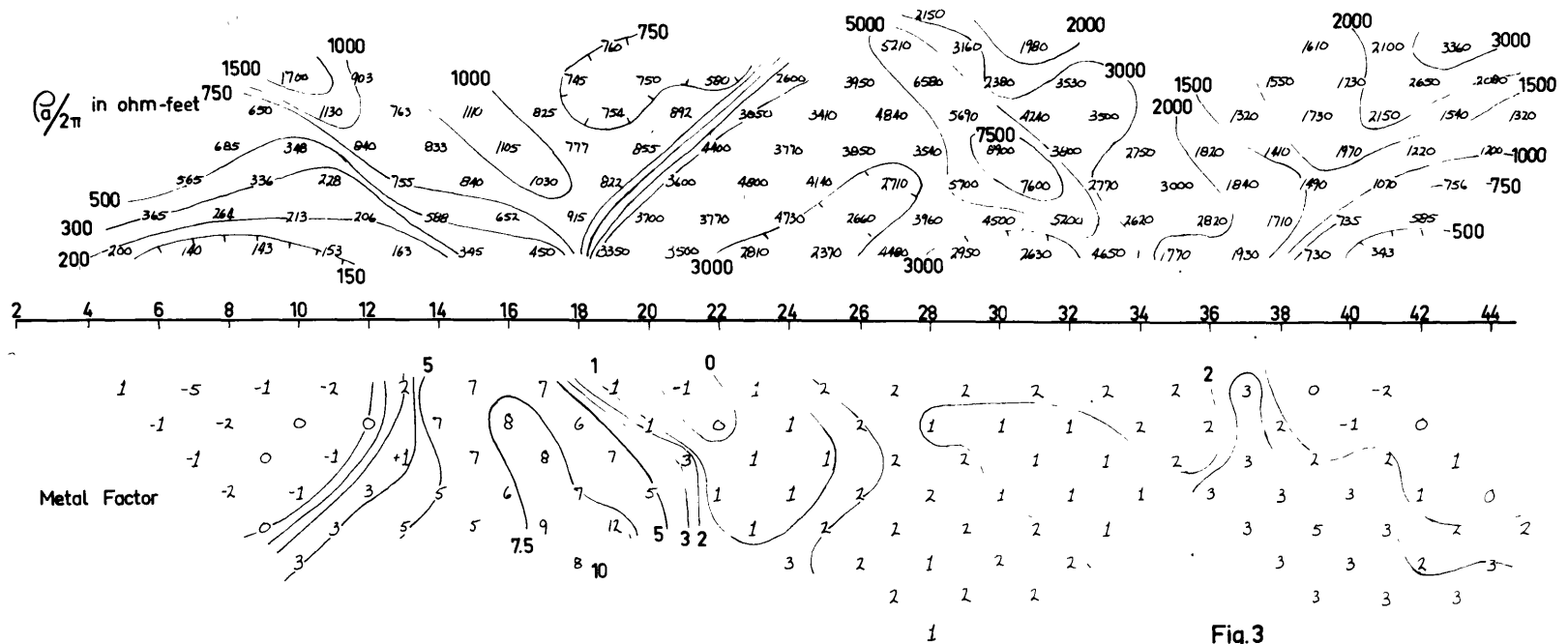
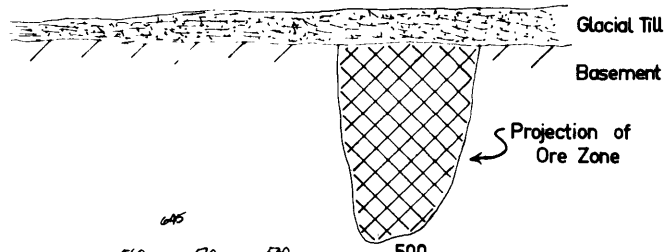
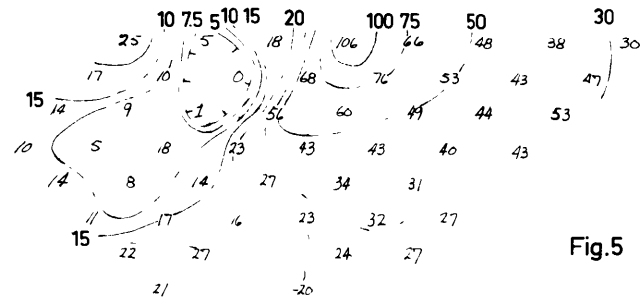
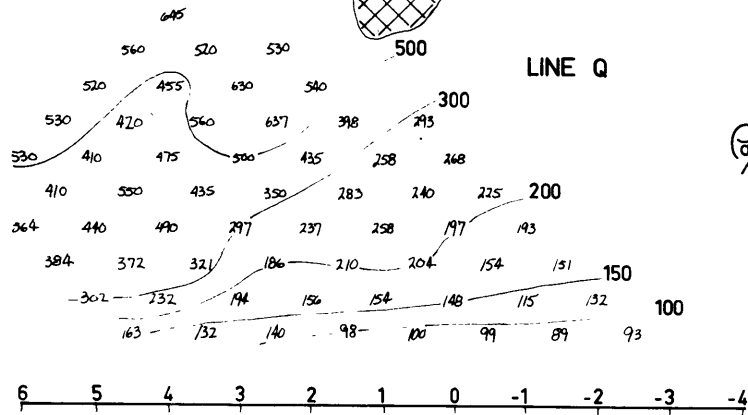


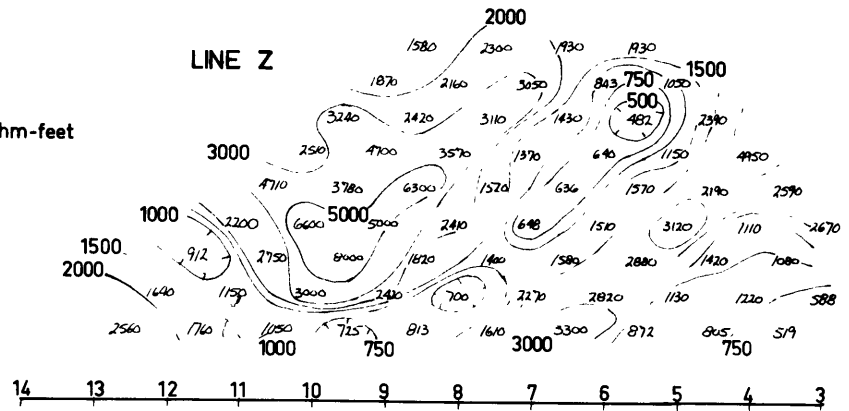
Fig.3



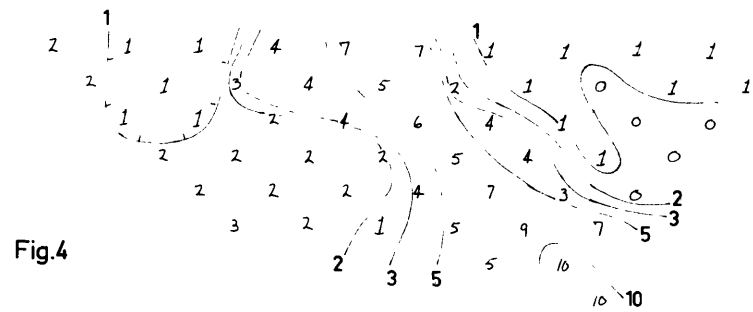
MINDAMAR

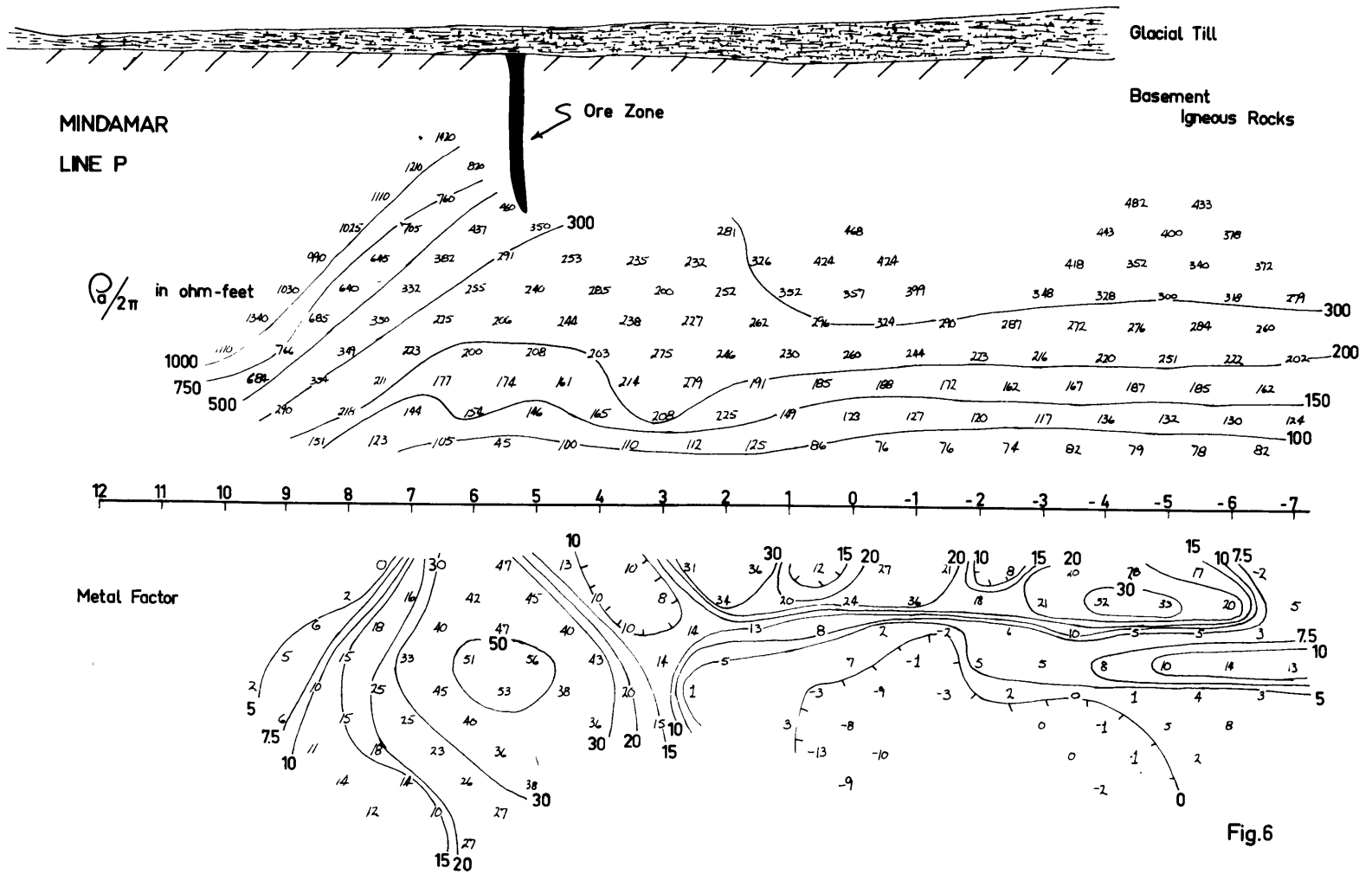


$\frac{\rho}{2\pi}$ in ohm-feet



Metal Factor





3.6 Integration to Get the Potentials

There is one other advantage to collecting the data in this way and that is we have enough information from either the dipole-dipole or pole-dipole configurations to allow us to integrate to get the theoretical potentials for a single current source. All that must
→ be assumed are the potentials at large separations.

As we shall see when we examine more field data, the first or second derivative measurements are often so influenced by small local variations in resistivity that the resistivity maps are not effected by a more remote conductor such as an ore body. In this situation it is an advantage to be able to calculate the theoretical pole-pole data since the potential is less sensitive to small resistivity variations and is more likely to give evidence of a deeper, excellent conductor such as an ore body.

the pole-dipole
or dipole-dipole

Fig. 7 will help us to see that we do have enough data to calculate the exact potentials. In the top map are plotted, instead of apparent resistivities, a schematic representation of the potential measured in a dipole-dipole spread, from which the appropriate apparent resistivity would be calculated. Since we have two current and two potential electrodes there are four separate pole-pole potentials involved in the measurement. For instance, the number (25) represents the potential at the point (5) if a single current source were located at the point (2). Likewise for (37) and for (45).

INTEGRATION TO GET POTENTIALS FROM 2nd DIFFERENCES

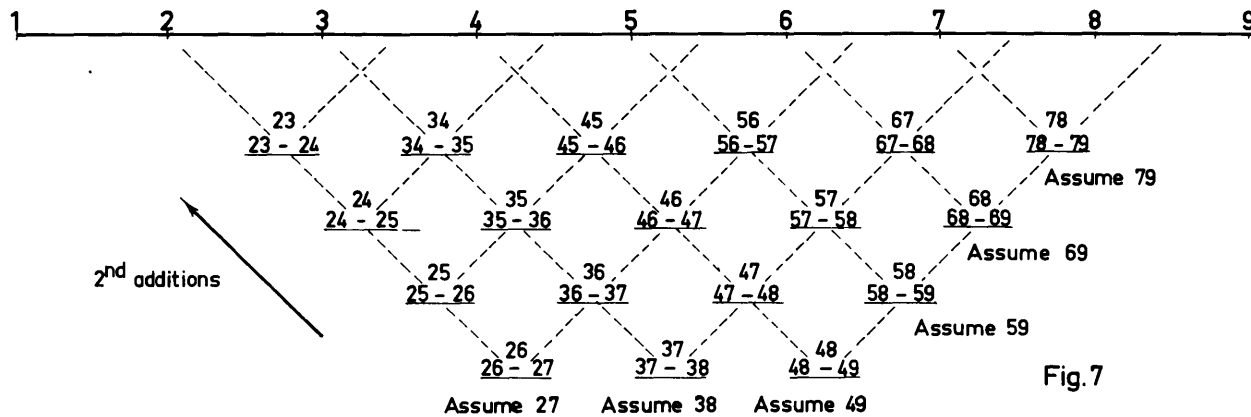
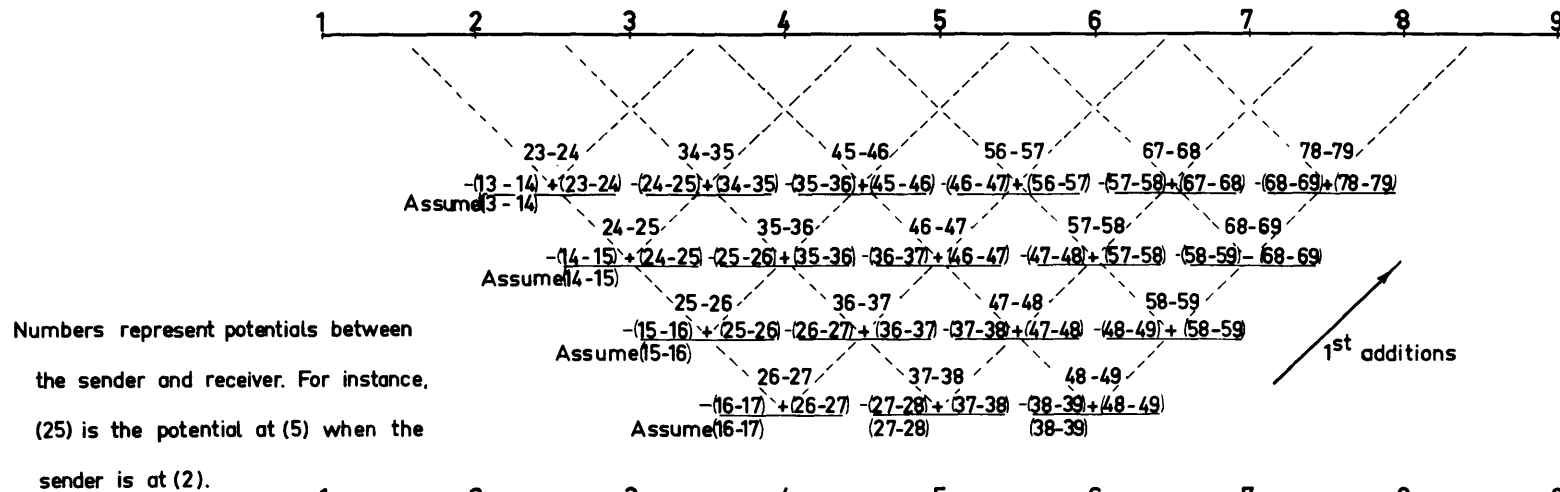


Fig. 7

When the potentials are collected as in the upper figure, we can see that a few assumed first differences will give us enough information so that we can get all of the other first differences by addition. For example, if we assume the potential (16-17) and add it to $-(16-17) + (26-27)$ we have left (26-27) which is just the value we need to add to the next second difference to get (36-37). Thus, by adding upwards to the right we can calculate all of the first differences for that column.

When we have performed all of these additions, we have left just the potential differences shown in the lower map; those that we would have measured if we'd started with a pole-dipole configuration. The assumed first differences are not too critical nor is a choice of value difficult to make. In the first place, we have the apparent resistivity from the dipole-dipole spread. If we assume a value of first difference in potential that will give the same apparent resistivity at the same point on the contour map, we shouldn't be too wrong with the guess. A consideration of the size of the numbers involved will help us to understand why the choice isn't too critical. The first differences fall off roughly as $(\frac{1}{r^2})$ from the pole source. Thus the potential difference at a separation of 800 feet will be considerably smaller than those in close. Then also, the assumed number is added to another bigger than itself. This new number is in turn added to a third, still larger in value. It is obvious that very quickly an error of 25 or 50% becomes negligible.

The additions to get the potentials are just as simple. By looking at the lower diagram on Fig. 7, we see that by assuming (27) and adding upwards to the left we can calculate (26), (25), etc. in turn. We are then left with the potential data we would have measured if we had been able to make a pole-pole measurement. From these the pole-pole apparent resistivities can be mapped. The same sort of argument regarding the assumed values of the potentials applies here as was used in the previous step. If we have taken data out to 800 or 900 feet our integrated data is probably quite accurate out to 500-600 feet and this separation, i. e. , the shallower spreads, are the ones we are generally most interested in.

Since the earth is a linear system we would expect that reciprocity should hold, and indeed it does. Several times an opportunity has presented itself to interchange the sender and receiver, and in each case, the readings were duplicated within the error of measurement. This only holds though if the sender and receiver are of the same kind. If a pole-dipole configuration is used reciprocity does not hold since the dipole has finite length and only approximates the first derivative. This is important when considering the symmetry of a resistivity or induced polarization anomaly. If the geometry of the earth is symmetric with respect to the line of measurement, we would expect the maps to be symmetric if we have the pole-pole or dipole-dipole data. The pole-dipole data will not be symmetric in any case.

In a test of the ease and accuracy of this integration, some data were collected at an old nickel mine at Dracut, Mass. The results are shown in Fig. 8. A narrow vein of mineralization outcropped between stations 14 and 15. Resistivity data was collected using both the dipole-dipole spread and the pole-dipole spread. The first differences and the potentials were calculated from the former using the simplest possible value for the assumed values needed to make the additions. These data appear in the first three maps in Fig. 8. In order to do the integrations the assumption was made in each case that an average apparent resistivity prevailed at the end of the line. I used a constant value for both the assumed first differences of the potential and the assumed potentials.

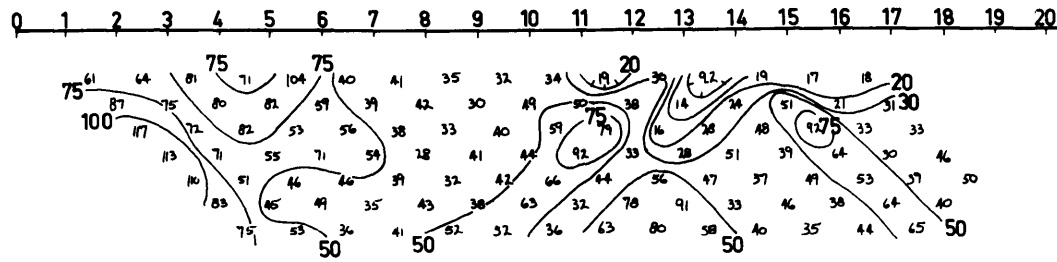
The fourth map in Fig. 8 is the measured apparent resistivity map of the same line using a pole-dipole spread for the measurements. Comparison with the calculated first difference map reveals excellent agreement in the main features of the map, particularly for the upper 1/2 or 2/3 of the maps. Much better agreement is reached if the assumed starting potentials for the integration are picked with a little more discretion.

The smoothing involved in the integration is quite evident from the maps. The apparent resistivities from the potentials are quite smooth with very little variation. The anomaly from the conducting ore body tends to be smaller in magnitude and broader in size.

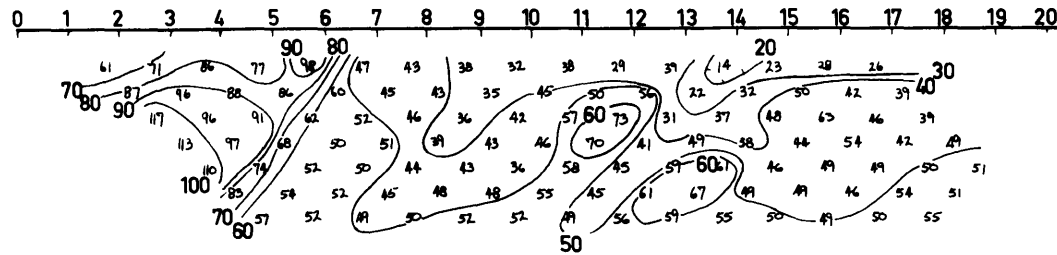
DRACUT RESISTIVITY

Value Plotted is $\frac{\rho}{2\pi} / 100$
from:

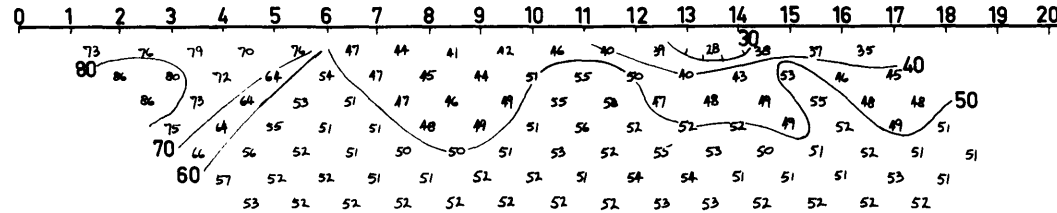
Measured 2nd Differences



Calculated 1st Differences



Calculated Potentials



Measured 1st Differences

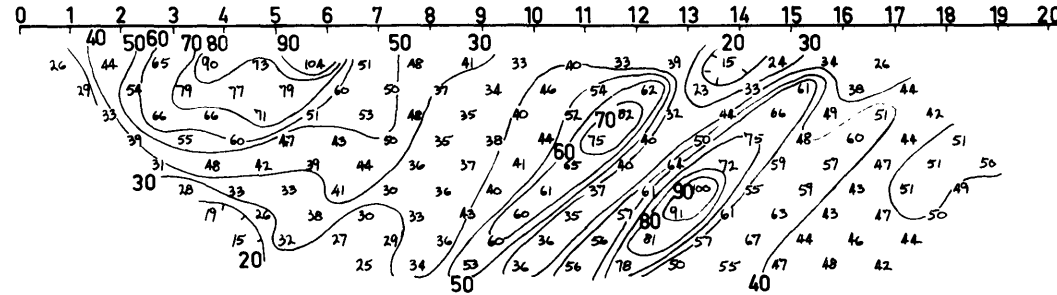


Fig.8

The integration of the resistivity data has not been used to any great extent in the work described in the thesis because as we shall see the induced polarization maps always serve to outline the ore bodies studied. Nevertheless, in at least one case integration of the resistivity maps helped to clear up the picture and to point out a resistivity anomaly that could not be seen in the second derivative data.

IV. FIELD RESULTS

4.1 General Discussion and Methods

Using the method described in the previous section, resistivity and induced polarization maps have been plotted from measurements made in three areas with three different types of ore bodies. The results definitely show the superiority of the induced polarization measurement in locating metallic conductors. In each case though, the resistivity maps do indicate the presence of the conductor. The fact that any resistivity anomaly at all can be picked out is largely because the method of plotting the data gives a better chance to keep track of apparent resistivity variations.

The field procedure in each case was similar but not exactly the same. The field equipment has undergone continual change as experience has suggested improvements. Basically though, the kind of measurements were the same.

At each station a D. C. and an A. C. apparent resistivity measurement was made. The D. C. resistivity was used for the resistivity map and the apparent metal factor was calculated using both according to the formula

$$(M.f.)_a = \frac{\left[\frac{\rho_{a\ dc}}{\rho_{a\ ac}} - 1 \right] \times 100}{\frac{\rho_{a\ dc}}{2\pi} \times 10^{-3}}$$

The source of power in the field was a 300 watt, 60 cycle, gasoline motor driven generator. The D. C. measurement was made

in each case by rectifying the out-put of the generator and putting this D. C. signal into the ground through the current stakes. The current level was measured by a D. C. ammeter.

At the potential stakes the D. C. signal was first filtered to remove any A. C. background. The voltage was then read on a high impedance battery operated V. T. V. M. by converting it into an A. C. square wave signal. The conversion was accomplished using a mechanical switching system operated by a spring driven motor.

The A. C. apparent resistivities were measured in two ways. Originally the 60 cycle output of the generator was used directly and the A. C. potential was read on the same A. C. meter used for the D. C. reading. The use of 60 cycles proved inconvenient since almost all of the background voltages in the ground were 60 cycles also. They originate from power lines, houses, etc. A later system converted the D. C. signal of the rectifier into a low frequency (10-14 cycle) signal which was used. The frequency range of the portable voltmeter was such that it could still be used at this frequency. The 60 cycle background was largely eliminated by using a low pass filter in the potential circuit.

This new system extended the range of the equipment in most areas because with the lower background smaller voltage reading could be measured with confidence. A more detailed description of the field equipment can be found in the 1955 M. I. T. Bachelor's thesis by N. Ness, (Ness, 1955). The equipment is mounted on packboards and can

be carried quite easily by three or four men into almost any area where measurements are desired.

4.2 Results from a Vertical Ore Body

The first results are from two lines over a vertical ore body on the property of Mindamar Metals Corporation at Stirling, Nova Scotia. The geology of the mine area can be found in a report by P. W. Richardson (1953). The ore body was tabular, about 15-20 feet thick, 150-175 feet long, and continued down at about 200 feet below the sub-outcrop. The sub-outcrop was under 60 feet of glacial till. Line P was roughly at right angles to the strike of the ore zone and line Q was paralleled to the strike.

The ore zone is itself a mineralized portion of a vertical shear zone in the basement rocks. It is typical of base metal deposits found in metamorphic rocks in several parts of the world. Some features that these so-called massive sulphide deposits have in common are , a high content of metallic minerals, extremely fine grain size, relatively simple mineralogy - pyrite, sphalerite, chalcopyrite, and galena being most common - and thinly layered structure in the ore. The principal ore at Mindamar was sphalerite, but there was some chalcopyrite present and quite a bit of pyrite so that metallic minerals made up a large part of the ore zone.

This area is an excellent test of the induced polarization method because of the glacial till. As we have seen, the resistivity contours on the maps from this area are mirror images of the thickness

of the glacial overburden. However, the current flow in the till, since it is more conductive than the basement, will be as in parallel with the current in the basement rocks and the calculation to get the metal factor will to a large extent eliminate the effect of the conductive surface layer.

The two lines P and Q intersect over the ore body, so that P5 very nearly coincides with Q0. Both lines were run with the dipole-dipole spread and the stations were 100 feet apart. Fig. 6 shows line P while line Q is on Fig. 5. The idealized sections I have shown above the maps were drawn using the available drill hole data. Since line Q did not pass directly over the ore body, it was off set by about 25 feet, the outline of the ore body on this sketch is its projection on the plane of the map.

Consider first the resistivity map on Fig. 6. On the right hand side of the map the thickness of the till is constant and as before, the contours are flat. The dominating feature on the left side of the map is the rapid approach of the contours to the surface. The till thinned to practically nothing in a creek bed at station 13 and the shallow bedrock is responsible for the higher resistivity values for short spreads at the left of the map. There is a hint that the contours are bent up between stations 4 and 7, but it would be difficult to attribute this to a good conductor at depth, because the 45° contours caused by the thinning till mask everything else.

The metal factor map is a different story. There is a very definite induced polarization anomaly associated with readings when the sender and receiver were straddling stations 5 and 6. Moreover, the contours begin to close on top indicating that the source of the anomaly has some depth. Indeed, the maximum metal factors were obtained when the center of the sending and receiving dipoles were 600 feet apart. The fact that the dipole-dipole metal factor anomaly is more or less symmetric also suggests that the ore body is roughly symmetrical with respect to the data line.

The resistivity map in Fig. 5 is also completely dominated by the contours approaching the surface. Here the presence of the conducting ore zone is not evident in the contour pattern created by the thinning till.

The M. f. map is more interesting here than on line P. The anomaly is larger both in magnitude and size. This is taken to mean that the metallic conductor plays a bigger part in the current conduction in line B than in line P. The anomaly is also much less symmetric in this case. The high readings end quite abruptly on the left side, but the right hand part is less definite. As a matter of fact, the line doesn't extend far enough in this direction to determine where the anomaly really ends. This fact suggests a more gradual beginning for the mineralization in this direction.

These few general statements are about all that can be said

from intuition concerning the data from lines P and Q; I will return to these maps when there is more on which to base an interpretation.

4.3 Results from a Horizontal Ore Body

The next group of maps are from the lead-zinc district of southeastern Missouri, near Fredericktown. They were done on the property of National Lead Company over an ore body that had been outlined by exploration drilling. It was an excellent chance to test induced polarization in a well controlled situation. Powers, etc., (1953), give a brief description of the ore occurrence in the area and other numerous papers on the area can be found in the geologic literature, (James, 1949).

The granite basement rocks, which outcrop further west in the Ozark uplift, are from 100-600 feet deep in the Fredericktown area. Numerous knobs and hills on the old erosion surface protrude up into the overlying sediments. The basal member of the sedimentary section is the La Motte s. s. which laps up onto and pinches out against many of the old granite hills. There are several limestone formations on top of the sandstone and granite and they are the surface rocks in the area today.

The lead-zinc deposits are found in the lowest limestone bed or the upper few feet of the sandstone but always closely associated with the pinchout of the sandstone. This strange control in the mineralization is much argued by the geologists of the area, but it is a fact that almost all of the major ore bodies have been closely associated with the

sandstone pinchout. Geophysics has been successful only in locating the buried granite hills. This is done with ground magnetic surveys; nothing else in the way of geophysics has been very successful. Powers, etc., (1953), describe some resistivity measurements using the Wenner spread, but this has not been too successful in the past. Electro-magnetic methods also have been tried without much satisfaction.

A total of three resistivity and induced polarization lines were run over one ore body that had been pretty well drilled. The measurements were all made with the dipole-dipole configuration using 100 feet between stations. The data are presented in Fig. 9 - Fig. 14. The ore body was about 250 feet deep and was flat lying. It was roughly 500 by 1000 feet, and the lines were over one end of it. The drill holes showed a scattering of pyrite mineralization in one of the upper limestones throughout the whole area. One of the aims of the survey was to see if the induced polarization measurements could differentiate between this light upper mineralization and the ore zone.

Figures 9, 10 and 11 are the maps from three lines at Fredericktown, and over each map I have drawn an idealized section of the information in the nearest drill holes. The hatched section on each line represents the shadow of the ore zone on the surface as indicated by the induced polarization measurements. They can be seen, in all three cases, to correspond very well with the actual location of the ore.

In Fig. 9, line A, we can see that the metal factor values are

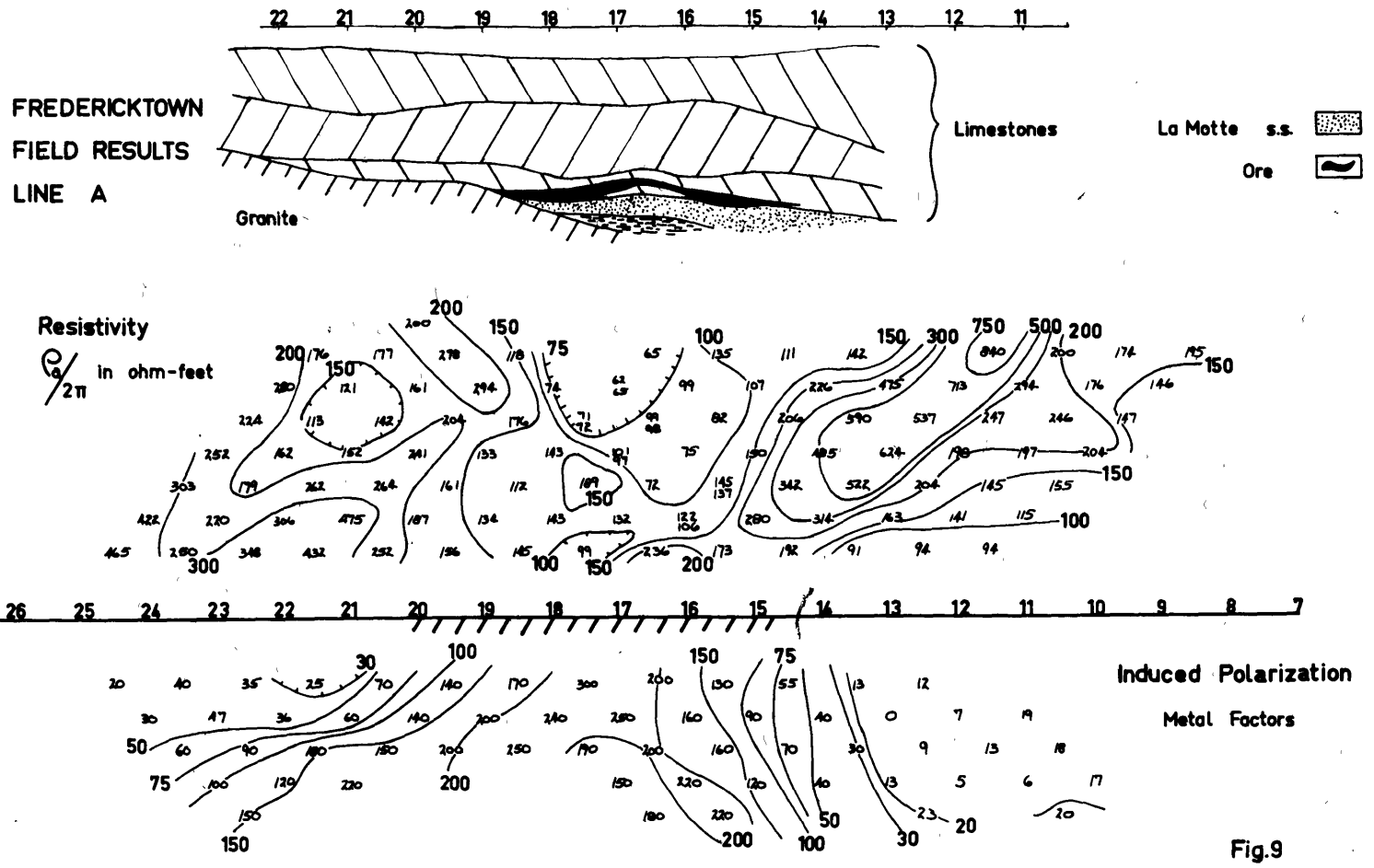


Fig.9

quite high for receivers past station 15 and for senders less than station 20. The anomaly is very definite in shape and seems to be more or less symmetric. The resistivity map is very confused with a lot of 45° contours, and nothing can be said about it except that there does seem to be a general area of lows if the sender and receiver are astraddle the ore zone.

Fig. 10 shows line C which is a roughly parallel line, and both the resistivity and induced polarization maps have much the same character as in line A. One feature of both of the induced polarization maps is a region of low metal factors directly under the center of the anomaly. This is curious, but we shall see later from the modelling work, that it is expected.

On the extreme left hand end of line C, we can see that the metal factors are getting bigger again. This is because the line has extended over the granite knob and these high metal factors are from a small ore zone on the other side of the hill as is shown in the section.

The resistivity map for line C is also very confused. The weathered surface and soil thickness were varying on the limestone surface, and this, undoubtedly, gives rise to lateral variations in resistivity. The dipole-dipole spread, of course, magnifies these variations. Again, as in line A, though, the lowest apparent resistivities are when the sender and receiver are across the ore body, although the anomaly is not very definite.

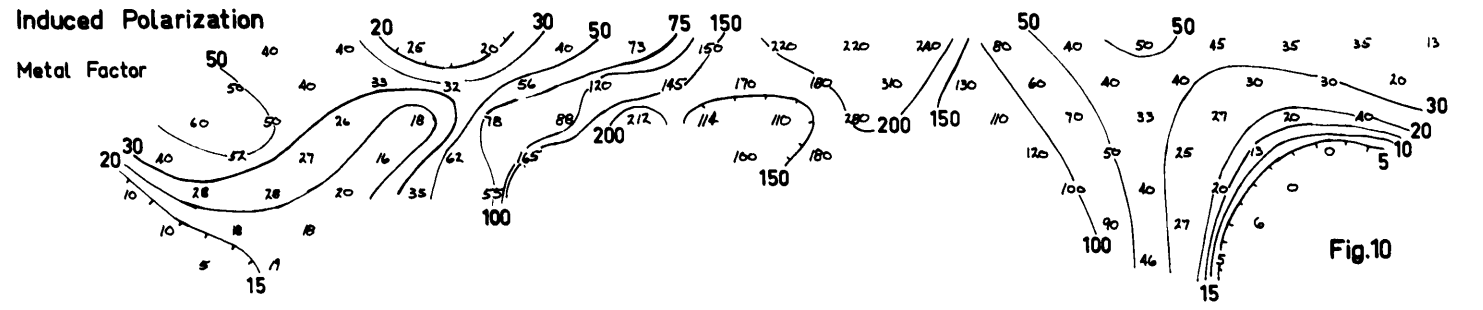
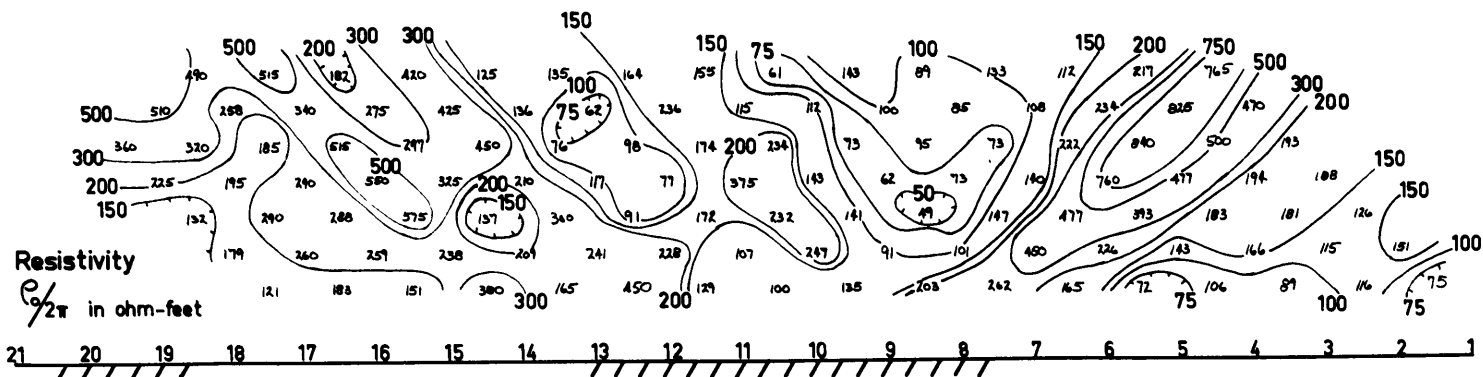
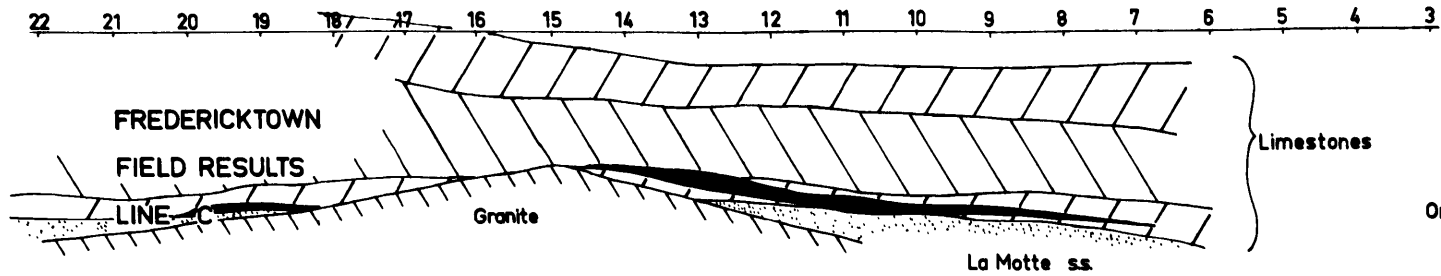


Fig.10

01
0

The data from line B is shown on Fig. 11. Line B was roughly at right angles to A and C and was parallel to the buried hill over the pinchout of the sandstone. On these maps the beginning of the induced polarization anomaly is much less abrupt. This is because the ore zone limits were not as definite in this direction. On the right part of the map there seems to be a small metal factor anomaly, but the drill hole data doesn't support this. The resistivity data is dominated by a region of high values on the right where the soil cover became very thin. Again, the resistivity maps give little or no indication of the conductor.

Most of the metal factor contours are open on top and give no indication that there was much depth to the source of the anomaly. The first readings are obtained when the center of the dipoles are 200 feet apart, and for this separation the ore body at 250 feet might begin to have an effect; but the possibility that the shallow mineralization was the source of the anomaly still needed investigation. Line Csh was run on line C using 20 foot spreads for the dipole-dipole configuration. The metal factor map on Fig. 12 very definitely shows that the values get bigger with the longer separation and are not too shallow. The resistivity map for this line shows a shallow low with an increase of resistivity with depth. There is very little that can be said about the depth to the anomalous region from these maps.

The shallow mineralization was widely scattered throughout

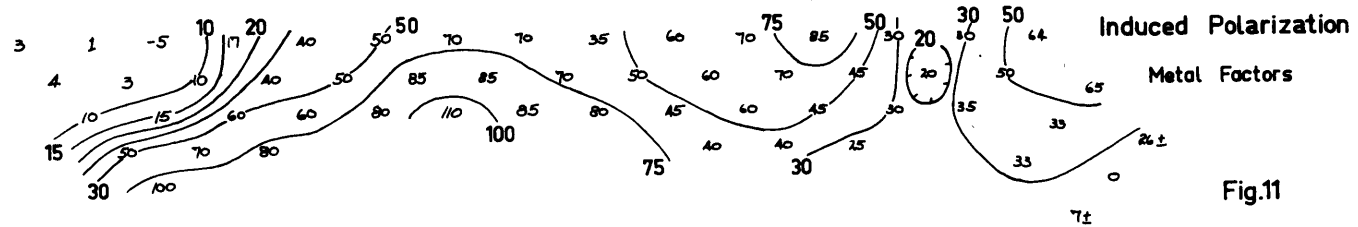
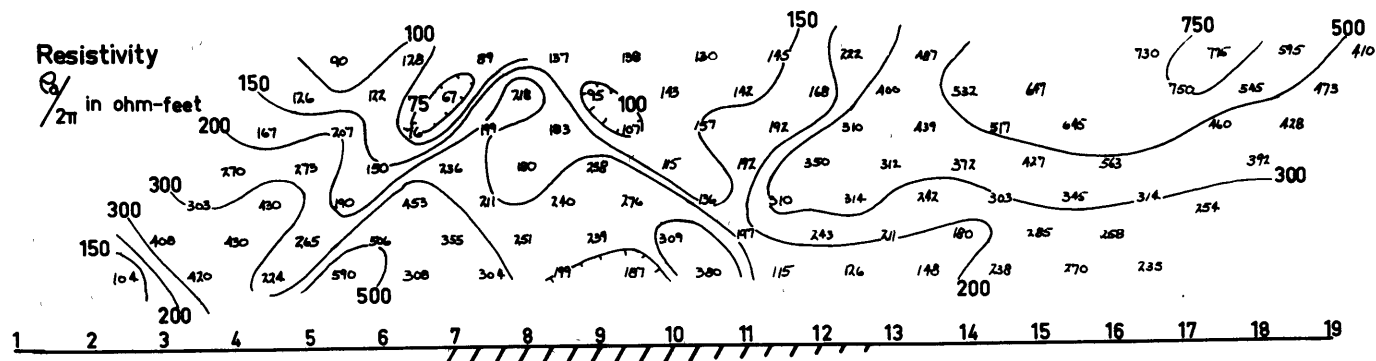
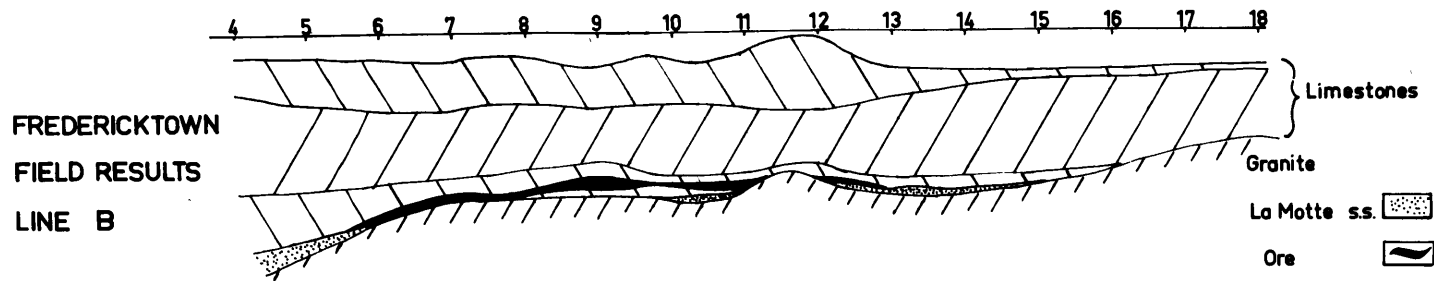


Fig.11

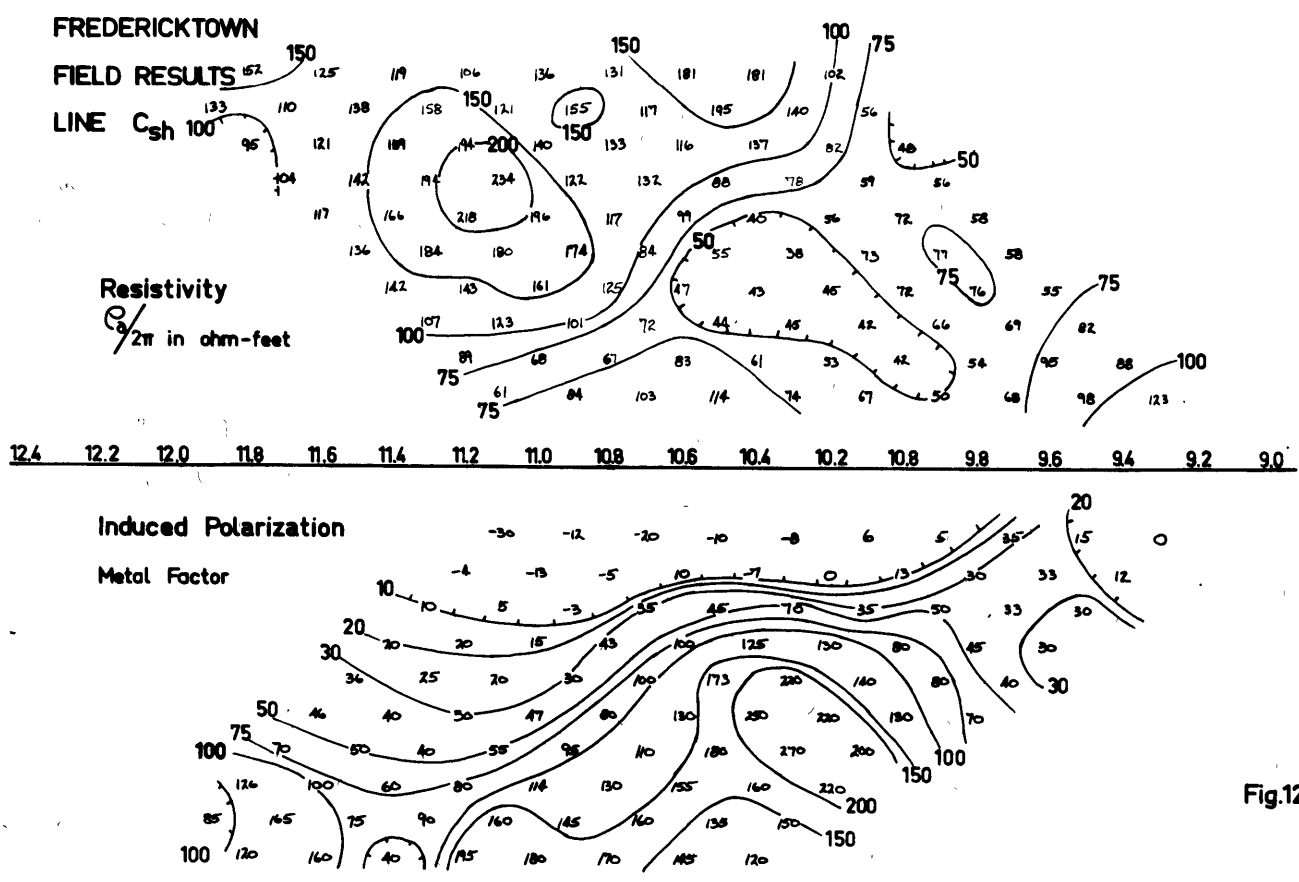


Fig.12

S
W

the area and was present in most of the drill holes as traces of pyrite. The excellent correlation of the high metal factors with the ore zone seems to indicate that the more widespread traces of pyrite are not directly responsible for the anomaly. They may, though, be the reason for the rather high background of metal factors on some of the lines. T.R. Madden, (1956), has suggested that there is extra mineralization over the ore zone and associated with it that was logged as traces of pyrite in conformity with the other drill holes. If this were true, it might account for the fact that the metal factor contours do not close on top and therefore give little indication of depth for the source of the anomaly.

On Fig. 13 are the three apparent resistivity maps that have been plotted using the potentials obtained by integrating the second derivative data from the dipole-dipole spread measurements. In this case, the starting values of the first differences in potentials and the potential were not considered constant but were weighted according to the apparent resistivity from the original map. The maps are much smoother than the derivative maps, and the resulting lows in apparent resistivity correlate very well with the induced polarization anomaly. However, the ore body does not cause a reversal in the apparent resistivity values as the separation of the pole sender and pole receiver is increased. The anomaly is caused by the fact that the normal increase of resistivity with separation is slowed down over the ore zone. This gives rise to the low zones of apparent resistivity.

FREDERICKTOWN FIELD RESULTS

$\frac{e}{2\pi}$ from Integrated Potentials

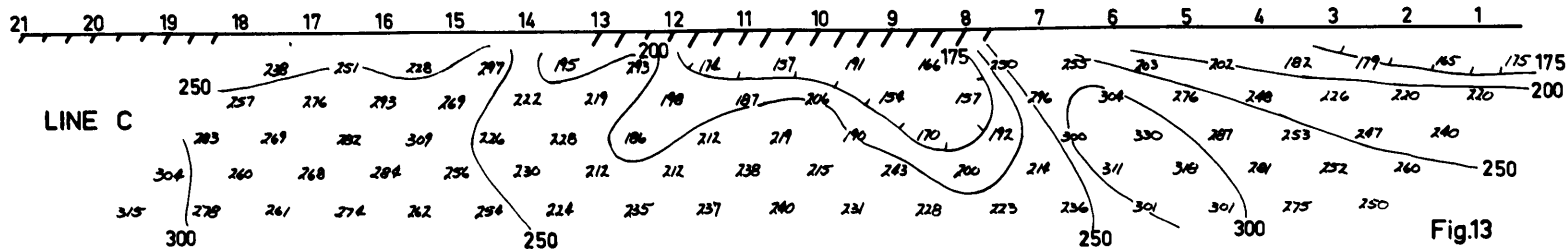
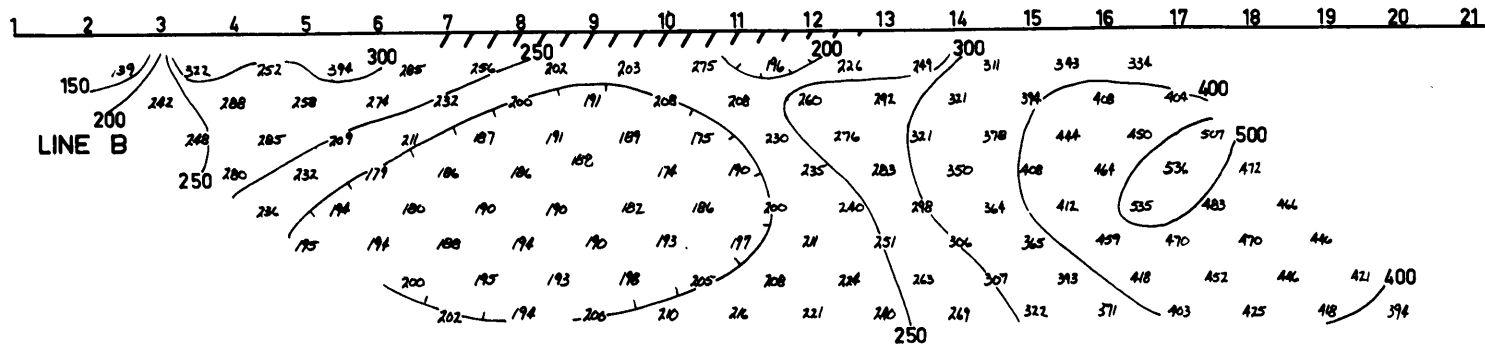
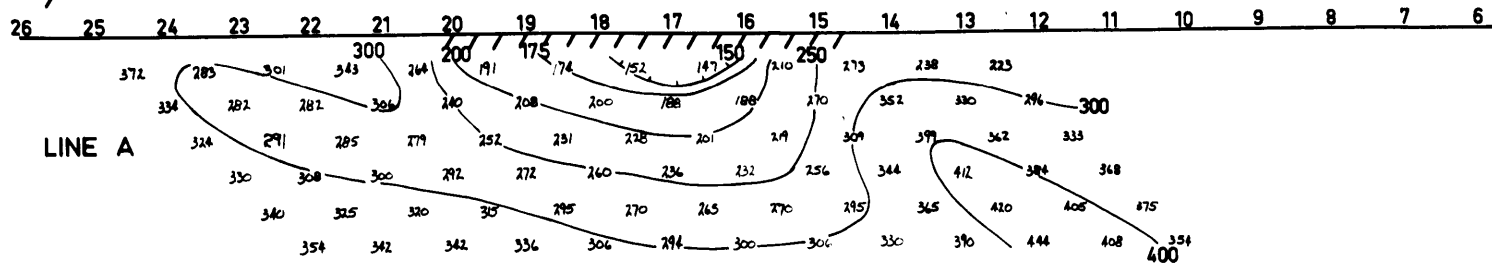
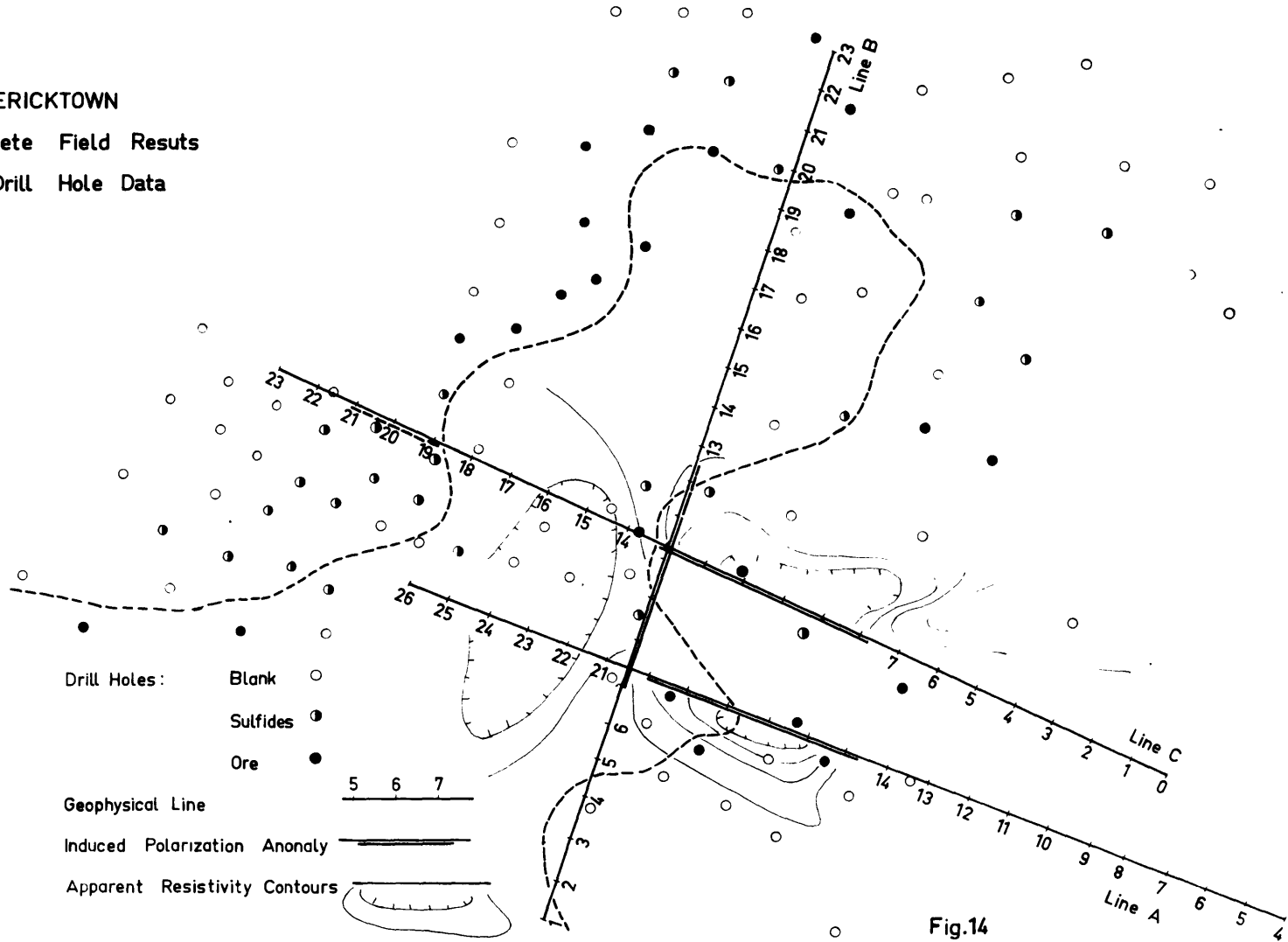


Fig.13

One important thing to see from the maps is that a single line of data is not enough to differentiate the anomalous region. Thus, an expanding spread centered over the ore body would only measure an apparent resistivity that increased with separation. The lateral changes in resistivity as the electrodes moved horizontally would alter the apparent resistivity data more than the presence of the conducting ore zone at depth.

All of the information from lines A, B, and C is plotted on a composite map in Fig. 14 along with the existing drill holes. The dotted line is the pinchout line of the LaMotte s. s. and the ore location is seen to be very closely associated with this pinchout. The three lines on which data were collected are located in their respective geographic positions and the induced polarization and the integrated apparent resistivity anomalies are indicated. As indicated by the idealized sections, the correspondence of the anomalies with the location of the ore is very good. Over this ore body, at least, induced polarization measurements seem to be adequate in outlining the ore. In an area such as this where the area of interest can be narrowed down in advance, in this case by magnetic location of the buried hills, the slower induced polarization method has definite advantages over others such as the E. M. technique. The major advantage being, of course, that the method can locate the ore zone. In a localized area it doesn't require too long to make a complete survey, even with the number of measurements that are needed to plot the data in the manner used here.

FREDERICKTOWN
 Complete Field Results
 and Drill Hole Data



4.4 Resistivity and Induced Polarization Results from Vertical Interfaces

The third set of field maps is from a region that is very different from the other two. These measurements were taken in one of the great porphyry copper areas in the southwestern United States on a property of Kennecott Copper Corporation. In this case, the measurements were more exploratory in nature. There was practically no drilling data available along these lines, so there was little control; however, the contour maps were more interesting than the others, especially so because the simple case of vertical interfaces is one of the few that can be done theoretically, so that we can calculate exact maps.

The large open pit mines in the west which extract the enriched porphyry copper ore are among the biggest in the world. The lateral and vertical extent of these ore bodies is measured in thousands of feet. Much larger areas are covered by the unenriched porphyry. Chalcopyrite is the ore mineral, but pyrite is always present in larger amounts. The ore is usually economical if the copper is enriched to 2-3%; in this ore there is likely to be as much as 6-8% pyrite. In the unenriched zones the metal content is much less. Because of the nature of the ore occurrence, we might expect the porphyry copper ore to be good targets. The tiny grains of metallic minerals are redeposited in the solution channels so that each has a maximum effect on the induced polarization measurements. The geometric location of the metallic particles is an

important factor in the size of the induced polarization effect and is discussed more fully in T. R. Madden's thesis.

The size of the ore zones makes them good targets, but geophysics has not had much success in this area either. In the dry southwest there is little or no water flowing through the rocks to flush away dissolved salts, and as a result, the water more or less tightly held in the small cracks in the rocks is quite salty. This is the water through which conduction takes place, and therefore the resistivity of the rocks in this area is quite low. Also, since weathering is slow there is a great deal of clay in the soils and they have a high conductivity. Since the ore zones only have a few percent of metallic constituents, their resistivities are not much lower; in short, they are poor electrical targets compared to the surrounding country rocks. Most electrical methods have been tried in this area but with little success.

In this case, the measurements were made with the pole-dipole spread. The stations were set every 100 feet, but in order to increase the speed of the operation, the pole sender was only set up at every other station. For each sender the dipole receiver still occupied each position along the line. The problem of choosing the scale of the measurements and the number of sending positions to use is largely dictated by the situation. If the ore body we are looking for is only 50 feet or so in dimension, we are obviously not going to use a long spread. On the other hand, if the target is 500 or 1000 feet long, it is a waste of time to look for it by

moving your sender along 100 feet at a time. The important thing is to have enough values on the map so that it can be contoured intelligently. Of course, such things as the expected depth of the conductor and the size of the anomalous values are also important.

Figures 15 and 16 show the first half and last half respectively of the same line. Fig. 17 is the last part of another line that crossed the first near the end of both. Station number 28 on line W. A. is very close to station 25 on line A. H. The angle between the two is about 60°.

The drill holes that were in the area were all along the first part of line W. A. The drill logs showed that the top of the ore was about 250 feet deep under station 0 and came very close to the surface at station 5. The last drill hole was between stations 6 and 7 and was out of ore. The resistivities between stations 5 and 9 are high and the equivalent metal factors are low. As we shall see later, the shape of the contours in this region suggest a vertical blank zone. However, past station 9 the metal factor values picked up again and continued high, with several shallow lows, until about station 26. When the sender was past this station, the metal factors were all small and the resistivities increased.

The metal factors, as high as 3000-5000, are the largest we've seen in the field work, and the fact that they seem to be increasing with separation hints that the metal factors in the ground get bigger at depth. The resistivity contours show the same behavior. The lowest

LINE W.A.

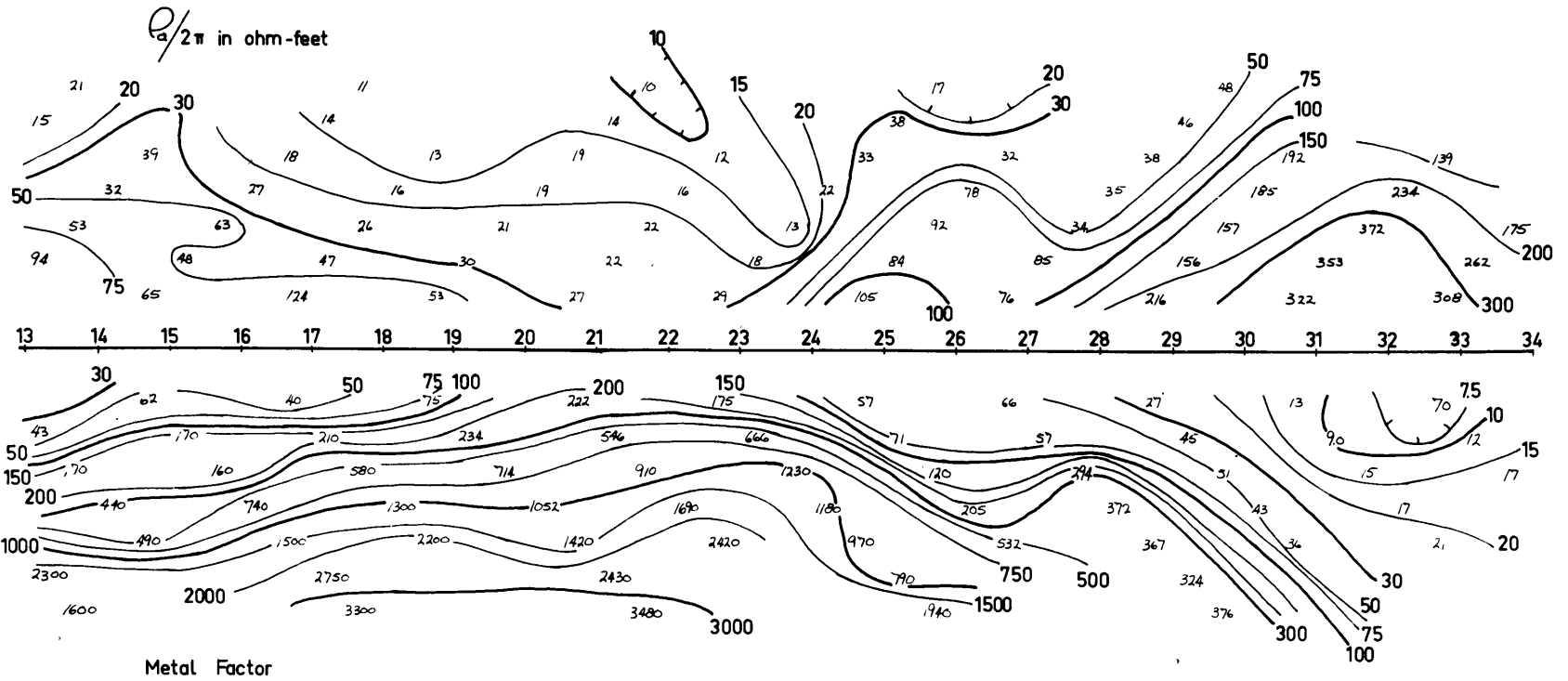


Fig.16

LINE A.H.

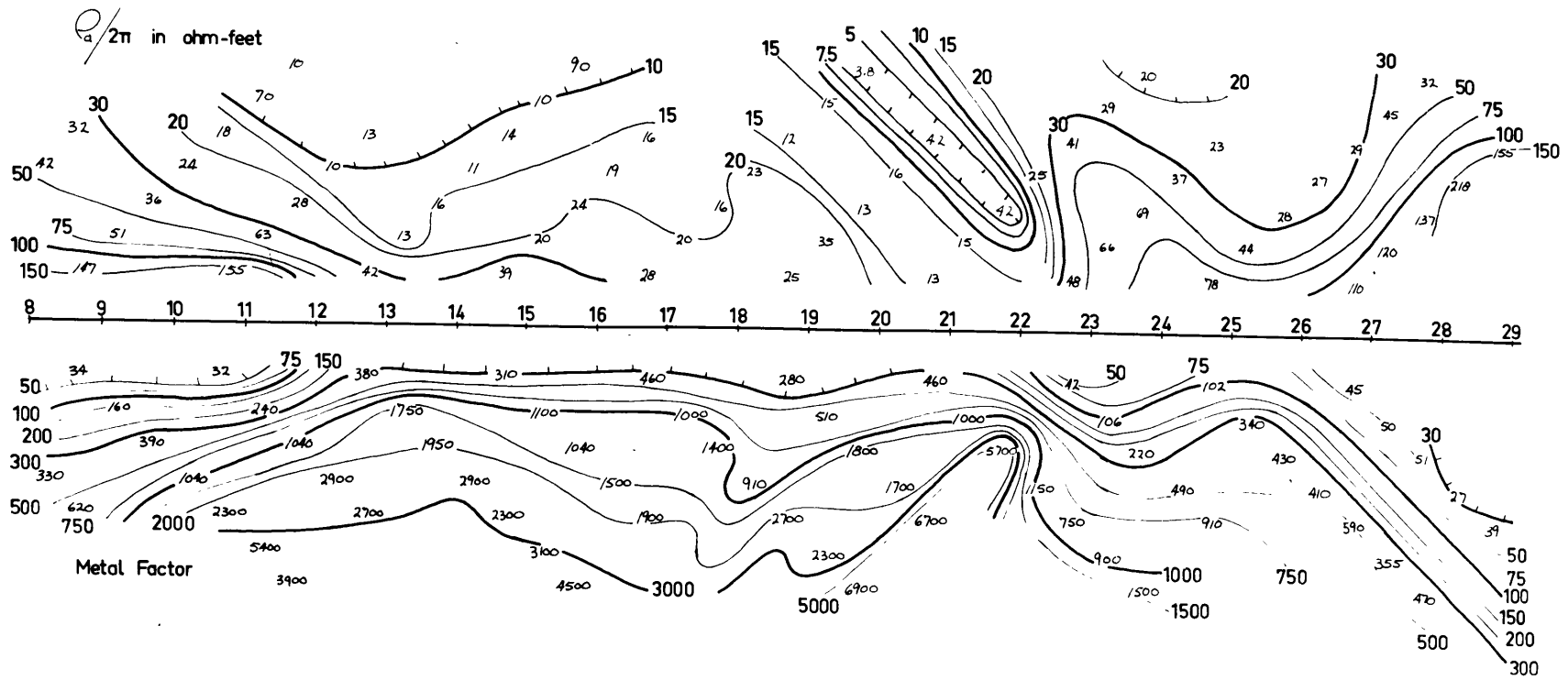


Fig. 17

resistivities are those from the largest separations. However, it would be difficult to determine the region of decreased resistivity with only one line of data. All of the contours on the map are necessary to give the correct picture.

The metal factors reproduce so well the known drill hole data at the beginning of the line, the plunging from station 5 to 0, that it probably is safe to say that we can map the ore with metal factor measurements. If this is true then we can say that the ore reaches from station 9 to station 26 along line W. A.

At the beginning of line A. H. Fig. 17, the metal factors were already large for the bigger separations. The contours stayed more or less parallel until the sender passed station 24; then the metal factors dropped very quickly. The resistivity pattern is very much like that on line W. A. The lowest apparent resistivities are for long separations and then a very rapid increase when the sender is past station 24. In fact, the ends of both lines are very similar, as it should be, since they cross very near the end of the region of high metal factors and low resistivities.

Despite the fact that the resistivity maps have enough character to allow the detection of the ore zone there is no doubt that the metal factor maps do a much better job. For one thing, there are more contours on the induced polarization maps. The maximum and minimum values on the maps are M. f. 's of 6900 and 5. The resistivity contrast is much less. A measurement in a nearby open pit where

the sender and receiver were both directly in the ore gave a metal factor of 10,000. On these lines the ore zone is big enough, so that for long spreads we are virtually seeing only the ore itself. The apparent metal factor values should then be approaching the value in the ore itself; they do get bigger and bigger as the spread increases.

In the measurements at Mindamar and in Missouri, the apparent metal factor anomalies were much smaller despite the fact that the ore itself was much more massive and must have had a higher metal factor. Later, it will be shown that the apparent metal factor drops off very quickly with distance from the anomalous region. This is the reason for the smaller anomalies. In neither of these cases, were we able to sample enough of the ore body to get anything like a true estimate of the metal factors in the ore zone. Only in the extremely large deposits such as the porphyry copper ores can we get a fair sampling of the properties of the ore itself from surface measurements.

4.5 Conclusions

The field measurements reported here and other work at these same locations and others seems without a doubt to show that the induced polarization measurements have at least another order of magnitude more resolving power than ordinary resistivity measurements. However, I think that the field maps reported here have also shown that more can be gotten out of resistivity measurements than is ordinarily used. By separating the sender and receiver and moving each separately and then

plotting the results on a two-dimensional plot the resistivity data can become useful, even in areas where the Wenner spread measurements would have become very confused because of lateral as well as vertical resistivity changes. This amount of data also allows us to perform some operations on the potential data, such as integration or differentiation, which sometime are of use in clearing up the resistivity picture.

There are, of course, a large number of measurements involved in gathering this kind of data; this makes the method slow when compared to some of the new tools of mining geophysics. The airborne electromagnetic and even the ground electromagnetic methods can cover ground faster. They are both very adequate to determine conducting zones in areas like the Canadian Shield where resistivity contrasts are high. The E. M. methods are not effective in areas where the country rock is more conducting; also, the E. M. methods can't differentiate between a metallic conductor and a shear zone filled with water, for instance. Neither method can, of course, do much about graphite. T. R. Madden feels that being a semi-conductor, the graphite will act as an electronic conductor and have an induced polarization effect.

There are other electro-chemical phenomena that have been suggested as possible sources of frequency dependent resistivities in the ground. Several papers have appeared describing the conduction

characteristics of clays and apparently they do have polarization properties; however, the processes involved are essentially mechanical in nature, and as such, have long time constants; much longer than 10 seconds probably. Madden, in his thesis, has considered clays and other materials and finds that their effect can probably be eliminated or reduced, (Madden, 1956).

There are, of course, ways of speeding up the operation; you can give up resolving power for speed by merely skipping sender locations as were done on lines W. A. and A. H. Other lines were run over these porphyry areas by using pole-dipole spreads with a 200 foot dipole and pole location every 400 feet. The longest measurements ever taken were with a dipole-dipole configuration and the dipoles 500 feet long. A greater length of line can, of course, be covered in any given period of time using these longer spreads. How far this extension can be carried before inductive coupling becomes important depends upon the conductivity of the rocks over which you are working and the frequencies you are using. There is work now going on in the Department of Geology and Geophysics on extending the measurements to separations of miles by considering the inductive coupling.

As mentioned before, the situation largely dictates the kind and length of spread to use. If the problem is to outline an ore body or to extend known mineralization in a region well controlled, small scale measurements are in order. For reconnaissance over an area measured in thousands of feet a larger scale must be considered.

V. FURTHER THEORETICAL TREATMENT

5.1 General Discussion

Two things were made clear by the field results discussed in the previous chapter. The first was that the induced polarization measurements do a much better job of outlining metallic conductors than resistivity measurements. Indeed, it gives positive results in areas where the apparent resistivity measurements were badly confused by lateral resistivity variations or where the metallic conductor was too small or too deep to give a large anomaly.

The other fact to come out of the field work is that for both the apparent metal factors and the apparent resistivities, the two dimension method of plotting the data is superior to the usual one dimensional plotting of apparent resistivities from lateral and vertical profiling. The two dimensional plot permits the detection of trends in the apparent resistivities that would be missed by single line measurements. This success justifies a further study of the resistivity maps gotten from simple geometries for the resistivity in the ground.

5.2 Vertical Interfaces

However, there is very little information available on the potential field from a single pole of current for instance. Almost all of the data that have been published, both theoretical and experimental, is for the Wenner electrode spreads. Recently though, the journal "Geophysical Prospecting" has published curves compiled by Schlumberger for the instantaneous first derivative and the potential

in a horizontally layered media. Even then, as discussed in section 2.3, only a few theoretical cases have been solved. For those cases, a consideration of the field from several sender locations would give enough data to plot some two dimensional maps. The most completely studied problem is for horizontal layers and we have seen that this case gives rise to horizontal contours. Another problem that can be solved exactly but that has not been completely covered in the literature is that of vertical interfaces and vertical layers. Logn. (1954) has shown that the problem is exactly analogous to the treatment of horizontal layers which was first discussed by Stefanescu, (1930). However, in his treatment Logn uses the method of images which is inexact, and also solves the problem only for very thin layers. The exact treatment of the general case is possible and will be demonstrated below.

The problem to be solved is that demonstrated in Fig. 18 where current is applied at the surface of the ground, which is the (YZ) plane in a system of rectangular coordinates. Since the air is an insulator, no current will flow across the surface. What we are seeking is the potential U everywhere in the half space when a current I is applied to the surface. If we use the Z axis and the axis of rotation of a circular cylindrical system and ν as the cylindrical radius then

$$\nu^2 = x^2 + y^2.$$

If we consider the problem in which all the resistivities in the ground are mirrored above the surface and in which a current

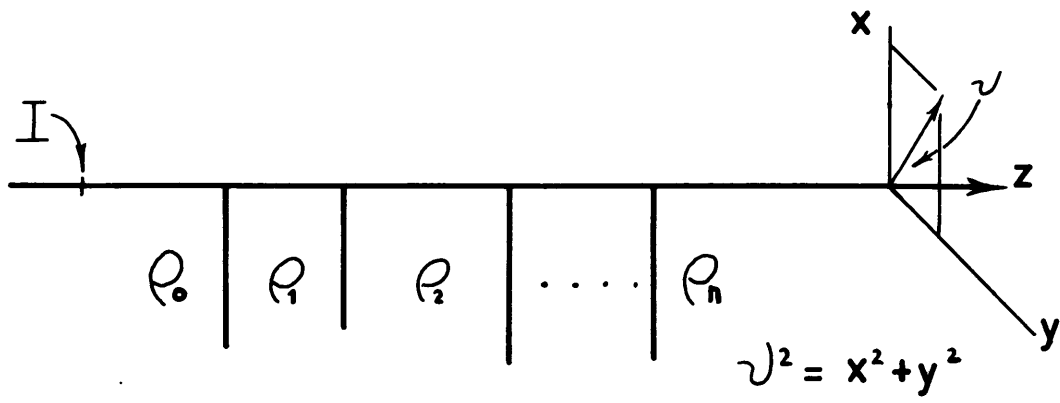


Fig.18

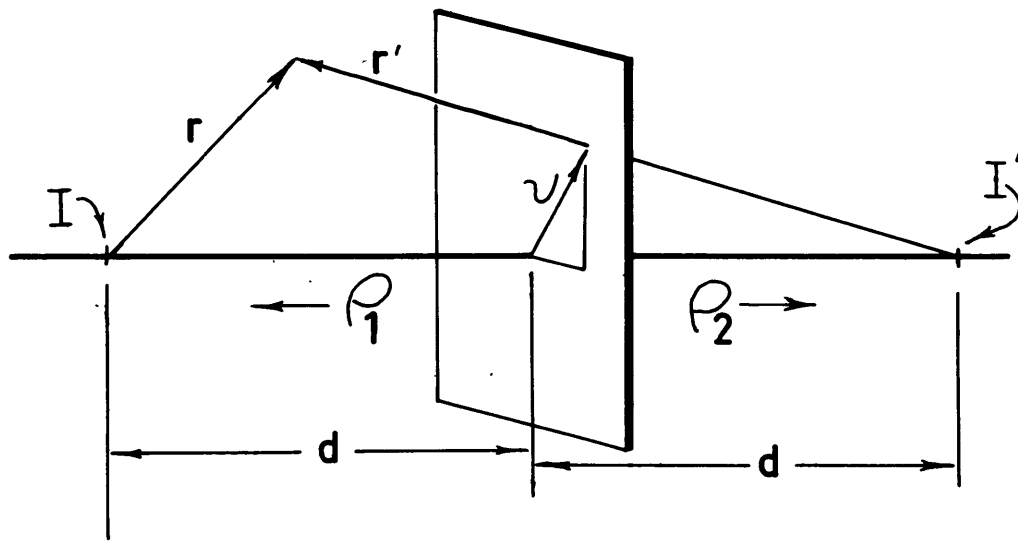


Fig.19

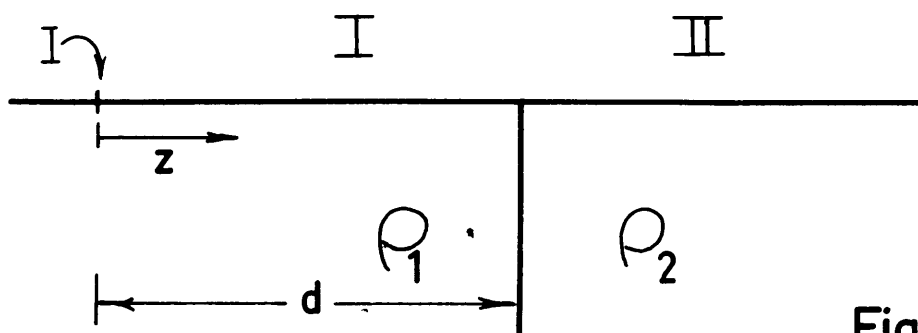


Fig.20

2I is applied at the same point, we see that in this case also, no current will flow across the YZ plane and furthermore, that the potential U will be exactly the same in both cases. We now have a problem that fits into a coordinate system which is separable. All of the theoretical resistivity problems thus far solved have been done in this way. The geometry must be such that a mirroring in the surface makes the surfaces of discontinuous resistivity coincide with the constant coordinate surfaces in some separable coordinate system.

5.2a The simplest problem is the one of a single discontinuity of resistivity and has been solved in many ways. The easiest is, I think, the method of images. In Fig. 19 if the current is applied a distance from the interface, we consider the image point at I' and r and r' the distances from the source and the image. By assuming a form for U given by

$$U_1 = Q \left(\frac{1}{r} + \frac{M}{r'} \right) \quad \text{for } 0 \leq z \leq d$$

$$U_2 = Q \frac{s}{r} \quad \text{for } z > d$$

where, as shown by Sunde (1949) on page 20 the term Q is equal to $\frac{\rho I}{4 \pi}$ for the whole space problem. By satisfying the conditions of continuous potential and normal current flow at the boundary we can arrive at the following for the potentials.

$$U_1 = \frac{\rho I}{4 \pi} \left[\frac{1}{\sqrt{z^2 + v^2}} + \frac{\rho_2 - \rho_1}{\rho_2 + \rho_1} \frac{1}{\sqrt{(2d - z)^2 + v^2}} \right]$$

$$U_2 = \frac{\rho I}{4 \pi} \left[\frac{2 \rho_2}{\rho_2 + \rho_1} \frac{1}{\sqrt{z^2 + v^2}} \right]$$

These expressions hold when the current source is on the left of the interface and the potential is measured always to the right of the current source in the diagram of Fig. 19.

Now, in the case where we are interested in resistivity measurements on the surface of the earth, we consider the case for $v = 0$ and $Q = \frac{\rho I}{2 \pi}$. Furthermore, we are going to calculate all of our apparent resistivities for the pole-dipole spread where the dipole is 1 unit long and the nearest electrode is z units from the pole. The dipole measurement is then made from station (z) to station ($z + 1$). The geometry is shown in Fig. 20. By taking the difference of the appropriate potentials and multiplying by the factor $\frac{2 \pi}{I \rho_1} [z(z + 1)]$ we can then calculate

the following expressions for the normalized apparent resistivities.

For the sender in region I

$$\frac{\rho_a}{\rho_1} = 1 - \left(\frac{\rho_2/\rho_1 - 1}{\rho_2/\rho_1 + 1} \right) \frac{z/d \cdot (z+1)/d}{(2 - z/d)(z - z'/d)}$$

For

$$0 < z \leq d$$

$$\rho_a/\rho_1 = 2 \frac{\rho_2/\rho_1}{\rho_2/\rho_1 + 1}$$

For

$$z \geq d$$

For the sender in region II

$$\rho_a/\rho_1 = \rho_2/\rho_1 \left[1 - \frac{\rho_2/\rho_1 - 1}{\rho_2/\rho_1 + 1} \frac{z/d \cdot (z+1)/d}{(z+z/d)(z+z'/d)} \right]$$

For

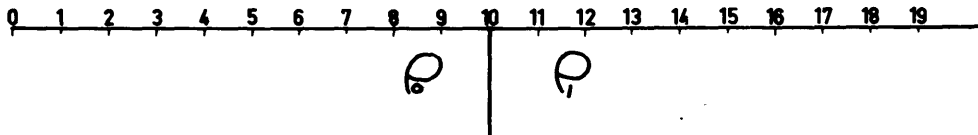
$$z \geq 0$$

One case was calculated using these expressions and the data are shown in figures 21, 22 and 23. Fig. 21 is the apparent resistivity map using the potentials while figures 22 and 23 were calculated using the above expressions for the normalized apparent resistivities from the pole-dipole measurement.

The potential data are quite smooth, increasing from a value of (1) to a constant value of (1.9) when the sender and receiver are astraddle the contact and then as the sender passes over the interface the values gradually build up to (18) which is, of course, the true resistivity in region II.

The first derivative measurements are quite different because they are not as smooth. In Fig. 22, when we are going from a conducting region to a more resistive one, the apparent resistivities decrease

VERTICAL INTERFACE APPARENT RESISTIVITY MAPS



Pole Receiver $\rho_0 = 1 ; \rho_1 = 18$

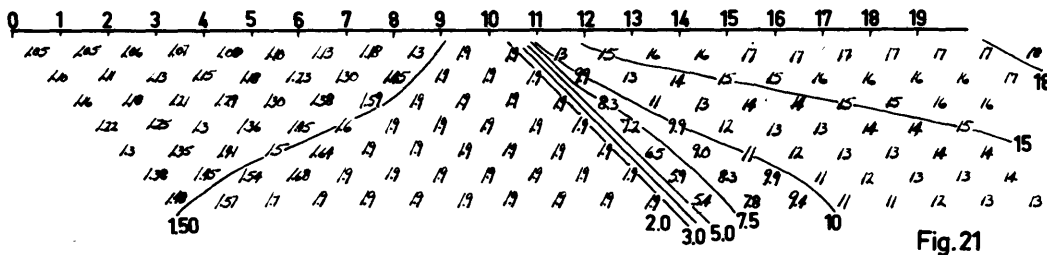


Fig.21

Dipole Receiver $\rho_0 = 1 ; \rho_1 = 18$

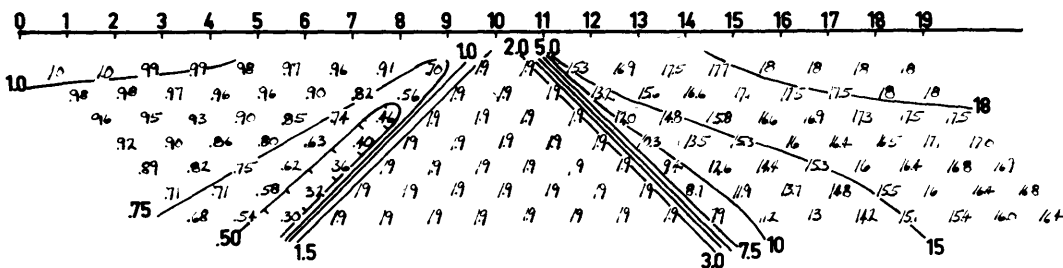


Fig.22

Dipole Receiver $\rho_0 = 1 ; \rho_1 = \frac{1}{18} = .056$

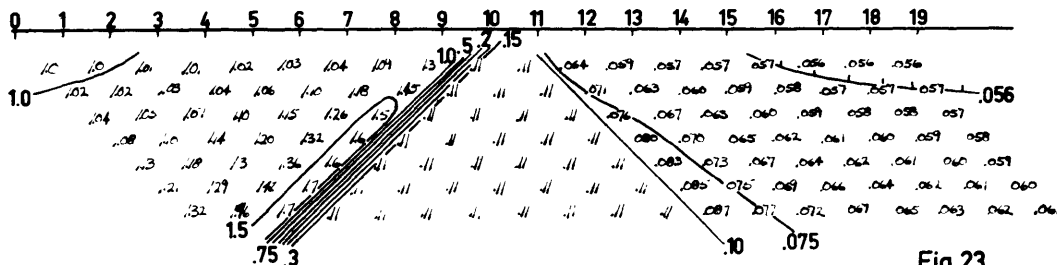


Fig.23

in value as the sender approaches the interface with a low value of (.3) which is much lower than any true resistivity in the ground. We then have on the contour map a triangular region of constant resistivities corresponding to the readings when the pole and dipole are astraddle the interface. The values then return, more quickly than for the pole-pole, to the value of (18).

The case in Fig. 23, when we are going from the resistive region into the conducting is exactly the opposite of Fig. 22. As we approach the conducting zone, the apparent resistivity increases to a value of (1.7) and then the values become constant when the interface is between the sender and receiver.

In fact, the last half of all three maps looks very similar for the pole-pole and the pole-dipole configurations. The apparent resistivity maps get very rough when the dipole receiver passes over the region of changing resistivity, but when the pole passes over the anomalous regions the readings are smooth regardless of what kind of receiver we have. If another differentiation were performed on the data, we would have two areas where the data varied quickly; one when the dipole receiver passed over the contact and one when the dipole sender was in the region of the interface.

In section 4, 4 field maps were shown of two lines that were interpreted from the induced polarization data as running over the edge of a porphyry copper deposit. This situation could be approximated

by the geometry of Fig. 22 and if we compare it with the right hand part of the apparent resistivity maps in figures 16 and 17, we can see if this theoretical map strengthens the original interpretation.

On line A. H. the region between stations 18 and 30 duplicates exactly the contour map on Fig. 22. The three main regions of a very narrow low at 45° with a triangular region of constant values followed by an increase in the apparent resistivity are all present on the map of the A. H. line in Fig. 17. As a matter of fact, the values of (4, 2; 25 and 150-200) are just about ten times the values on the calculated map. The great similarity makes the interpretation that a resistivity change of about 18/1 takes place at station 24 on line A. N. quite definite.

The region between stations 20 and 31 on Fig. 16 is also very similar to the theoretical map in Fig. 22. The three features are again present on this field map, although not as clearly defined as on the other. In this case, the vertical interface would be picked at station 26.

If the interpreted location of the interface is joined on a plan map of the two lines, which intersect very close to these points, the strike of the interface is roughly at right angles to line A. H. while it intersects line W. A. at a much shallower angle. This fact probably explains the fact that the contour features on line A. H. are much more distinct and sharp than on line W. A.

In section 4.4 when we were discussing the field maps on

Figures 15, 16 and 17, we noted that since the apparent resistivity decreased with sender and receiver separation while the apparent metal factors increased that the mineralization must increase with depth. If this is true, the simple geometry assumed here isn't exactly correct; however, since the theoretical results compare so well with the field results it must be true, in this case at least, that a surface layer over the vertical contact doesn't change the general shape of the contours. This is probably a good assumption if the surface layer isn't much more conductive or much more resistive than the rocks underneath. The influence of the surface layer is best seen in the triangular region. On the theoretical map, the values in this region are constant while on the field maps the contours form the triangular region, but there is still a decrease of apparent resistivity with separation.

Because the induced polarization effect can be looked at as being a resistance problem, theoretical apparent metal factor maps could be calculated. This is done by calculating two apparent resistivity maps with different contrasts; if the absolute resistivity of the background is assumed to be the same for both cases, we then have the case where the resistivity for D. C. current flow and the other is the resistivity for A. C. current flow, we can then give the resistivity of the background a resistivity in ohm-feet and then calculate the metal factor of the anomalous zone as well as the apparent metal factors from the two apparent resistivity maps.

This was not done in this case though, because a glance at the theoretical map gives a clear picture of what would happen. On the extreme left we would get a constant apparent metal factor that would be equal to the true metal factor in region I. As the interface was approached the value would increase to a maximum value in the area of the low trough as the resistivity map. There would be a region of constant metal factors when the interface was between sender and receiver and then as the sender passed over the interface the apparent metal factor values would go to zero, the true metal factor in region II. This general description compares very well with what happens to the apparent metal factor contours on the field maps.

5.2b The next most complicated problem that can be considered is for two interfaces with resistivities in the layers of ρ_1, ρ_2, ρ_3 . This problem was considered by Logn (1954) and solved partially, but I will include all of the derivation here for completeness.

We will consider that the geometry is as shown in Fig. 18 except that here we shall use (r) as the cylindrical radius and (R) as the distance between any two points. We will consider that the current is applied in one of the regions and that we want to determine the potential in all of the vertical layers. We have seen that if we use $\frac{\rho I}{2\pi}$ for our source term that we can consider the half space problem in the same way as the whole space problem.

In the layers where there is no source the potential must be a solution of Laplace's equation. In the layer with the source, we must add to the solution of Laplace's equation a function that has a singularity at the source, in all of the following the source is considered to be at the origin. From potential theory we know that this singularity must be of the order of $(\frac{1}{R})$ where (R) is the distance from the origin, (Morse and Feshbach, Chapter VII).

We can set up Laplace's equation in cylindrical coordinates and separate it to find the required eigenfunctions. Since by symmetry we can have no dependence on the polar angle our solutions must be combinations of the functions $e^{\pm\lambda z} J_0(\lambda r)$. We can also get a representation of our source term $\frac{1}{R}$ in terms of these same eigenfunctions.

It is

$$\frac{1}{R} = \int_0^{\infty} e^{-\lambda|z|} J_0(\lambda r) d\lambda = \frac{1}{\sqrt{z^2 + r^2}}$$

(Morse and Feshbach, Chapter X)

The boundary conditions that must be imposed on our solutions of Laplace's equation are that the normal flow of current across each boundary and the value of the potential at each boundary be continuous. There can be no current flow across the surface of the ground, but we know that in the whole space problem, we are considering that this is assured by symmetry. Finally, the potential must remain finite everywhere, except at the source. (Stratton, pages 163 and 483). As discussed previously, our source Q will be located at the origin and will be of a strength $Q = \frac{\rho I}{2\pi}$ where the resistivity ρ is that of

the region in which the source is located.

The general solution in the n^{th} layer takes the form,

$$U_n(r, z) = Q \int_0^\infty \left[f_n(\lambda) e^{+\lambda z} + g_n(\lambda) e^{-\lambda z} \right] J_0(\lambda r) d\lambda$$

where the f 's and the g 's are arbitrary functions of (λ) . The integration is over the whole range of (λ) since the integral expression is a solution of Laplace's equation for any value of (λ) .

The complete problem may be broken into the consideration of three cases; i. e. , the cases when the source is in each of the three layers, regions (I, II, III) as shown in Figures 24 and 25. In Appendix A, the exact expressions for each of the potentials for the three locations of the source are derived in a straightforward manner for the three layers having resistivities (ρ_1, ρ_2, ρ_3) respectively.

However, we are only going to consider the simplest case here, the case of a vertical dike in an otherwise uniform half space. In the expressions in Appendix A we have only to let $\rho_1 = \rho_3 = \rho_0$ to get the appropriate potentials. Because of the way the apparent resistivity maps are drawn we need only consider in each case the potentials which are used in calculating apparent resistivities for positive values of z , when the current is considered to be at the origin. Therefore, we need;

- a) for the sender in region I $U_{a1}; U_{a2}; U_{a3}$
- b) for the sender in region II $U_{b2}; U_{b3}$
- c) for the sender in region III U_{c3}

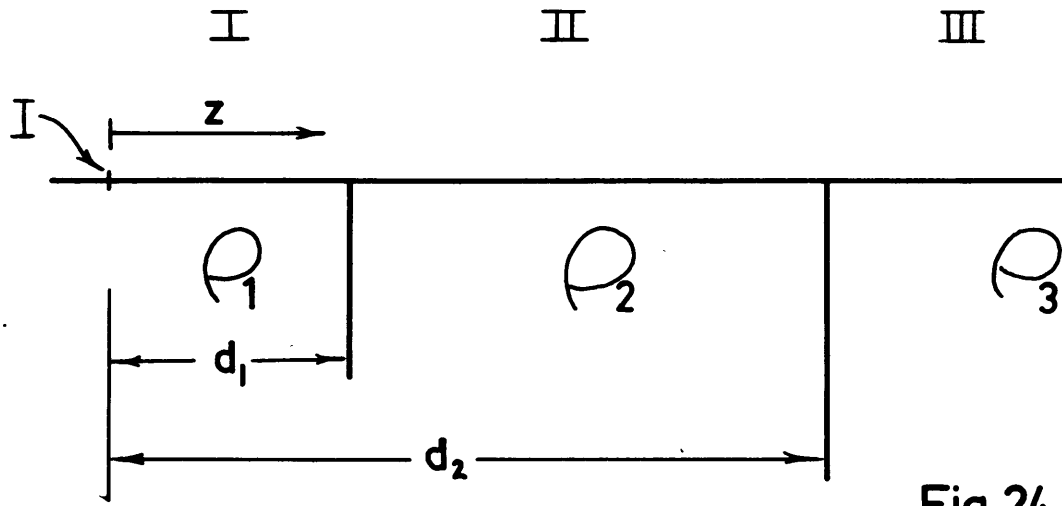


Fig.24

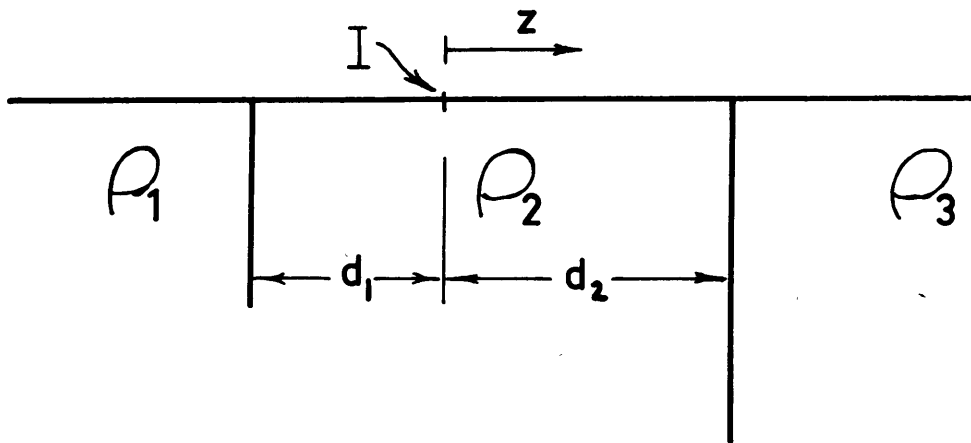


Fig.25

We have therefore, if $\rho_1 = \rho_3 = \rho_0$; $\rho_2 = \rho_2$ in the results of Appendix A,

$$K(\lambda, \tau) = 4 \rho_2 / \rho_0 \frac{1}{\left[1 - \rho_2 / \rho_0\right]^2} \frac{1}{\left[\frac{1 + \rho_2 / \rho_0}{1 - \rho_2 / \rho_0}\right]^2 - e^{-2\lambda\tau}}$$

$$= 4 \rho_2 / \rho_0 \frac{1}{\left[1 - \rho_2 / \rho_0\right]^2} \frac{1}{D - e^{-2\lambda\tau}}$$

where

$$\sqrt{D} = \left[\frac{1 + \rho_2 / \rho_0}{1 - \rho_2 / \rho_0} \right]$$

Finally, since we are making our measurements on the surface of the ground along a line that is at right angles to the strike we can set $r = 0$ in all of the expressions. Since $J_0(0) = 1$ the Bessel functions will drop out and we have left only the integral of exponentials in (λ) . Using these substitutions, we may write our potentials in the following way.

$$U_{a1} = \frac{I \rho_0}{2\pi} \int_0^\alpha \left[\sqrt{D} (\sqrt{D}-1) \frac{e^{-\lambda(2d_1-z)}}{D - e^{-2\lambda\tau}} - e^{-\lambda(2d_1-z)} + (\sqrt{D}-1) \frac{e^{-\lambda(2d_2-z)}}{D - e^{-2\lambda\tau}} + e^{-\lambda|z|} \right] d\lambda$$

$$U_{a2} = \frac{I \rho_0}{2\pi} \int_0^\alpha \left[\sqrt{D} (\sqrt{D}-1) \frac{e^{-\lambda z}}{D - e^{-2\lambda\tau}} + (\sqrt{D}-1) \frac{e^{-\lambda(2d_2-z)}}{D - e^{-2\lambda\tau}} \right] d\lambda$$

$$U_{a3} = \frac{I \rho_0}{2\pi} \int_0^\alpha \left[D-1 \right] \frac{e^{-\lambda z}}{D - e^{-2\lambda\tau}} d\lambda$$

$$U_{b2} = \frac{I P_2}{2 \pi} \int_0^\alpha \left[\sqrt{D} \frac{e^{-\lambda(z d_2 - z)}}{D - e^{-2\lambda\tau}} + \frac{e^{-\lambda(2\tau - z)}}{D - e^{-2\lambda\tau}} + \frac{e^{-\lambda(2\tau + z)}}{D - e^{-2\lambda\tau}} \right. \\ \left. + \sqrt{D} \frac{e^{-\lambda(2d_1 + z)}}{D - e^{-2\lambda\tau}} + e^{-\lambda|z|} \right] d\lambda$$

$$U_{b3} = \frac{I P_2}{2 \pi} \int_0^\alpha \left[\sqrt{D} \frac{e^{-\lambda z}}{D - e^{-2\lambda\tau}} + \frac{e^{-\lambda(2\tau + z)}}{D - e^{-2\lambda\tau}} + (\sqrt{D} + 1) \frac{e^{-\lambda(2d_1 + z)}}{D - e^{-2\lambda\tau}} + e^{-\lambda|z|} \right] d\lambda$$

$$U_{c3} = \frac{I P_0}{2 \pi} \int_0^\alpha \left[e^{-\lambda|z|} - e^{-\lambda[2d_2 + z]} + \left[\sqrt{D}(\sqrt{D} - 1) \right] \frac{e^{-\lambda(2d_2 + z)}}{D - e^{-2\lambda\tau}} \right. \\ \left. + (\sqrt{D} - 1) \frac{e^{-\lambda(2d_1 + z)}}{D - e^{-2\lambda\tau}} \right] d\lambda$$

The geometry for these is the same as Figures 24 and 25 if $P_1 = P_2 = P_0$.

A check of each term of each integral expression will reveal that in the region of (z) where they are defined each of the potentials can be put in the form;

$$\int_0^\alpha \frac{e^{-\lambda\theta}}{D - e^{-2\lambda\tau}} d\lambda$$

where τ and θ are positive constants.

The simple change of variable $\chi = e^{-\lambda \theta}$ transforms the integral into the finite one,

$$\frac{1}{\theta} \int_0^1 \frac{d\chi}{D - \chi \frac{2\tau}{\theta}}$$

Considered as a function of the values of D and $\frac{2\tau}{\theta}$, this integral will henceforth be designated as $G(D; \frac{2\tau}{\theta})$.

That is to say,

$$G(D; a)$$

For any given value of D and (a) the value of this integral can be determined as accurately as desired by numerical methods. Since the constant D contains all of the information about the resistivities it will remain constant for any given case being considered. The factor (a) will change as the location of sender and receiver points is moved along the line.

If we put the expression for the potentials in this form, we will have;

$$U_{a_1} = \frac{I\rho_0}{2\pi} \left\{ \frac{1}{2d_1 - z} \left[\sqrt{D}(\sqrt{D}-1) G\left(D; \frac{2\tau}{2d_1 - z}\right) - 1 \right] + \frac{\sqrt{D}-1}{2d_2 - z} G\left(D; \frac{2\tau}{2d_2 - z}\right) + \frac{1}{|z|} \right\}$$

$$U_{a_2} = \frac{I\rho_0}{2\pi} \left\{ \frac{\sqrt{D}(\sqrt{D}-1)}{z} G\left(D; \frac{2\tau}{z}\right) + \frac{(\sqrt{D}-1)}{2d_2 - z} G\left(D; \frac{2\tau}{2d_2 - z}\right) \right\}$$

$$U_{a3} = \frac{I P_0}{2 \pi} \left\{ \frac{(D-1)}{z} G \left(D; \frac{2 \tau}{z} \right) \right\}$$

$$U_{b2} = \frac{I P_2}{2 \pi} \left\{ \frac{1}{|z|} + \frac{\sqrt{D}}{2d_2 - z} G \left(D; \frac{2 \tau}{2d_2 - z} \right) + \frac{1}{2\tau - z} G \left(D; \frac{2 \tau}{2\tau - z} \right) \right. \\ \left. + \frac{1}{2\tau + z} G \left(D; \frac{2 \tau}{2\tau + z} \right) + \left(\frac{\sqrt{D}}{2d_1 + z} \right) G \left(D; \frac{2 \tau}{2d_1 + z} \right) \right\}$$

$$U_{b3} = \frac{I P_2}{2 \pi} \left\{ \frac{1}{|z|} \frac{\sqrt{D}}{z} G \left(D; \frac{2 \tau}{z} \right) + \frac{1}{2\tau + z} G \left(D; \frac{2 \tau}{2\tau + z} \right) \right. \\ \left. + \frac{(1 + \sqrt{D})}{(2d_1 + z)} G \left(D; \frac{2 \tau}{2d_1 + z} \right) \right\}$$

$$U_{c3} = \frac{I P_0}{2 \pi} \left\{ \frac{1}{2d_2 + z} \left[\sqrt{D} (\sqrt{D} - 1) G \left(D; \frac{2 \tau}{2d_2 + z} \right) - 1 \right] \right. \\ \left. + \frac{(\sqrt{D} - 1)}{2d_1 + z} G \left(D; \frac{2 \tau}{2d_1 + z} \right) + \frac{1}{|z|} \right\}$$

An investigation of what typical values of the variable (a) might be in any resistivity geometry being studied reveals that even for very thin dikes, as small as .05 of the length of the dipole receiver, (a) never gets less than .01 for the range of z needed to get the complete resistivity pattern. For infinitely thin dikes, the values of (a) get smaller than this, but in this case, an approximate treatment

such as Logn's will give good results. As (a) gets large, we can see that $G(D;a) \longrightarrow 1/D$ very rapidly. For values of $a = 10$ the integral already has an almost constant value. Therefore, we can assume that values of $G(D;a)$ for $.01 \leq a < 10$ are about all that we will ever need in practice to determine the apparent resistivities for the vertical dike problem.

Some statements can also be made about the general case. The expressions for the potentials derived in Appendix A for $\rho_1 \neq \rho_3$ can also be put in terms of $G(C;b)$. In this case, the value of C depends upon all three of the resistivities but the range of values is much the same as in the dike problem. A little work has been done on the case of four vertical layers and it appears that the same kind of integral can be used to evaluate the potentials obtained in this case also.

It appears then that the problem of vertical layers will be completely solved if we have a tabulation of the values of $G(D;a)$ for various ranges of D and (a) . The integral can be evaluated simply by use of Simpson's rule or some other numerical integration procedure. The integral was first evaluated using a desk calculator for 7 values of D with values of the variable (a) from .02-2.0 using Simpson's rule. Five divisions were used in evaluating the integral. Recently, the integral was evaluated by N. Ness of the M. I. T. Geophysics Department using the IBM 650 digital computer. He evaluated in all 27 cases for various values of D . For each value of D he has calculated the

value of the integral at 10 values of (a) from .01-10. He also used Simpson's rule but with 10 divisions of the integrand. His results are therefore more accurate than the hand calculated ones; however, in the one case common to both tables, the hand calculated results agreed to within 1% with the machine results. Tables I and II in Appendix B contain the results of both calculations. In Appendix B also is a list of the values of D and the corresponding ratio of which gives that value of D for the case of the vertical dike in a homogeneous half space. It is interesting to note that the value of D is independent of whether the ratio

$$\rho_a/\rho_0 = x/1 \text{ or } \rho_2/\rho_0 = 1/x$$

i. e. , whether the resistivity of the dike is x times larger or x times smaller than the background resistivity.

Among other things, this means that if our dipole receiver is on the other side of the dike from the sender, it will measure the same potential if the dike is more resistive than the country rock as it would if the dike were more conducting. This is because the potential U_{a3} depends only on the factor D. A closer look at the potential U_{a3} shows that it depends only on the thickness of the dike (τ) and the distance from the source z. Therefore, it is impossible to tell from the potentials on the other side of the dike just where it

is between the sender and receiver. This is analogous to the one interface problem in which the potential in the second medium is independent of the location of the interface as long as it is between the sender and receiver.

As a matter of fact, a general statement about this can be made after a study of the potentials for the vertical dike. In the form in which they are written, each potential depends upon z , the distance from the source; \mathcal{T} , the thickness of the dike; and the distance from the source point to the interfaces not between the sender and receiver. The distances to the interfaces between the measuring point and the source do not appear explicitly in the expression. Their only effect is through the thickness \mathcal{T} .

Using the calculated values of the integral the case of a dike 3 units wide with a resistivity contrast of 1/18 and 18/1 was calculated and plotted for two sender and receiver combinations. Since the formal expressions give the potential itself the apparent resistivity maps for the pole-pole spread can be drawn. From the pole-pole potentials, the potentials for a one unit dipole receiver were obtained by subtraction and a pole-dipole apparent resistivity map drawn. The curve of $G(1, 25; a)$ is shown on Fig. 26 and was used to make the calculations. The apparent resistivity maps are shown in the Figures 27-30.

The first case studied was for $\rho_2/\rho_0 = 1/18$. The dike was three units thick and located between stations 10-1/2 and 13-1/2.

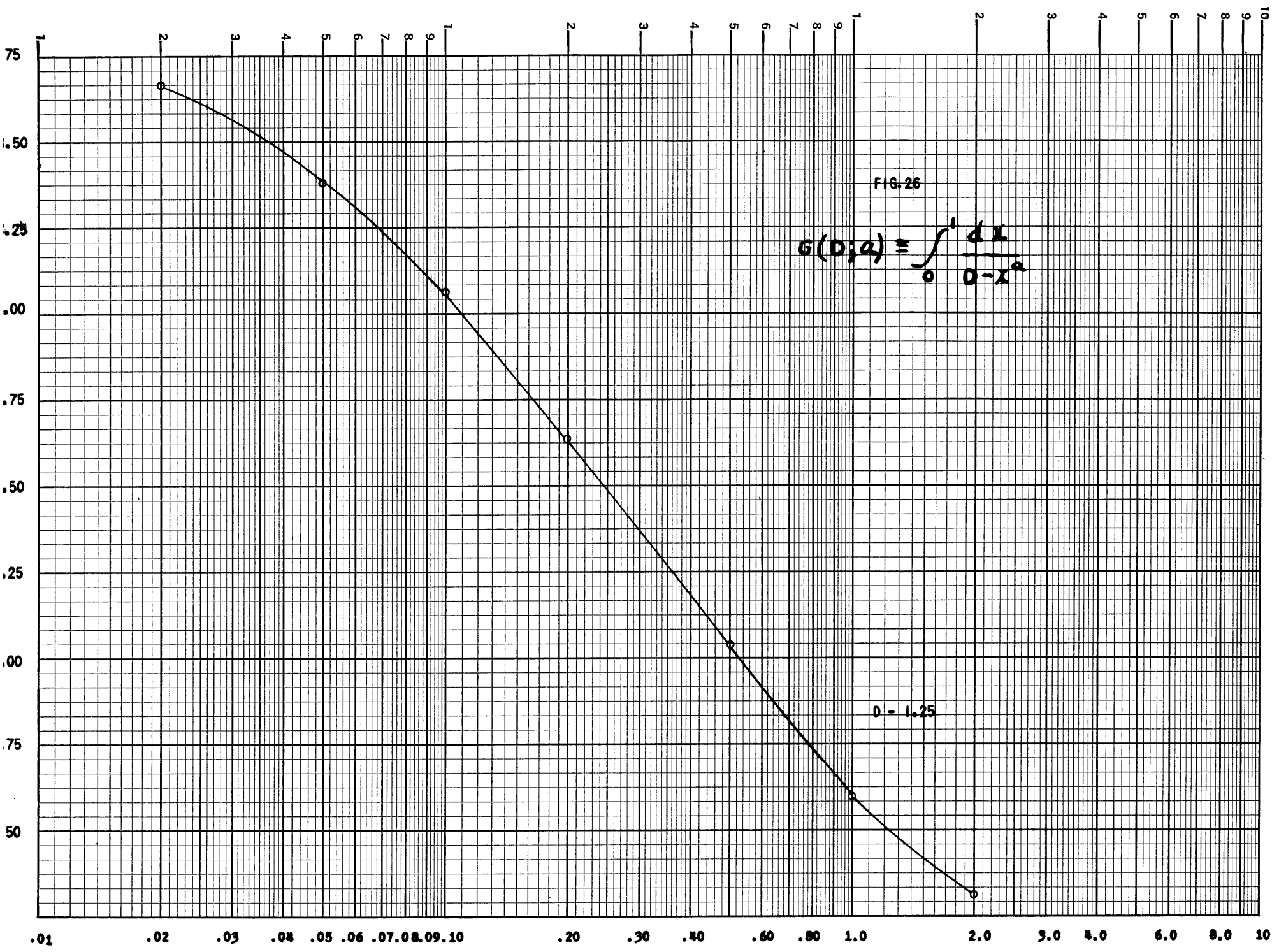


FIG. 26

$$G(D; a) = \int_0^1 \frac{dx}{D-x^a}$$

D = 1.25

APPARENT RESISTIVITY MAPS
for
ONE VERTICAL LAYER

$$\frac{\rho_2}{\rho_1} = \frac{1}{18} = .056$$

ρ_a from Potentials

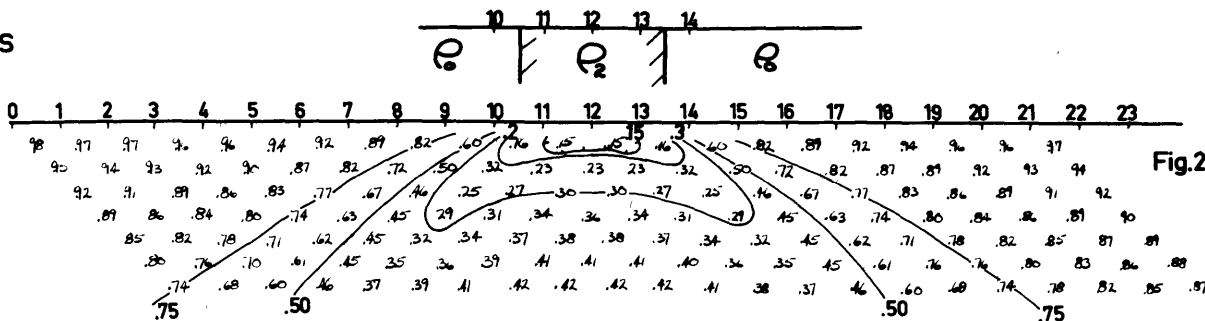


Fig.27

$$\frac{\rho_2}{\rho_1} = \frac{1}{18} = .056$$

ρ_a from 1st Differences
in Potential

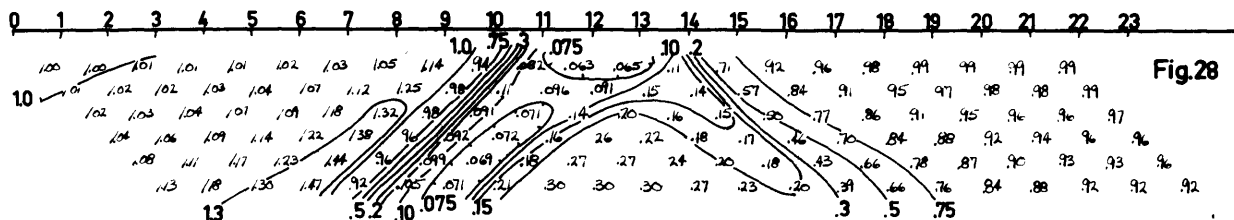


Fig.28

$$\frac{\rho_2}{\rho_1} = \frac{18}{1}$$

ρ_a from Potentials

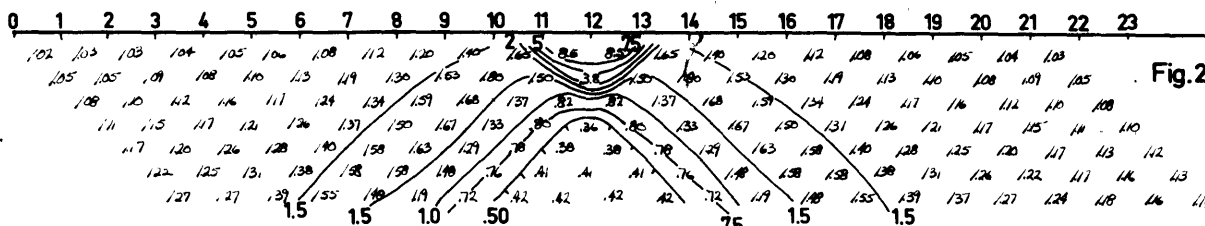


Fig.29

$$\frac{\rho_2}{\rho_1} = \frac{18}{1}$$

ρ_a from 1st Differences
in Potentials

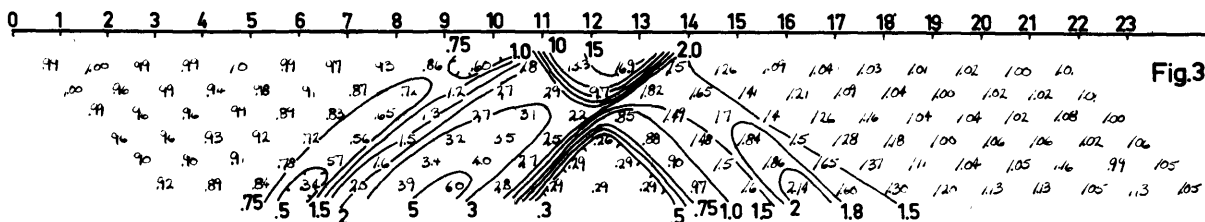


Fig.30

The apparent resistivities from the calculated potentials are shown on Fig. 27. The contours are quite smooth with a low zone when the sender and receiver are both in the conducting zone. The values when the sender and receiver are astraddle the dike depend only upon the separation. This gives rise to a triangular zone in which values along a horizontal line are constant; however, the values have little variation so that no contours are present in this region. In general, the values go from 1.0 on the left to the low of .15 and then back to 1.0 on the right. The lowest value of .15 is three times the true value of the resistivity in the dike.

The second map, Fig. 28, is gotten from the first by taking the first differences of the potentials and then calculating the apparent resistivities. As usual, the first derivative map has a much rougher appearance. The maximum low, when the sender and receiver are both in the dike, is much closer to the true value of the resistivity in the dike. There is another low associated with all receivers in the dike and a lesser one when the pole sender is in the dike. As in the case of one interface there is an increase of apparent resistivity just before the receiver gets to the conducting dike.

Fig. 29 is the map for the apparent resistivities when the potentials are calculated for a resistive dike. In this case, it has a resistivity of 18 times that of the background. Here, we have a high of 8.5 when the sender pole and receiver pole are both in the dike.

This is less than $1/2$ the true resistivity of the dike. Below the high contours is the triangular region for the values when the sender and receiver are astraddle the dike. These are the same values as in Fig. 27 but on this map, they appear as a low. The rest of the contours are quite smooth.

Again, the first derivative map in Fig. 30 has many more contours than the potential map. It is a general property of these derivative maps that the variations in apparent resistivity are larger than the potential apparent resistivity maps, but that the variations take place in a smaller portion of the map. This means that the derivative maps have more contours and that they are crowded into a smaller space.

Fig. 30 has more contour features than the other. The high of 16.9 when the sender and receiver are both in the dike is much closer to the true value than is the corresponding map when the apparent resistivities are calculated from the potentials. Immediately under the high zone, there is the familiar triangular low region when the sender and receiver are on opposite sides of the dike. There is also a high associated with every receiver position in the dike and a high zone of smaller value when the sender is in the resistive zone. Finally, there are low values of apparent resistivity for the receiver positions just in front of the resistive dike.

In section 4.4 we discussed Fig. 15 which was a portion of a

line done over a porphyry copper ore zone. I said then that a drill hole between stations 6 and 7 on line W. A. was out of the ore zone and was the last hole drilled along the line. If the section of the apparent resistivity map of line W. A. between station 3 and station 10 is compared with Fig. 30 the reason for the blank drill hole can be seen. The apparent resistivity map of this part of line W. A. is very similar to that of a vertical resistive dike. The three features of the map in Fig. 30 are all present in this part of line W. A. The high apparent resistivities for short separations over a triangular region of low values for large separations and the more localized low associated with one receiver position are all present on both contour maps. In the field case also, the resistive zone seems to be about 300 feet wide.

The fact that the apparent metal factors build up again to high values on the other side of the blank zone is further indication that the reason for the high apparent resistivities and low apparent metal factors is a vertical zone, about 300 feet wide, that has less mineralization than the surrounding rock.

Another important thing that this interpretation tells us about the zone under station 6, is that it is different in character from the other resistivity highs along lines W. A. and A. H. There are other places along the lines where comparatively high apparent resistivities were measured for small separations. The contours

in these regions though had none of the characteristics of the map for a vertical dike. The region under station 6 is then a blank zone with some depth while the others are apparently shallow surface features of less mineralization.

5.3 Usefulness of the Vertical Layering Solutions

The usefulness of the solutions derived in Section 5.2 depends upon how they are used. Theoretically, of course, the resistivities in any vertical layering geometry could be measured by taking measurements with small enough spreads in each zone. Practically though this is a useless procedure. First of all, if any kind of cover of soil or weathering is present, the whole surface of the ground will appear much the same and therefore there will be no indication of where to begin the small scale measurements. The second objection to this plan is the most important. With very small spreads, there will be the problem of small local surface variations in resistivity. If a thin surface layer is present, very small scale measurements will not be of much use in determining the geometry of the underlying rocks.

At best, a resistivity measurement is an averaging of the properties of various blocks of the ground, and if you try to make small scale measurements, you are not averaging anymore. You are investigating the properties of very small segments of the earth and on a small scale large variations are present. While the overall resistivity of a large block of the ground may be comparatively constant, there are

almost always variations of a smaller scale present and measurements of the same scale as these variations will not give a good indications of the average resistivity of the rock mass.

The question of cover, of course, also places a limitation on the usefulness of the theoretical work. A layer on top of the half space with vertical layers is a departure from the assumed geometry. If, however, the cover is of the same general resistivity as the layers and is not too thick, it will not alter the radial flow of current much. In this case, we might expect that the general features of the contour maps from the two cases would be similar. This was certainly true in the three field cases studied here in connection with the theoretical maps. The fact that the values of both metal factors and resistivities were changing with separation shows that some vertical variation was present. The contours though still have great similarity with the theoretical cases. The thinner the cover is in relation to the dimensions of the spread, the smaller the effect it will have. Thus, 10 feet of soil cover would greatly effect measurements using a dipole 20 feet long and with 20 feet between stations. At the same time, that much cover would not greatly alter measurements made on a 100 foot scale.

One quite valid criticism of the theoretical work is that it only gives the apparent resistivities along a line which is perpendicular to the strike of the resistivity discontinuities. For the case of the

single interface the calculations for a skew line are not much more difficult than those presented here. For the three layer case though the difficulties introduced by an angled line are more serious. The solution then involves an infinite integral with Bessel functions and exponents and could not be treated in the simple manner presented here. In the field this problem could be overcome by first determining the strike of the layering with two parallel lines and then gathering data on a third line that is normal to the strike. Again, the field results presented here demonstrate that the contours for lines not quite at right angles to the strike are only slightly different from those on the theoretically perpendicular line.

I'm sure, that even considering these limitations, that that calculation of theoretical apparent resistivity maps for the vertical layering problem can be of assistance in the interpretation of field results. A program has been written for the IBM 650 and N. Ness will soon have calculated resistivity maps for various resistivity contrasts and thicknesses of the dike. The tabulation of the values of $G(D;a)$ makes hand calculation of any particular problem of interest quite simple and quick so that any field map can be quickly compared with an assumed model.

5.4 Conduction in Anisotropic Layers

One perturbation on the general theory of conduction in layered media, both horizontal and vertical, is anisotropic conduction.

It is certainly not unreasonable to suppose that in a thinly bedded rock the conduction along the layers will be greater than the conduction across the layers. It is certainly true in a rock that is mineralized or graphitic along closely spaced planes. Several authors have mentioned anisotropy in papers on resistivity but always in a very general way. (Geneslay, 1939; Maillet, 1947; Mooney, 1954; Pirson, 1936 and 1948). After the derivation of the equations of conduction in transversely anisotropic media some statement is usually made about a change of scale in the anisotropic direction and then the solution is carried no further. The derivation of the exact integral expressions for the potentials in anisotropic layers, both horizontal and vertical, is not much more difficult than that outlined in Appendix A for homogeneous isotropic layers. In Appendix C I have included, in some detail, a discussion of the effect of anisotropic conduction in layers.

The general conclusions that can be drawn from the results in Appendix C are few. Apparently, in conduction in anisotropic rocks the correct conductivity dependence can be gotten from the corresponding potentials in the isotropic case by assigning an isotropic conductivity of $\sqrt{a} \sigma$ to the anisotropic zone; where (a) is the degree of anisotropy. In the simple two layer cases where there is only one boundary between the isotropic and anisotropic media the only other effect is a change of scale in the direction at right angles to the layering. This

change of scale, $[z' = \sqrt{\alpha} z]$, only occurs when the current is being applied in the anisotropic layer.

If more than one boundary is present however, the distance factors in the potential expressions are changed in an unsymmetric manner and no single statement can describe the whole effect. The problem becomes very complex and the interpretation correspondingly difficult.

VI. FURTHER EXACT RESULTS

6.1 The Need for Modelling Results

The possible geometries that can be solved theoretically have already been discussed. The problem of horizontal layers has been studied in the greatest detail and several references have been given. The work described in Section V and Appendices A and B makes the calculation of apparent resistivities for any vertical layering very straight forward. Few other useful geometries can be solved in the case when the earth's surface must be considered. The only problem that can be solved that could be of use in studying buried, finitely dimensioned resistivity contrasts is the buried sphere discussed by Van Nostrand (1953). He uses bi-polar coordinates for which solutions of Laplace's equation are necessarily complicated. Because of the symmetry of the Wenner spread he is able to derive partial results, but the kind of data we require for our two dimensional maps would involve long and tedious calculations for each case considered.

This brings us to the possibility of using an analogue computer to give us the desired surface potentials for certain resistivity geometries. In this case, the computer would simply be a scale model of the earth geometry for which the data are desired. There are two reasons why these data are needed.

First of all, exact data from known and controllable geometries is needed for comparison with results from some approximate methods.

These approximate methods are discussed thoroughly by K. Vozoff (1956) and I will repeat the major points in the next section of this thesis. The modelling results are needed so that a quantitative idea can be formed concerning the accuracy of the approximations. The data are also necessary in a study of the parameters effecting the approximation so that we can find out when the approximate calculations will give good results and when they are likely to be poor. A further discussion of these points will be given in chapter VII.

The second need for the modelling results is even more immediate. There is little doubt, after the field results reported here, that induced polarization measurements can be an important tool in prospecting for metallic minerals. It is particularly important because it gives good results in some mineralized areas where all other geophysical methods have given poor results or failed completely. Until some theoretical techniques are developed to aid in the interpretation of field measurements of induced polarization, or resistivity for that matter, experience will be the important factor in interpretations. Just about all of the experience available for interpreting this kind of induced polarization measurement is presented in Section IV. Several other lines of field measurements have been taken in these same areas but they add very little to the picture. One way to get results from geometries that are of interest is to construct the geometries in a

scale model and then take measurements in such a way that the most can be learned from data. A great deal of experience can be gained in a short time in this manner.

I have pointed out several times that since the metal factor is calculated from apparent resistivity values, an apparent metal factor map can be plotted from any two apparent resistivity maps. As a matter of fact, since the apparent metal factor depends on the value of $\rho_a/2\pi$ in ohm-feet, an infinite number of apparent metal factor maps can be constructed from two apparent resistivity maps. They are, of course, not independent though.

In the resistivity modelling, all of the resistivities can be normalized to the value for the background material. This simply means that we consider this material to have a resistivity of 1 in whatever units we want to use. The important thing is that the simulated ore zone has a resistivity of 1/10 or 1/20 or 1/100 of the simulated country rock. The apparent resistivity values gotten from surface measurements can then be used for comparison with any field case where the geometry and the resistivity contrast are the same as in the model. The apparent resistivity when plotted in this way is a dimensionless quantity that depend only on the geometry of the model and the contrast.

The apparent metal factor can not be made dimensionless

though because the value of $\rho/2\pi$ in ohm-feet appears explicitly in the calculation. Apparent metal factor maps can then be plotted from the modelling data only for specific cases. A value of $\rho/2\pi$ in ohm-feet must be assigned to the material representing the country rock. This fixes the resistivity of the ore zone for the models. Then two models are used with different contrasts, the model with the highest resistivity for the ore zone can be considered as being the D. C. case and the other the A. C. case. This fixes the values of the D. C. and A. C. resistivity of the ore zone and these two values are enough to determine the true metal factor for the ore zone under these assumptions. The apparent metal factor values can then be calculated and plotted using the two apparent resistivity maps and the assumed value of $\rho/2\pi$ for the country rock. By changing the value of $\rho/2\pi$ assigned to the country rock, we change the metal factor of the ore zone and the apparent metal factors measured on the surface.

Using the model, it has been possible to get enough maps so that for the first time some definite statements can be made about how the apparent metal factor anomalies are changed when the parameters of the ore zone are changed. Such things as the depth of the ore body, its attitude, its resistivity and its metal factor are all important in determining the size and shape of the surface anomaly. Since the only technique we have at present for interpreting these anomalies

is a sort of "curve fitting" it is important to have results from as many cases as possible.

6.2 Methods and Procedures

As in the case of the field equipment, I don't think that a detailed discussion of the equipment used in the modelling is necessary. As in all scale modelling, experimental errors and mistakes are best eliminated by practice and I think that a statement of the major pitfalls to be avoided would be of more use to future experimenters than a very detailed description of the particular equipment I used.

The equipment used in all of the modelling was the same. A current of 20 cps was used so that if the filtering of 60 cycle background and pickup became necessary it would not be difficult. As it turned out, grounding of all the equipment completely eliminated the pickup so that the background voltages measured were essentially zero. This is partially due to the fact that I used a battery operated V. T. V. M. for all of the potential measurements. The fact that the meter was portable eliminated any pickup that might arise from the connection with the A. C. supply in the lab. An A. C. ammeter was used for the current readings. The fact that the comparatively low frequency of the current might affect the reading of the ammeter was unimportant since a set current of 15 ma was used for all of the experiments.

An oscillator and a power amplifier were used as the current

source. They gave a very constant current themselves but the level of the output of the oscillator was changed by changes in the line voltage. A voltage regulator was used to regulate the line voltage and then the current applied to the model was steady over long periods of time. By removing the transformer a large distance from the location of the model the effect of its magnetic field was completely eliminated.

The first measurements were made on two dimensional models. A commercial conducting paper marketed by A. T. & T. was used. Contacts were made with very small nails that were driven into the paper. The contacts were greatly improved by applying a little silver paint around the nail where it entered the paper. Regions of the paper can be made more conducting by painting them with aquadag. Aquadag is a mixture of powdered graphite and water that is used as a conducting paint to assure or improve electrical contact. The desired shape of the geometry to be modelled was merely painted on the paper. Successive coats of aquadag each increased the surface conductivity of the paper in the region where they were applied.

There were three major problems in this work as well as in the later three dimensional modelling. They are,

- 1) The problem of accurate measurement

In this respect, field measurements are more accurate than

model results. In the field, a surveying error of two feet in one hundred produces an error that is completely neglectable. Since the resistivity maps are all contoured using logarithmic intervals a 2% error is completely lost. In the models though, where the station interval is 1/2 inch a slight error in placement of the electrodes could change the readings considerably. The electrodes themselves were of considerable size when compared with their separation and in this respect, the model measurements are really averages over the finite size of the electrodes. The error in placement of the electrodes is eliminated at least in the first approximation by comparing all readings to a blank, i. e. , the apparent resistivities are calculated not from the current, distance and voltage readings, but by comparing the voltage at a given point with the voltage obtained when the model did not contain any resistivity contrasts.

2) The problem of uniform background material.

Calculation of the apparent resistivities by comparison with the reading when no ore body is present in the model also partially eliminated this problem. However, if the conductivity of the material changes between the blank measurements and the measurements when the ore body is present errors are introduced. The conducting paper did not have a uniform surface resistivity but the voltages for the blank measurements were affected also, so that by comparing the

voltages the effect of the inhomogenities was eliminated from the apparent resistivity calculations. This is very close to being exact because as we shall see in the next chapter in the first approximation each region of resistivity contrast has an effect that is independent of other regions of resistivity contrast. Since the variations in the paper are small compared to the contrast simulated by the aquadag this assumption is probably upheld in this case.

A more serious matter was the fact that the paper changed resistivity as the humidity of the air varied. These variations, of course, introduced errors into the apparent resistivity calculations since the blank readings could no longer be considered constant. During the late fall and winter when the laboratory was artificially heated, the humidity was constant enough so that the same readings, to within $\pm 6\%$, were obtained with as much as two weeks between measurements. However, in the spring when the windows were open accurate measurements could no longer be taken because humidity changes from day to day created large variations in the resistivity of the paper.

3) The problem of determining the resistivity contrast.

This is probably the largest source of error in the two dimensional modelling. When a section of the paper is painted with aquadag there is no sure way of determining exactly how much the resistivity has been changed. I was able to get an estimate by painting two

squares of the conducting paper with aquadag at the same time I painted an anomalous region on the model. By comparing the surface resistance of the two squares before and after the application of the aquadag I was able to get an estimate of the contrast I had created in the model. Because the magnitude of the decrease depended upon the thickness and uniformity of the coat of aquadag applied, serious variations occurred. The two squares frequently differed by as much as 15 or 20%. The possible errors in the assumed contrast on the model were at least this much.

These same problems were found in the three dimensional modelling, although in some cases, the method of solution was different. The three dimensional modelling was done in the modelling tank belonging to the Department of Geology and Geophysics. It is a concrete tank that is 10 feet long, 6 feet wide and 4 feet deep. For the modelling I did I filled the tank with tap water. There is a wooden superstructure built over the tank that holds sliding rails. There are holders that fit onto the rails and by moving the holders along the rails and the rails along the superstructure, you can locate the holder over any point on the surface of the water in the tank. One of these holders was fitted with a set of electrodes that were mounted in such a way that they could be raised or lowered in the holder as a group. In this way the electrodes could be lowered until they were just touching the surface of the water. The electrodes were considered to be placed

at 1 unit intervals. In this case they were placed 1/2 inch in the holder.

There were sixteen electrodes in all in the spread. The first was used as a current electrode. The other current electrode was located in a far corner of the tank so that it was effectively at infinity. The other electrodes were used for measuring the potentials and were wired to a switching box so that any two electrodes could be connected across a voltmeter and potential difference between them measured. When the measurements were to begin, the electrodes were located with the current electrode at a known position. The voltage readings at each station were then taken. I modelled the pole-dipole configuration in the three dimensional modelling so I took the voltage difference between two consecutive potential electrodes in each case. The readings were taken in exactly the same way as the field measurements with the receiver moving away from the current electrode. When all of the receiving positions had been occupied the current electrode was moved up one station and the procedure repeated.

The ore body model in all of the experiments was 4" x 2" x 1/2". It thus represented an ore body that was 8 x 4 x 1 units in dimensions. Another holder was fitted with an attachment that held the ore body. It was adjustable so that the depth and the dip of the ore body could be varied. The strike of the long dimension of the ore body was variable too, although all of the measurements I made were with the long dimension of the ore body at right angles to the line of measurement.

The problem in the three dimensional modelling could be classified into the same groupings as those discussed previously in conjunction with the two dimensional modelling. They are,

1) The problem of measurement

The source of the errors here and the solution to the problem were exactly the same as in the two dimensional case. Before the ore body was put into the tank, I made a set of measurements for comparison. The fact that the same set of electrodes were used for all of the measurements made them somewhat more reliable than in the 2-D case. These blank readings were always the same regardless of where along the line the electrodes were located. This was verification of the fact that the remote electrode and the images created by the insulating walls of the tank were sufficiently removed to have no effect. The ore body was located in position in the tank very carefully each time, so that errors introduced by uncertainty in its location were kept at a minimum.

Another problem concerning the electrodes was the depth to which they extended into the water. Once the electrodes were set they remained at the same level throughout the measurements. They were only moved once throughout the whole sequence of experiments reported here. They were adjusted very carefully each time so that they were just touching the water surface. The rails on which the holder slide were constructed to be parallel with the water surface so that as the

holder moved along the slides, the electrodes remained in the same position relative to the water's surface. In this way, the depth to which they extended into the water was kept constant.

Because of evaporation and to keep the temperature in the tank constant, a small flow of water was run into the tank at all times when measurements weren't being made. The level was maintained by a standpipe in one corner of the tank. Before each set of measurements were taken the water flow was turned off. The surplus water ran off very quickly and the level quickly became that of the top of the standpipe. To assure a constant relationship between the electrodes and the final water level on each day, the surface tension at the edge of the standpipe was destroyed each time by putting a drop of detergent on the surface of the water. In this way I was sure that from one day to the next the coupling between the electrodes and the water surface was the same. This was important if comparisons between different sets of measurements were going to be made.

2) The problem of uniform background material

This problem was not so difficult in this case. The resistivity of the water was constant as long as its temperature didn't change. By continually running water in at the bottom and draining it off the top the temperature difference between the top and bottom of the tank was kept to less than 2° centigrade. Most of the measurements were made during the winter months so that the water was quite cold. The

temperature was 9° centigrade throughout most of the winter and was very constant from day to day. However, when the water was turned off to make a set of measurements, the water began to warm from the top. It takes about three hours to make a set of readings of 25 sending positions with 14 potential readings for each sender. In this time, the upper surface of the water warms enough to lower its resistance by about 4%. The usual procedure was to make two sets of blank readings, one before and one after each run. The average of these two readings was compared with the potential measurement when the ore body was present, to determine the apparent resistivity. Thus the readings were probably accurate to within 2%.

3) The problem of determining the resistivity contrast

In the three dimensional modelling, the accuracy to which the contrast was known was much better than for the two dimensional modelling. The modelling material for the ore body was in this case gelatine made with conducting solutions. The resistivity of the gelatine depended upon the resistivity of the CuSO_4 solution used and also the temperature at which the resistivity was measured. Since the temperature of the tank was the temperature at which the model measurements were made this was used. A pyrex tube about 30 inches long was used to determine the contrast. Its resistance was first measured when it was filled with water from the tank at the

temperature in the tank. The tube was then filled with gelatine at the same time that the ore body was poured. When sufficiently cool, the tube was hung in the tank until its temperature was the temperature of the water in the tank. Its resistance was then measured and in this way an accurate determination of the resistivity contrast was gotten. For any given solution, these measurements repeated themselves from day to day to the accuracy with which the meter could be read.

The problem of getting any given resistivity contrast was largely a matter of trial and error. The resistivity of the gelatine was always slightly higher than that of solution from which it was made. The resistivity of the gelatine increased by about 18% when it was cooled from room temperature (20°C) to the tank water temperature (9°C). It was therefore difficult to predict how concentrated a salt solution should be used to get a certain contrast in the model. I kept a record of all the values of resistivity for the solution and the resistivity of the gelatine made from that solution. The measurements were made with the solution at room temperature and the gelatine at the temperature of the tank water. In this way, I had a sort of calibration curve that was fairly accurate, but since the temperature of the water in the tank changed from time to time, the resistivities predicted by the curve for the gelatine were sometimes not exactly accurate. In order to be very accurate, each case had to be calibrated separately. During the last measurements made, those for the horizontal ore body, the temperature of the tank water was changing slowly from day to day because of the warming weather and for this reason, the resistivity contrast is

slightly different from model to model. For the earlier experiments, the temperature was sufficiently constant to give the same resistivity for the gelatine in the tank throughout a whole series of measurements with one geometry.

The gelatine for the models was made using one envelope of commercial gelatine and 100 cc of the solution. The hot gelatine was poured into the mold for the ore body and the calibration tube at the same time. With this mixture the ore body, at the temperature of the tank, was quite solid and held its shape well. A qualitative measurement of the number of salt ions that diffused out of the gelatine ore body in a 48 hour period indicated that a negligible number would diffuse out in the comparatively short time that it took to make a set of measurements.

To give strength to the ore body, the gelatine was molded around a frame work made from 1/16 inch lucite rods and 1/32 inch bakelite sheeting. This served very well to strengthen the gelatine and the frame had a small enough volume so that it didn't affect the current flow to any measurable degree. Several measurements were made with the empty frame and the ore body holder in position in the tank and they always were independent of the position of the empty frame. The readings were in all cases the same as the blank readings when nothing was in the tank.

This discussion of the procedures used in the modelling has been brief, but I think that enough detail has been included so that a clear picture of how the data were obtained can be formed. The model data are shown on the maps described in the following sections. We shall see that these results can be very useful in interpreting field results, and also in making some general statements about the induced polarization effect and what effect variations in the parameters of the ore body have on the measured surface anomalies.

6.3 Two Dimensional Modelling Results

Many geologic structures have length in one direction and can therefore be considered as two dimensional. These structures include glacial till deposits, faults, many ore bodies and others. They are easiest to model in two dimensions. In two dimensions though the source is not very realistic. What is being modelled is the line source; i. e., a line of infinitesimally spaced point sources. The receivers are also equivalent to line receivers in three dimensions. This type of sender and receiver is never used in the field because it would be too cumbersome. The measurements on the two dimensional model are easy to make and, as we shall see, do have qualitative use so that even though the conditions simulated by the model are not directly realizable in field work, the modelling can be some help.

Several models were used but all of the cases except that of

a conducting hill on the surface of a half space have been duplicated in the later three dimensional work. In each case, for the vertical ore body for instance, the character of the contour maps from the two kinds of data were exactly alike. They both had highs and lows in the same places, although the magnitudes weren't exactly the same. The fact that at least the shape of the contours from the two dimensional model is useful is encouraging because features infinite in one direction are difficult to model in three dimensions.

The fact that the dipole-dipole configuration was used probably helped. In this case, the potential falls off as $(\frac{1}{r^3})$ from the location of the sender. If we consider the line source as being made up of many pole senders, we can see that those poles at a greater distance from the measuring point would have much less effect than those very close. Therefore, the line source probably acts very much like a point source spread out over a small region of the line. The point sources near the center would give most of the effect, and at a little distance from the source, the potentials would look much like those from a point source.

The apparent resistivity map shown on Fig. 31 is from the only geometry not repeated by the later three dimensional work. This is the geometry of a large surface feature that is more conducting than the half space on which it rests. In the case shown, the hill has been

2-DIMENSIONAL HILL MODEL

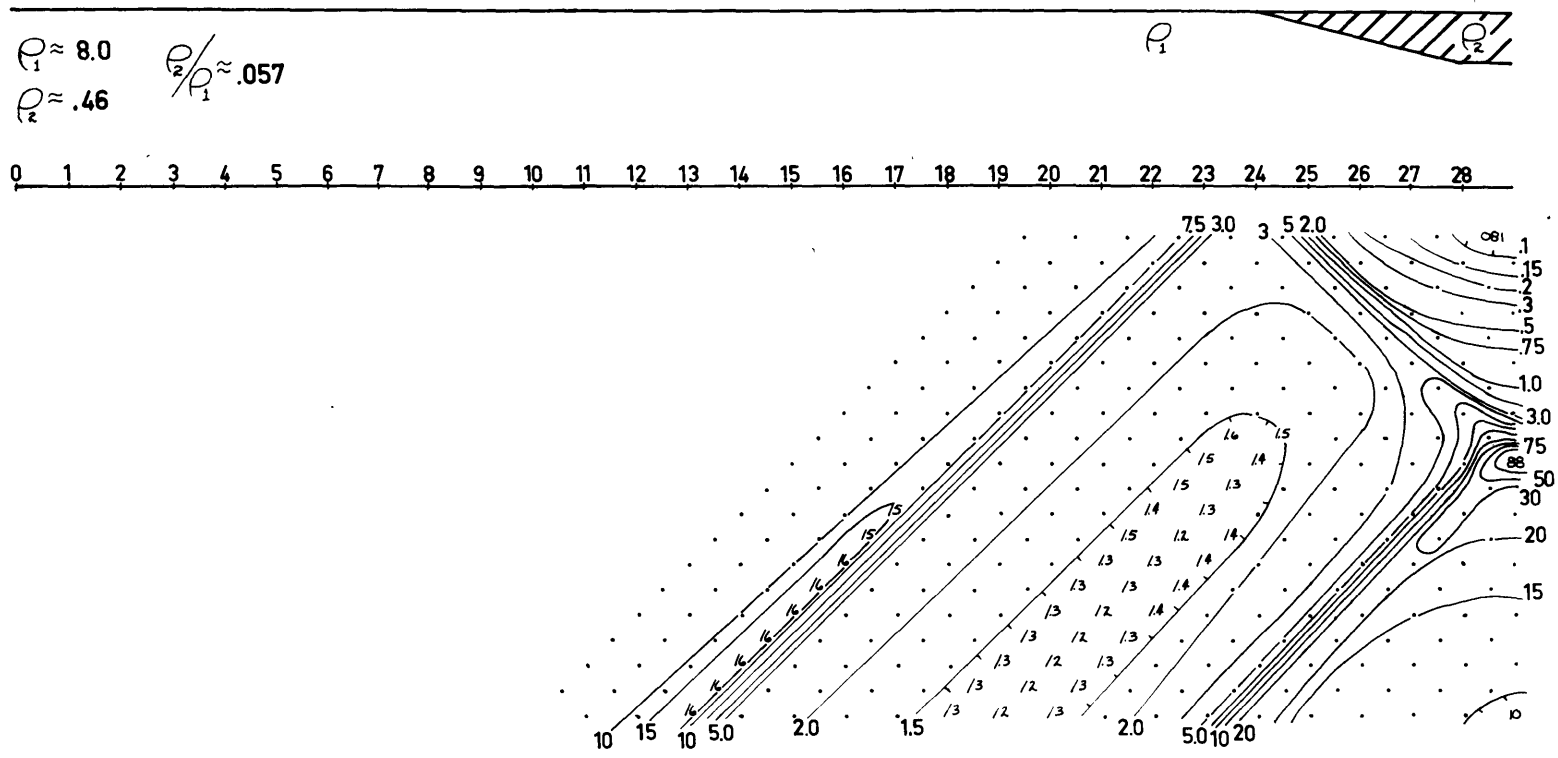


Fig.31

inverted to make the modelling easier, but the results are the same as they would be if the hill were raised.

In section 3.5 I pointed out that lateral changes in resistivity could be expected to give 45° contours, and as an example, Fig. 3 was discussed. It is an apparent resistivity map from a line that ran over a hill of glacial till and onto the basement rocks. The hill was very long in the direction at right angles to the line and could be considered to be infinite in that direction.

If the map on Fig. 31 is compared with the first half of line Y on Fig. 3, the similarity of the contours is apparent. The main features on both maps are the same. The low zone when both the sender and receiver were on the hill; the broader zone, not quite as low, when one set of electrodes was on the hill and the other on the high resistivity rock; the high zone for all senders when the receiver is just in front of the hill and the other high cutting across the low zones, when the sender is just in front of the hill. The region of really big apparent resistivities occurs when the sender and receiver are on either side of the hill and this feature isn't too large on the field map because the line didn't extend far enough.

All of the features on the left hand side of the resistivity map for line Y are caused by the hill; something that might not be predicted at first glance. In this case, the modelling was not able to give us quantitative information but it was helpful in interpretation.

6.4 Results from the Vertical Ore Body

In the next four sections, I will present the data from the three dimensional modelling measurements and describe the major characteristics of each set of contours. The first maps in each section are the apparent resistivity maps and the last maps are the apparent metal factors. I think that each map has on it all the information necessary to form a clear picture of what the model was simulating. The geometries are catalogued alphabetically from A-I. In Table II all of the geometries are listed while a diagram has been put on each of the resistivity maps demonstrating, in section, the location of the ore body. The third dimension (c) was in each case 8 units, four on each side of the electrodes, and all of the lines were at right angles to the strike of the ore body. The Roman numerals refer to the number of the run and are the index to which set of data were used to plot the maps. For the induced polarization maps, two run numbers are specified, one for the D. C. and one for the A. C. case.

The contours all have logarithmic intervals so that each contour is approximately twice the previous one in value. However, it must be pointed out that the value appearing on the apparent resistivity maps is not the value of the apparent resistivities measured at each station. What is plotted is the difference, in percent, of the measured value from the background value of 1.0. Thus, a value of (+9.5) means that the apparent resistivity at that station was (1.095), while a value of

(-25) means that the apparent resistivity was (0.75). Therefore, if these apparent resistivity maps were contoured on the value of apparent resistivity, as the field maps are, there would be much fewer contours. The first ones would be (+100) and (-50).

The induced polarization maps are contoured on the value of the apparent metal factor just as the field maps are. On both kinds of maps, the actual values are only on the maps in the regions of maxima and minima. The other values are represented only by dots. Experience with these contour maps has shown that once the contours are drawn, the actual values are neglected in observations. The true values can be gotten with reasonable accuracy by interpolation between the contours.

The apparent resistivity maps for the vertical ore body are on Figures 32-35. The main feature of these maps are a closed low centered at the location of the ore body and an area of small positive values for the receiver position just before the ore body. When the ore body is made more conducting, the negative values get more negative and the positive values get more positive, but not nearly in proportion to the increase in the conductivity of the ore zone.

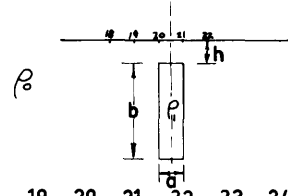
When the ore body is at a deeper depth the closed region of low values occurs for wider separations between sender and receiver. Also, as is expected, the actual value in the minimum is closer to zero.

APPARENT RESISTIVITY

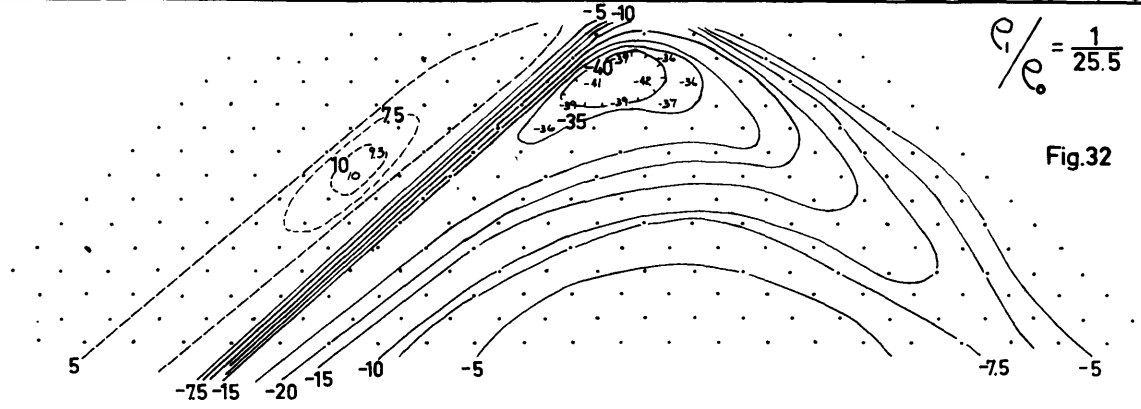
GEOMETRY A (Runs I & III)

Value Plotted is $\left[\frac{\rho_a}{\rho_0} - 1 \right] \times 100$

a = 1 unit
 b = 4 "
 c = 8 " (centered \perp line)
 h = 1 "



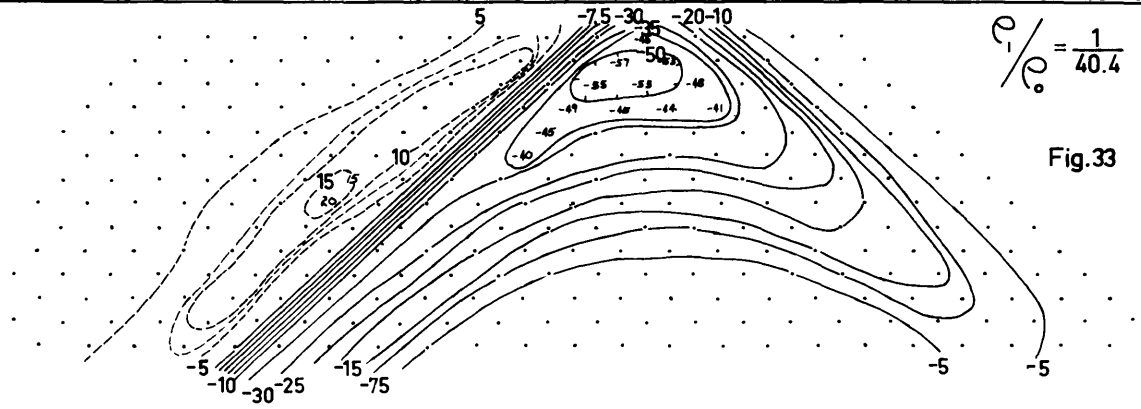
0 1 2 3 4 5 6 7 8 9 10 11 12 13 14 15 16 17 18 19 20 21 22 23 24 25 26 27 28 29 30 31 32



$$\frac{\rho_a}{\rho_0} = \frac{1}{25.5}$$

Fig. 32

0 1 2 3 4 5 6 7 8 9 10 11 12 13 14 15 16 17 18 19 20 21 22 23 24 25 26 27 28 29 30 31 32



$$\frac{\rho_a}{\rho_0} = \frac{1}{40.4}$$

Fig. 33

For the deeper ore body the small positive region has just about disappeared.

The apparent metal factor maps for the vertical ore body are on Figures 36 and 37. Using the values of the resistivity contrasts from the previous data and a $\rho/2\pi$ value of 750 ohm-feet for the background material, we get a value of 2000 for the metal factor of the ore zone. The apparent metal factor maps are asymmetric because the data is for a pole-dipole configuration.

A metal factor of 2000 is not very large and represents very little mineralization as a check in Table I will show. The induced polarization anomalies are quite distinct and since the background is zero the anomalies represent a level that is definitely well above background. When the ore body is one unit deep a resistivity contrast of 40 to 1 only alters the surface readings by 50% while the metal factor anomaly for the model representing just about the same degree of mineralization has a maximum of 96 compared to a background of zero.

These maps also disclose one of the drawbacks of the induced polarization effect. Although the induced polarization anomaly is much larger than the apparent resistivity for any ore body, it falls off much faster than the apparent resistivity anomaly as the ore body gets deeper. For a resistivity contrast of 40 to 1, the anomaly reduces from -55 to -22 when the depth to the top of the ore body was increased from 1 to 2

INDUCED POLARIZATION

Value Plotted is $\left\{ \frac{\left[\frac{\rho_{dc}}{\rho_{ac}} - 1 \right] \times 100}{\frac{\rho_{dc}}{2\pi} / 1000} \right\} \equiv \text{"METAL FACTOR"}$

Resistivity Values Used

$\frac{\rho}{2\pi} = 750 \text{ ohm-feet}$

$\left[\frac{\rho}{2\pi} \right]_{dc} = 29.4 \text{ ohm-feet}$

Metal Factor of Ore Body = 2000

0 1 2 3 4 5 6 7 8 9 10 11 12 13 14 15 16 17 18 19 20 21 22 23 24 25 26 27 28 29 30 31 32

GEOMETRY A (I & III)

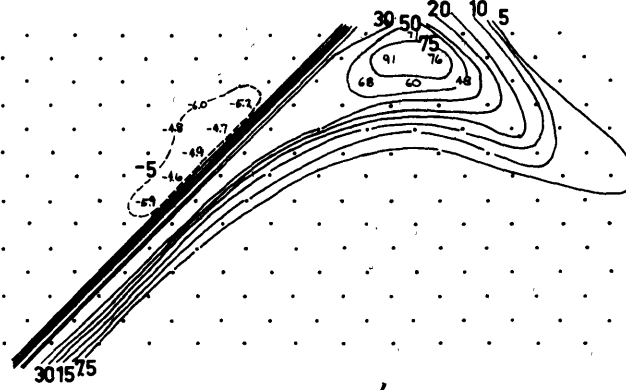


Fig.36

0 1 2 3 4 5 6 7 8 9 10 11 12 13 14 15 16 17 18 19 20 21 22 23 24 25 26 27 28 29 30 31 32

GEOMETRY B (II & IV)

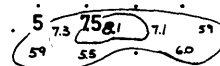


Fig.37

units. The corresponding apparent metal factors decreased from 90 to 8.1; however, at this depth the ore body would only have reduced the apparent resistivities by 20%, which wouldn't even show up on the contours of field data. The apparent metal factor anomaly of 8.1 is still an order of magnitude above background.

Something should be said about the small region of negative values on Fig. 36 because we will see larger negative values for some of the other models. These are a consequence of the fact that by introducing a conducting region into a uniform half space the lines of current flow are warped. They are crowded together in some places and spread out in others. This is why we can find places on the surface where the potential difference between two points is greater than it should be. We can therefore get apparent resistivities that are higher than any value in the ground itself. By making the anomalous region more conducting we make these apparent resistivities even larger. Thus, we calculate negative metal factors. They are a consequence of the way we measure the potential difference and not of the physical properties of the ground.

These negative metal factors are very seldom measured in the field. This is because there is almost always a background of metal factors in field measurements, as the field maps show. The background is usually due to slight mineralization present in most rocks like gabbro, or to instrumental inaccuracies. There are cases

though when very definite lows in the apparent metal factor maps are associated with sender or receiver positions adjacent to large high areas. Consider Fig. 6, the map for the vertical ore body. We see that there is a definite low on the induced polarization map just next to the region of positive values.

Line P, the map in Fig. 6, is from a geometry much like the vertical model. The field data was taken using the dipole-dipole configuration, but it is still quite similar to the model results. The closed metal factor anomaly is very similar to those in Figures 36 and 37. The fact that in the field there was a conducting layer over the vertical ore body has completely altered the character of the resistivity anomaly but the induced polarization anomaly is still characterized by the shape of the contours for a vertical ore body.

6.5 Ore Body Dipping Toward the Sender

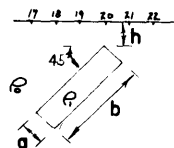
The apparent resistivity maps on Figures 38-41 are for the case of an ore body dipping at 45° toward the sender. There are several differences in the maps from the vertical case. For one thing, the region of positive values now occurs when the receiver is on the opposite side of the ore body from the sender. The character of the negative anomaly is also changed. There is still the closed low associated more or less with the location of the body, but now there is also a tendency to get very low values when the

APPARENT RESISTIVITY

GEOMETRY C (Runs V & VII)

Value Plotted is $\left[\frac{\rho_a}{\rho_0} - 1 \right] \times 100$

- a 1 unit
- b 4 "
- c 8 " (centered \perp line)
- h 1 "



0 1 2 3 4 5 6 7 8 9 10 11 12 13 14 15 16 17 18 19 20 21 22 23 24 25 26 27 28 29 30 31 32

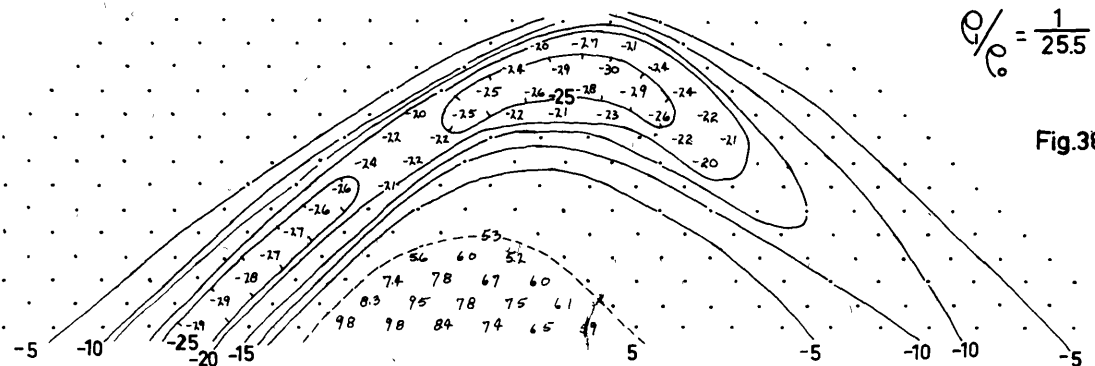


Fig.38

0 1 2 3 4 5 6 7 8 9 10 11 12 13 14 15 16 17 18 19 20 21 22 23 24 25 26 27 28 29 30 31 32

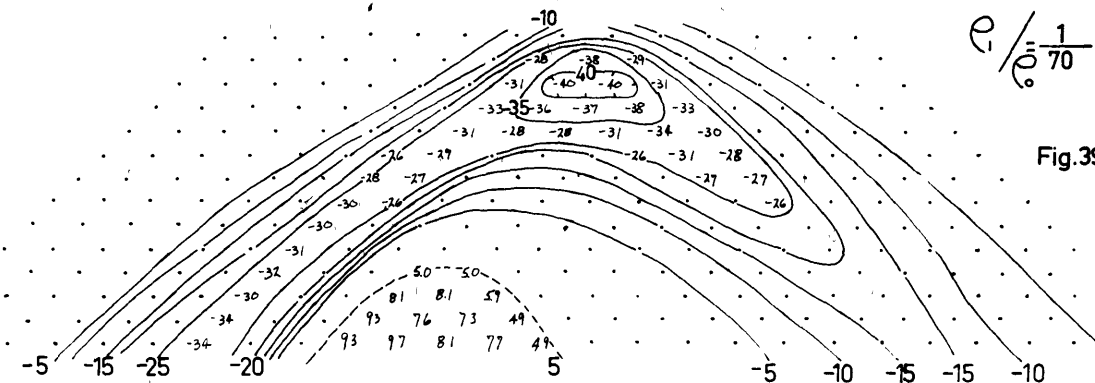


Fig.39

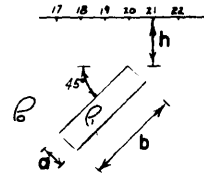
126

APPARENT RESISTIVITY

GEOMETRY D (RUNS VI & VIII)

Value Plotted is $\left[\frac{\rho}{\rho_0} - 1 \right] \times 100$

a=1unit
 b=4 "
 c=8 " (centered \perp line)
 h=2 "



0 1 2 3 4 5 6 7 8 9 10 11 12 13 14 15 16 17 18 19 20 21 22 23 24 25 26 27 28 29 30 31 32

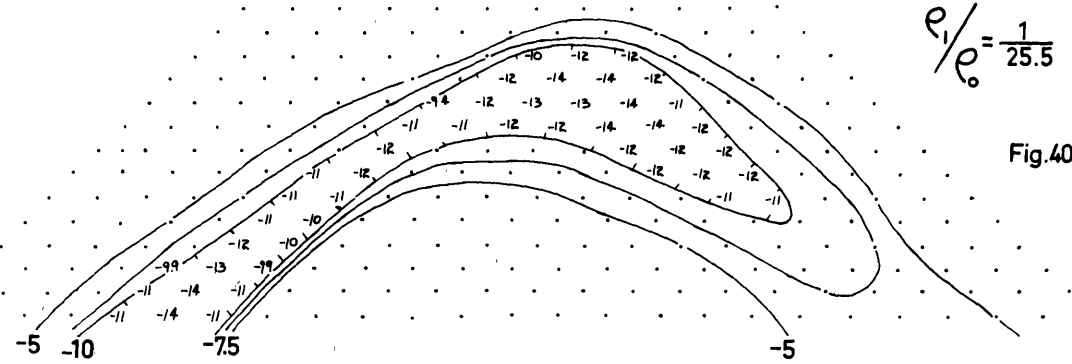


Fig.40

0 1 2 3 4 5 6 7 8 9 10 11 12 13 14 15 16 17 18 19 20 21 22 23 24 25 26 27 28 29 30 31 32

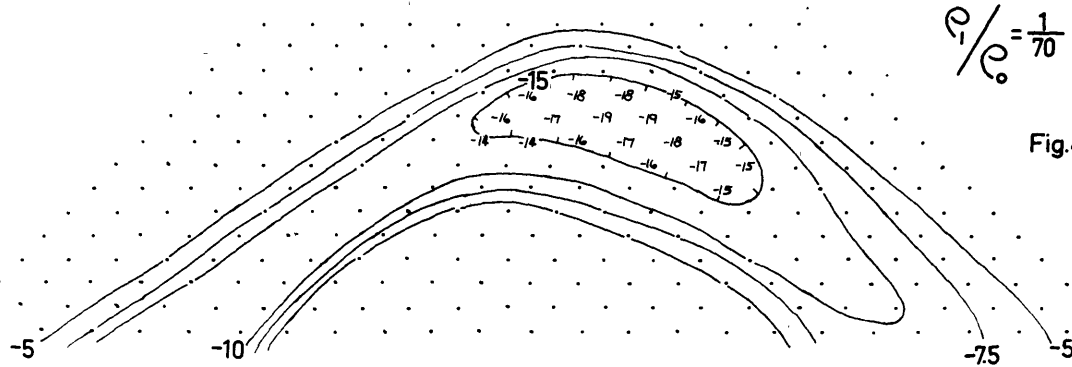


Fig.41

127

receiver is over the ore body but the sender is very far away. This shows up very well on Fig. 38. As the ore body is moved deeper the anomalies get smaller in magnitude and spread out, as in the vertical case.

The anomalies are all smaller than in the corresponding vertical case. In this case, the one unit depth refers to the uppermost corner of the ore body so that there isn't as much of the ore body at exactly one unit depth, but because of the dip, the center of mass of the ore body is shallower so that more of its volume is at a shallower depth. For instance, in Fig. 39 the contrast is 70 to 1 and the maximum anomaly is (-40), this wouldn't show up at all on a field map. When the vertical ore body is one unit deep a contrast of 40 to 1 gives a larger anomaly.

The metal factor maps on Figures 42 and 43 bear out the fact that this geometry gives relatively small anomalies. Because of the larger contrast used for the second case, the metal factor of the ore body comes out to be much larger in this case, about 6000. Still, the apparent M. f. anomalies are the same as or even smaller than the vertical cases when the top of the ore body was at the same depth. From these results then, it appears that the anomalies from a dipping body are quite small when the data is taken along lines such that the ore body is dipping toward the sender.

INDUCED POLARIZATION

Value Plotted is $\left\{ \frac{\left[\frac{\rho_a}{\rho_{dc}} - 1 \right] \times 100}{\rho_a^{dc} / 1000 \times 2\pi} \right\} = \text{"METAL FACTOR"}$

Resistivity Values Used

$\frac{\rho}{2\pi} = 750$ ohm feet
 $\left[\frac{\rho}{2\pi} \right]_{dc} = 29.4$ ohm feet
 Metal Factor of Ore Body = 5950

0 1 2 3 4 5 6 7 8 9 10 11 12 13 14 15 16 17 18 19 20 21 22 23 24 25 26 27 28 29 30 31 32

GEOMETRY C (V & VII)

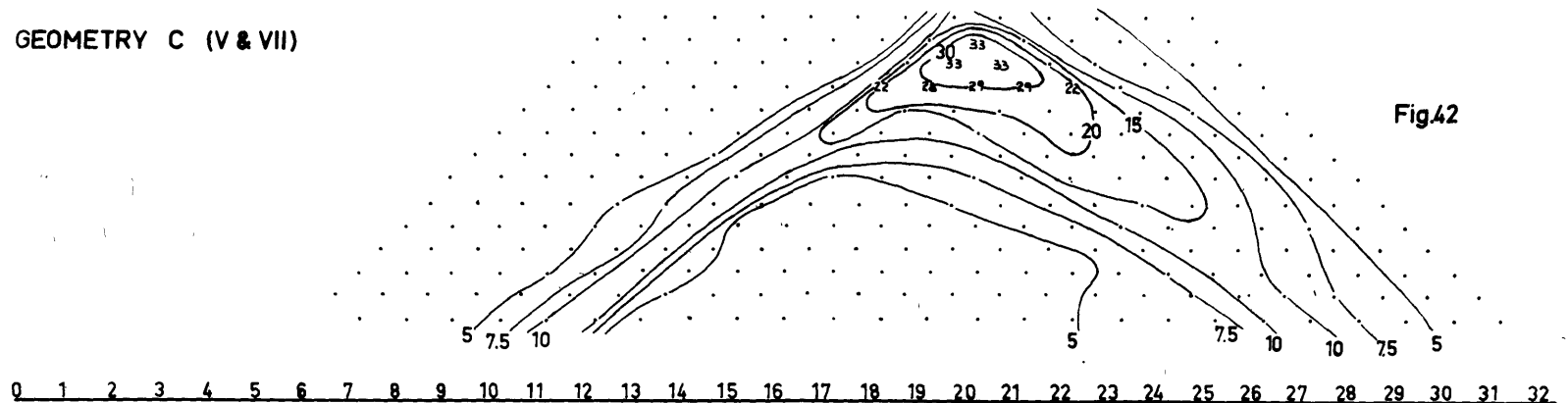


Fig.42

0 1 2 3 4 5 6 7 8 9 10 11 12 13 14 15 16 17 18 19 20 21 22 23 24 25 26 27 28 29 30 31 32

GEOMETRY D. (VI & VIII)

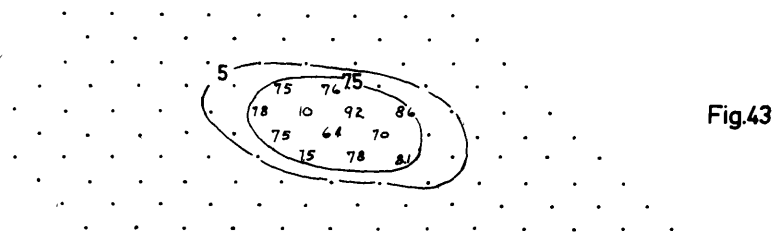


Fig.43

6.6 Ore Body Dipping Away from the Sender

A look at Figures 44-49 reveals that the situation is quite reversed when the ore body is dipping away from the sender. The apparent resistivity maps on Figure 44-47 are quite different from the other cases. For this geometry the anomalies are associated only with the location of the receiver and almost the same values are measured wherever the sender is situated. The sender does give some effect as it passes over the ore body, but it is very small compared to the larger anomaly when the receiver is over the ore zone. For this geometry both the positive and negative anomaly are open; i. e. , the separation between the sender and receiver doesn't affect the size of the anomaly as long as the receiver is over the ore body.

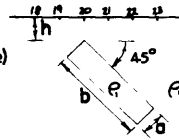
This is the first time too when a positive resistivity anomaly has been present when the ore body was two units deep. In fact, both of the positive regions were present when the ore body was only one unit deep. The size of the positive anomaly in front of the ore body is about the same as in the vertical case when the depth is one unit; however, when the ore body is moved to two units deep, the positive anomaly in the case of the vertical ore body becomes too small to measure and this is not the case in Figures 46 and 47. For the dipping ore body the positive values are smaller than when it was one unit deep but the anomaly is very definitely there.

APPARENT RESISTIVITY

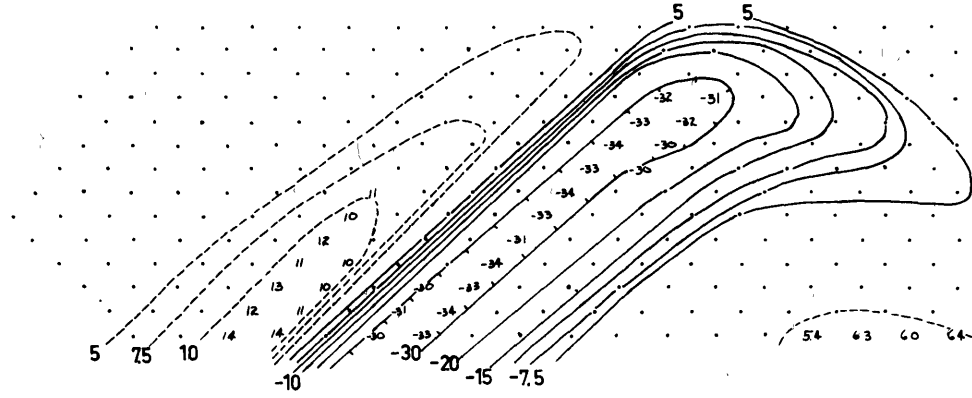
GEOMETRY E (Runs IX & XI)

Value Plotted is $\left[\frac{\rho_a}{\rho_0} - 1 \right] \times 100$

a = 1 unit
 b = 4 "
 c = 8 " (centered \perp line)
 h = 1 "



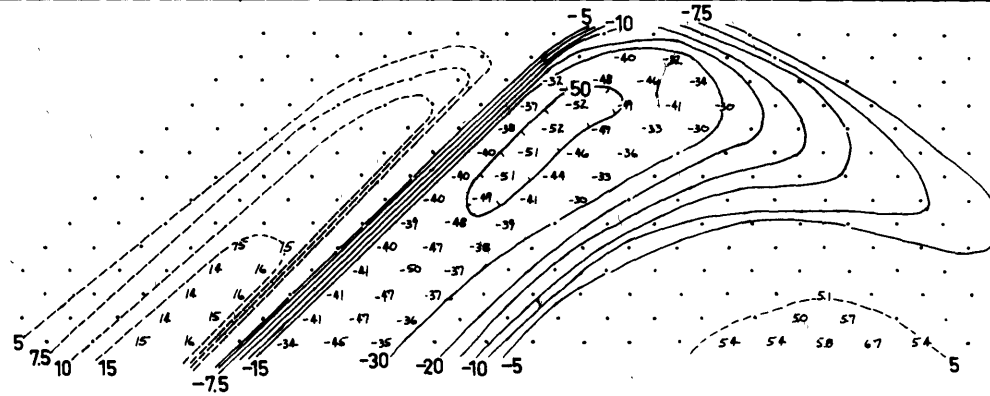
0 1 2 3 4 5 6 7 8 9 10 11 12 13 14 15 16 17 18 19 20 21 22 23 24 25 26 27 28 29 30 31 32



$$\frac{\rho_1}{\rho_0} = \frac{1}{24.8}$$

Fig.44

0 1 2 3 4 5 6 7 8 9 10 11 12 13 14 15 16 17 18 19 20 21 22 23 24 25 26 27 28 29 30 31 32



$$\frac{\rho_1}{\rho_0} = \frac{1}{73}$$

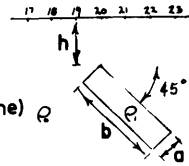
Fig.45

APPARENT RESISTIVITY

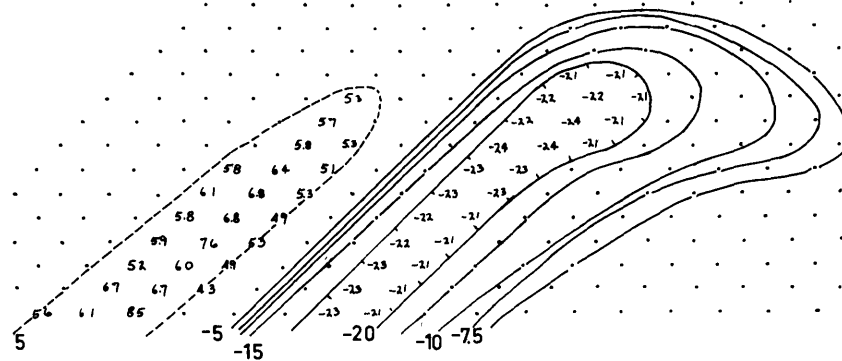
GEOMETRY F (Runs X & XII)

Value Plotted is $\left[\frac{\rho_a}{\rho_o} - 1 \right] \times 100$

a = 1 unit
 b = 4 "
 c = 8 "
 h = 2 " (centered \perp line)



0 1 2 3 4 5 6 7 8 9 10 11 12 13 14 15 16 17 18 19 20 21 22 23 24 25 26 27 28 29 30 31 32



INDUCED POLARIZATION

Value Plotted is $\left\{ \frac{\left[\frac{\rho_{dc}}{\rho_{ac}} - 1 \right] \times 100}{\frac{\rho_{dc}}{2\pi \times 10^3}} \right\} \equiv \text{"METAL FACTOR"}$

Resistivity Values Used

$\frac{\rho}{2\pi} = 750 \text{ ohm-feet}$

$\left[\frac{\rho}{2\pi} \right]_{dc} = 30.2 \text{ ohm-feet}$

Metal Factor of Ore Body = 6300

0 1 2 3 4 5 6 7 8 9 10 11 12 13 14 15 16 17 18 19 20 21 22 23 24 25 26 27 28 29 30 31 32

GEOMETRY E (IX & XI)

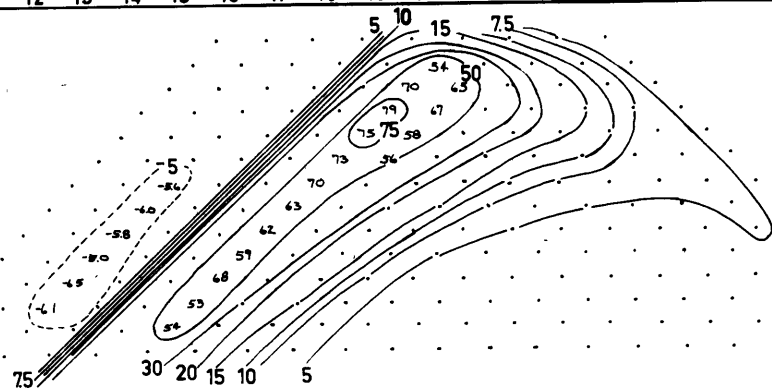


Fig.48

0 1 2 3 4 5 6 7 8 9 10 11 12 13 14 15 16 17 18 19 20 21 22 23 24 25 26 27 28 29 30 31 32

GEOMETRY F (X & XII)

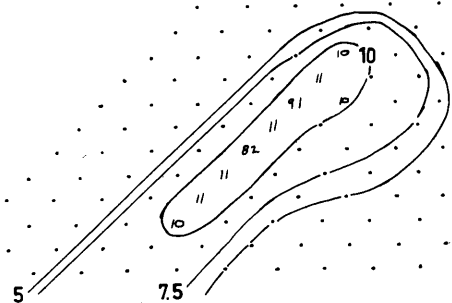


Fig.49

The negative anomalies are in size between the case for the ore body dipping the other way and the vertical case for the shallower depth. They seem to decrease less rapidly with depth though, so that while the anomaly in Fig. 32 is larger than that in Fig. 44, the situation is reversed for the deeper ore bodies and the anomaly in Fig. 46 is larger than that in Fig. 34.

The metal factors in Figures 48 and 49 are also bigger than those when the ore body is dipping the other way, although there is more difference for the shallow case than when the ore bodies are deeper. In this case, the metal factor of the ore zone is just about 6000 as it was before. The anomaly has a much different shape also. It must be remembered though that in the field it is only rarely that more than seven or eight readings are possible from each sender. If only the upper half of these maps are compared there is more similarity than if all the data were used.

It does seem that bigger anomalies are measured using the pole-dipole configuration if the lines are run so that the expected dip is away from the pole sender. Of course, if the proper subtractions were carried out on the potentials from both cases and the dipole-dipole second differences calculated, both cases must give the same values with the exception that they would be reversed. The maps would, of course, not be symmetric because the geometry of the resistivity contrast is not symmetric.

6.7 The Horizontal Ore Body

All of the current flow from a pole source could be described as more or less radial. At a point a couple of units from the source, all of the current in the upper few units of the half space is nearly horizontal. Because of this, all electrical measurements using current sources give their biggest effect for horizontal geometries. The fact that horizontal ore bodies have the biggest resistivity anomalies has long been recognized. For this reason, I considered the horizontal geometry to be more important than the rest and I did more horizontal modelling. The apparent resistivity maps from the modelling are on Figures 50-61 and the induced polarization maps are on Figures 62-70.

Since the effects were larger I was able to extend the horizontal to the case where it was 3 units deep to the top of the model. At each depth I took measurements for four resistivity contrasts, picked so that each contrast was roughly twice the previous one. This brought out one of the most important facts that can be learned from the modelling results. I've mentioned previously that if the contrast were doubled, the size of the anomaly was not increased in the same proportion; the modelling results from the horizontal model show that the higher the contrast the smaller the increase in the anomaly when the contrast is doubled! Apparently, a kind of saturation occurs so that after a reasonably high contrast is reached, the current lines can be altered

APPARENT RESISTIVITY

GEOMETRY G

Value Plotted is $\left[\frac{\rho_a}{\rho_0} - 1 \right] \times 100$

- a = 2 Units
- b = 4 " (centered, ⊥ line)
- c = 8 "
- h = 1 "

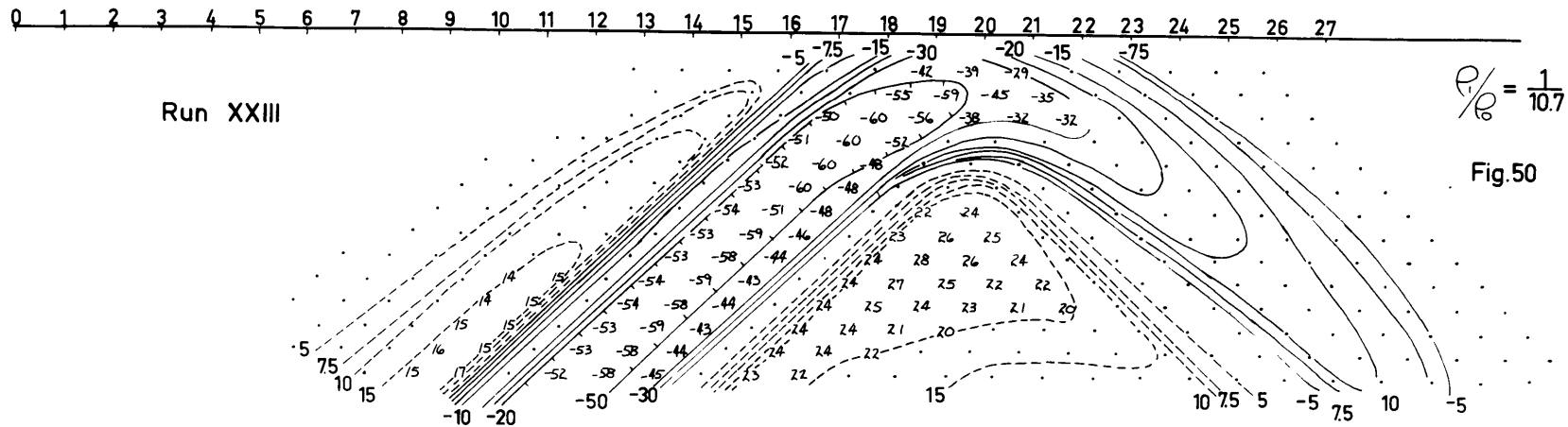
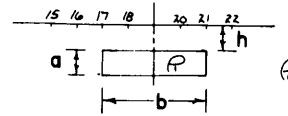


Fig.50

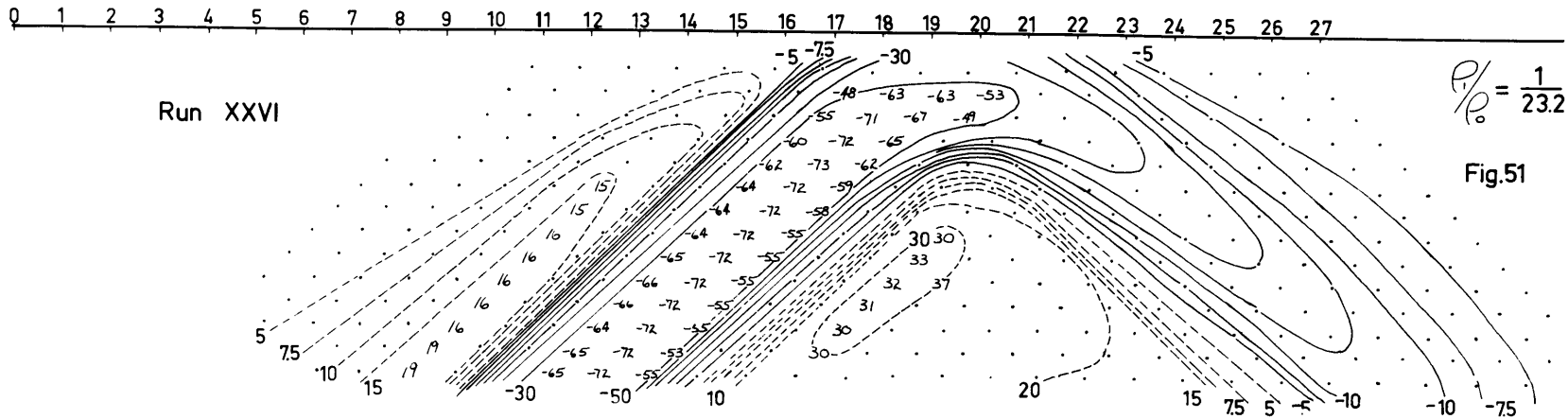


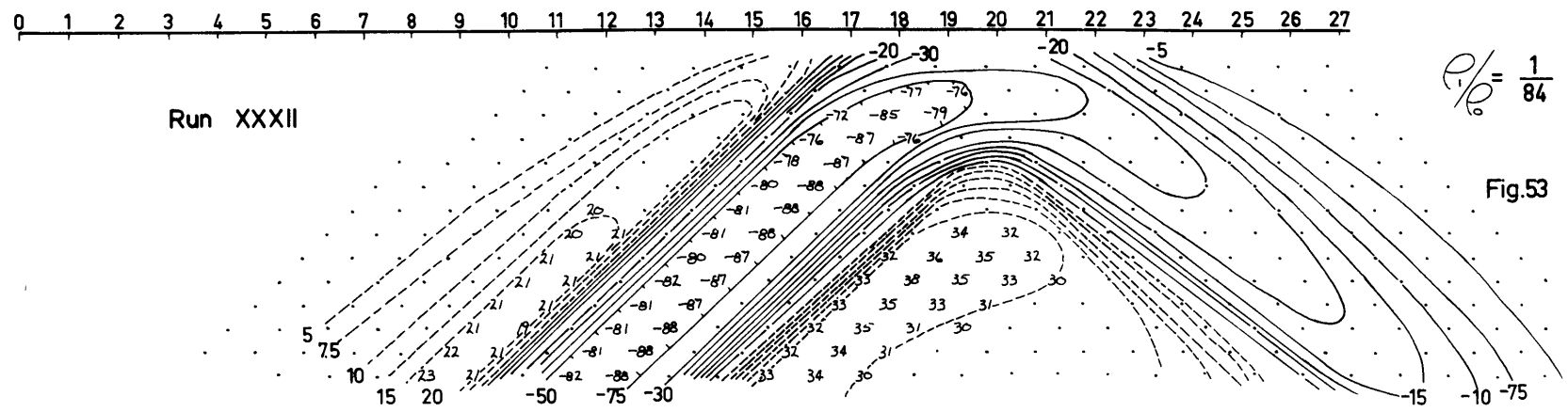
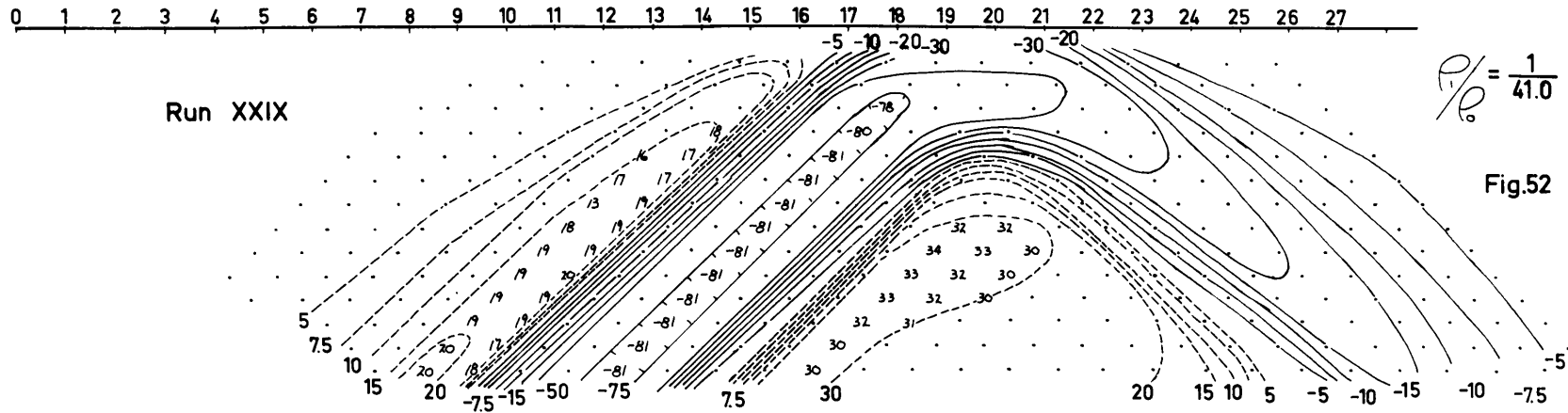
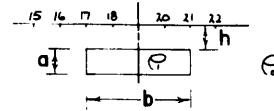
Fig.51

APPARENT RESISTIVITY

GEOMETRY G

Value Plotted is $\left[\frac{\rho_a}{\rho_0} - 1 \right] \times 100$

a = 1 Unit
 b = 4 "
 c = 8 " (centered, ⊥ line)
 h = 1 "

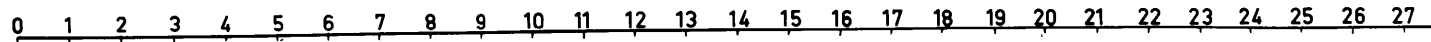
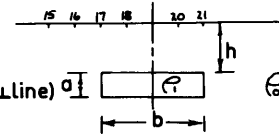


APPARENT RESISTIVITY

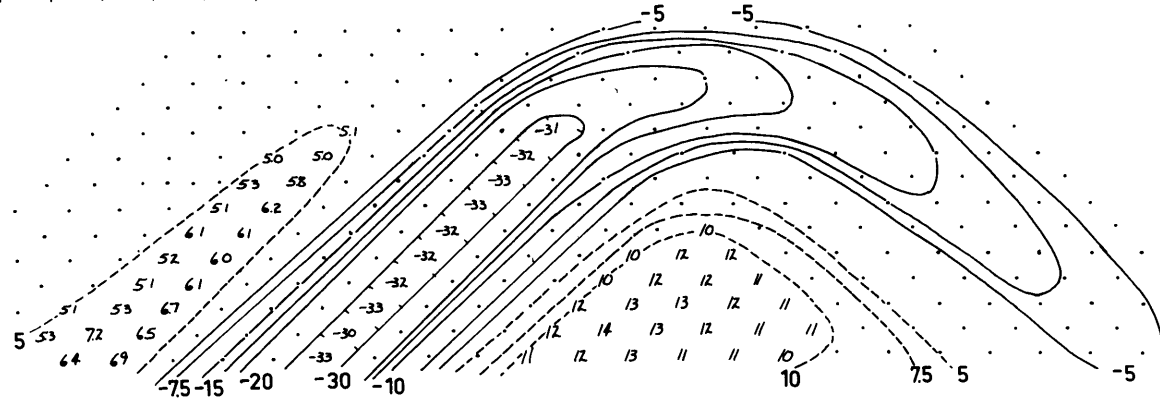
GEOMETRY H

Value Plotted is $\left[\frac{\rho_a}{\rho_0} - 1 \right] \times 100$

a = 1 Unit
 b = 4 "
 c = 8 " (centered, Lline)
 h = 2 "

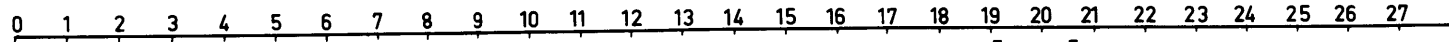


Run XXIV

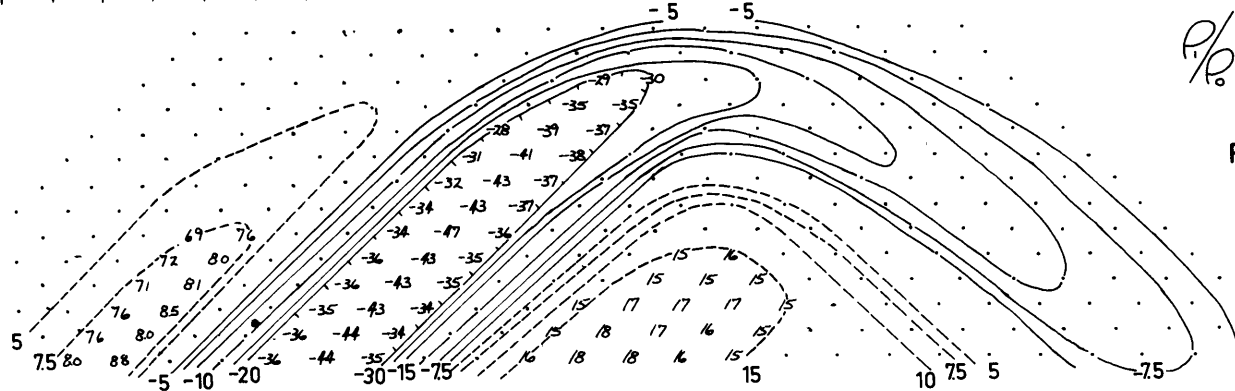


$\frac{\rho_a}{\rho_0} = \frac{1}{10.6}$

Fig.54



Run XXVII



$\frac{\rho_a}{\rho_0} = \frac{1}{23}$

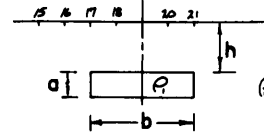
Fig.55

APPARENT RESISTIVITY

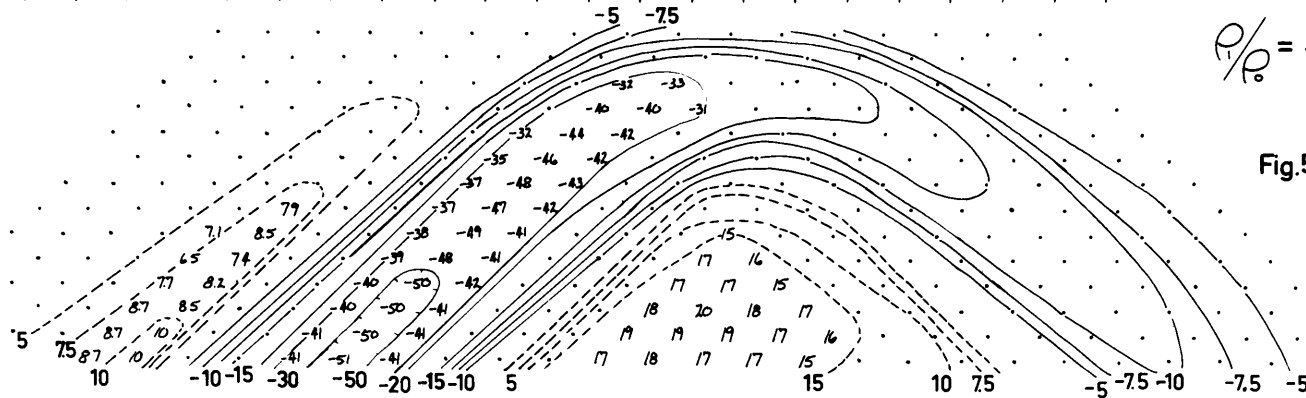
GEOMETRY H

Value Plotted is $\left[\frac{\rho_a}{\rho_o} - 1 \right] \times 100$

a = 1 Unit
 b = 4 "
 c = 8 " (centered, ⊥ line)
 h = 2 "

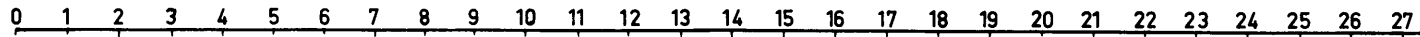


Run XXX

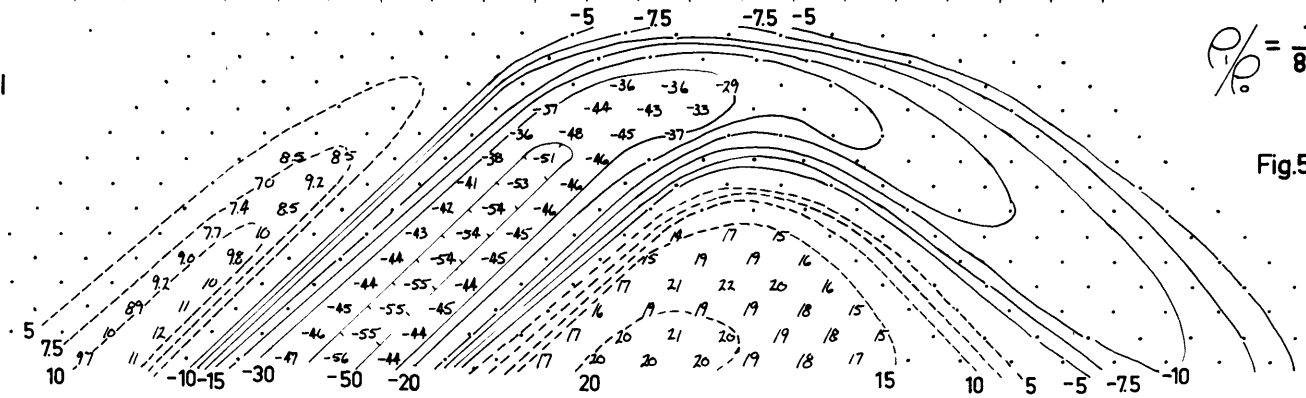


$\frac{\rho_a}{\rho_o} = \frac{1}{41}$

Fig.56



Run XXXIII



$\frac{\rho_a}{\rho_o} = \frac{1}{81.3}$

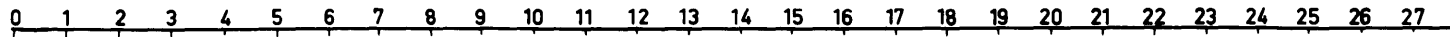
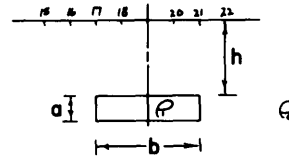
Fig.57

APPARENT RESISTIVITY

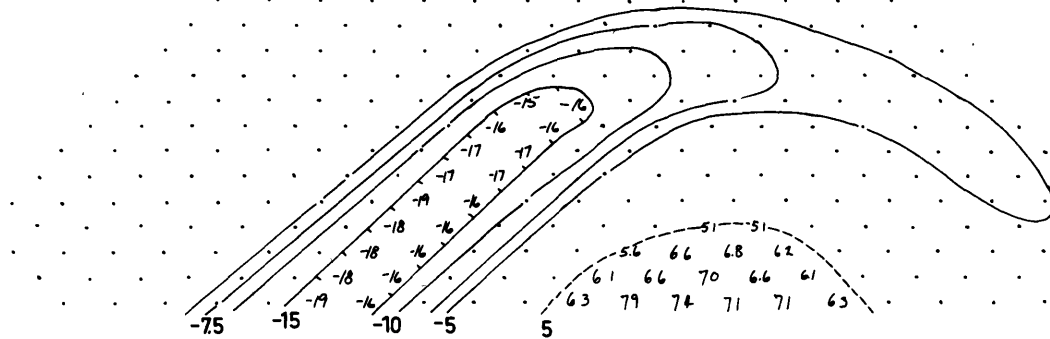
GEOMETRY I

Value Plotted is $\left[\frac{\rho_a}{\rho_0} - 1 \right] \times 100$

a = 1 Unit
 b = 4 "
 c = 8 " (centered, ⊥ line)
 h = 3 "

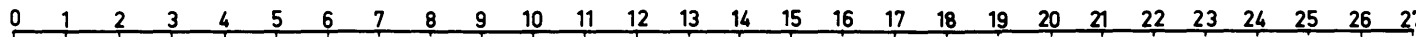


Run XXV

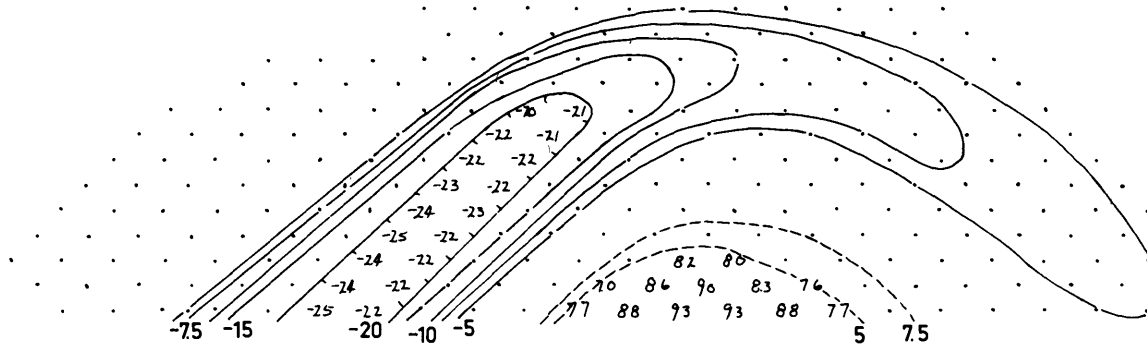


$\frac{\rho}{\rho_0} = \frac{1}{10.6}$

Fig.58



Run XXVIII



$\frac{\rho}{\rho_0} = \frac{1}{23.2}$

Fig.59

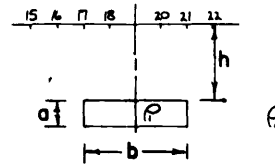
141

APPARENT RESISTIVITY

GEOMETRY I

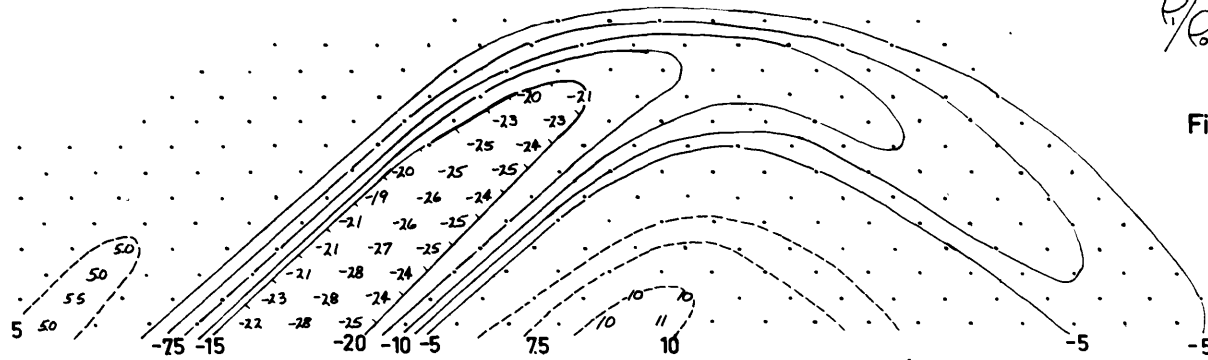
Value Plotted is $\left[\frac{\rho_a}{\rho} - 1 \right] \times 100$

- a = 1 Unit
- b = 4 "
- c = 8 " (centered, ⊥ line)
- h = 3 "



0 1 2 3 4 5 6 7 8 9 10 11 12 13 14 15 16 17 18 19 20 21 22 23 24 25 26 27

Run XXXI

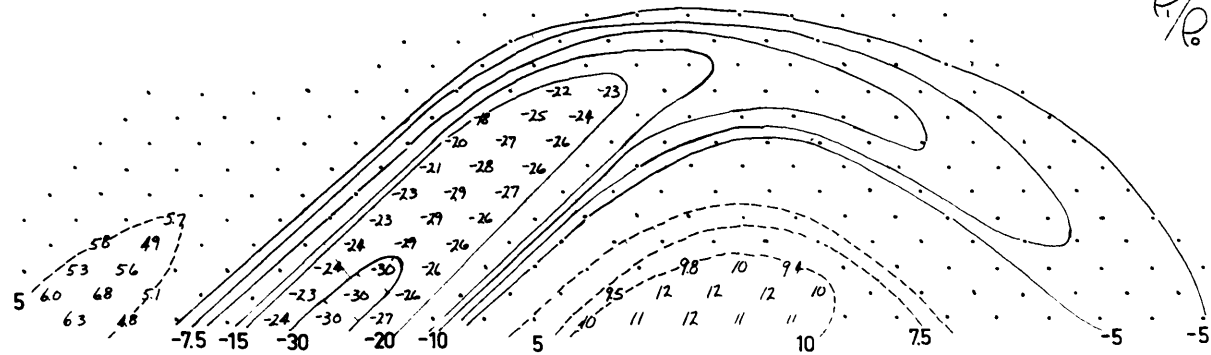


$\frac{\rho_a}{\rho} = \frac{1}{41}$

Fig.60

0 1 2 3 4 5 6 7 8 9 10 11 12 13 14 15 16 17 18 19 20 21 22 23 24 25 26 27

Run XXXIV



$\frac{\rho_a}{\rho} = \frac{1}{78}$

Fig.61

INDUCED POLARIZATION

Value Plotted is $\left\{ \frac{\left[\frac{\rho_{dc}}{\rho_a} - 1 \right] \times 100}{\left[\frac{\rho_{dc}}{2\pi} \right] \times 10^3} \right\} \equiv \text{"METAL FACTOR"}$

Resistivity Values Used

$\frac{\rho_0}{2\pi} = 750 \text{ ohm-feet}$
 $\left[\frac{\rho_1}{2\pi} \right]_{dc} = 32.6 \text{ ohm-feet}$

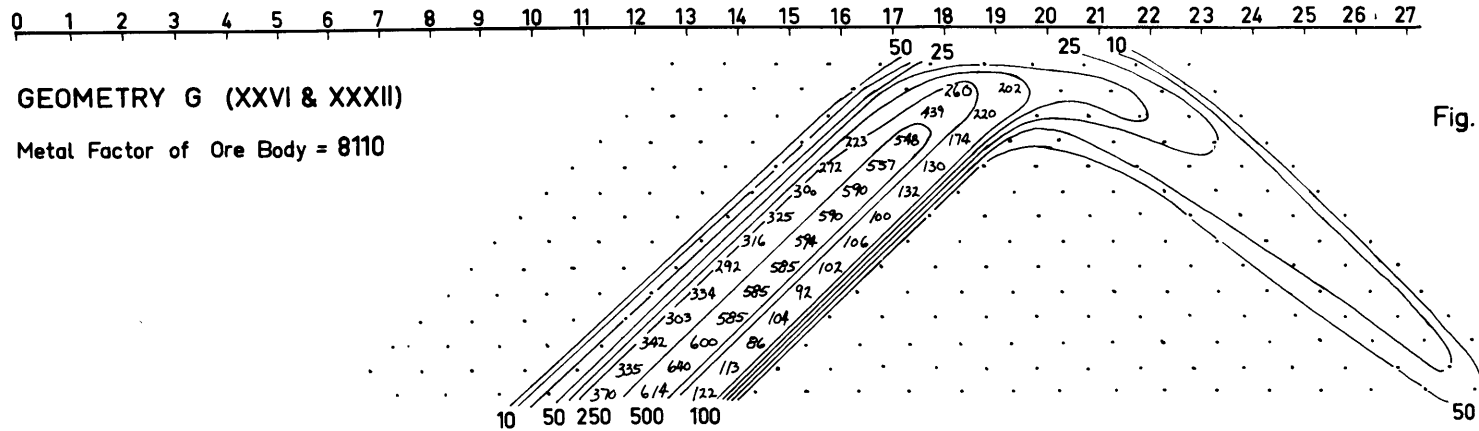


Fig. 68

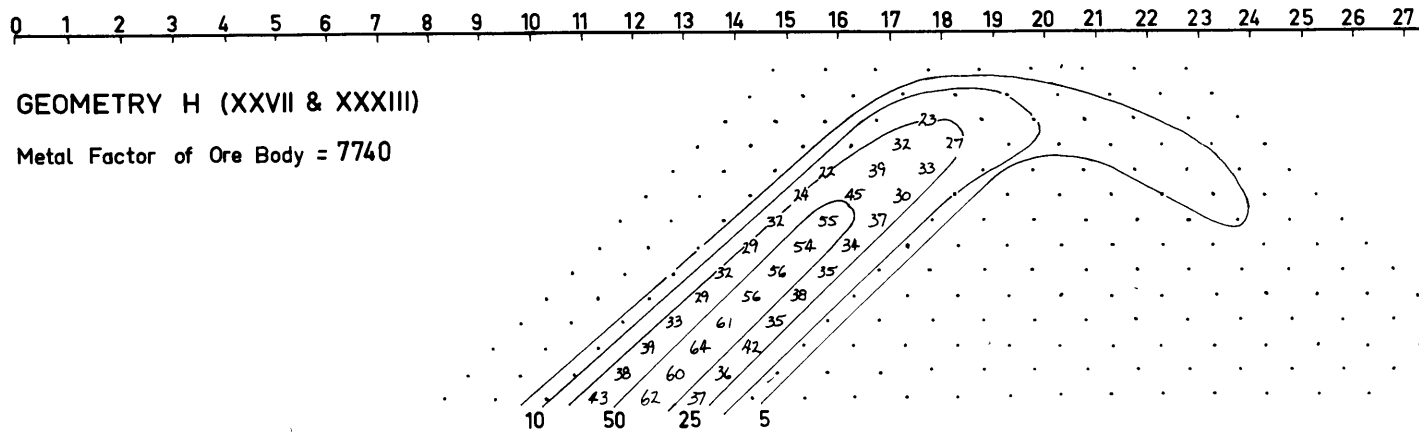


Fig. 69

145

very little by making the contrast higher. If the results of section 5.2 are re-examined, it can be seen that saturation is also indicated in the case of vertical layers. Vozoff (1956) has also pointed out that horizontal layers have this characteristic.

The horizontal model maps show large positive resistivity anomalies for the receiver positions on either side of the horizontal ore body. Also, for the first time, there is a relatively good sized anomaly when the pole sender is over the ore body. The values are much lower when the dipole receiver is over the ore body, but the sender did create lower readings for all the receivers when it was over the ore body.

For the shallow ore body there is a tendency for the contours to flatten out over the ore body. For the shorter separations, the potentials should depend mostly upon the distance between the sender and receiver because of the nearly horizontal layer appearance of the ore body near its center. As the ore body is moved deeper though the characteristic disappears as the anomalies become broader and smaller in magnitude.

The size of the anomalies is, of course, much larger for the horizontal geometry than for the others. Even when the top of the ore body is 3 units deep, the negative anomalies are quite large when compared with the other cases. At a depth of 3 units the positive anomalies in front of the ore body have all disappeared but the positive

anomaly under the negative anomaly is still present. As we shall see, this positive region is quite important in determining the shape of the induced polarization anomaly for a horizontal ore body.

Because of the amount of resistivity data I had, I was able to calculate several metal factor maps for each depth. The values were chosen so that several things could be investigated. We have already seen how the apparent metal factor depends very greatly on the depth of the ore body, but because we now have three depths for each ore body, we can tell more about this depth behavior. From these maps, we can also see something about how the apparent metal factor anomalies depend upon the metal factor of the ore zone.

To do this, I combined the resistivities in such a way as to keep everything constant but the metal factor in the ore zone. The resistivity of the country rock and the D. C. resistivity of the ore body were kept the same while the A. C. resistivity of the ore zone was changed to give a larger metal factor. This may seem to be slightly artificial at first but it is probably a good way to test the dependence of the surface anomaly on the values in the ore body itself. Certainly, in order to get a higher metal factor in the ore zone, it would have to be more heavily mineralized and it might be argued that this would change the D. C. resistivity also. However, if the description of the induced polarization effect given by T. R.

Madden is correct, there is very little conduction through the metallic particles at D. C. anyway so that adding more metallic particles might not change the D. C. resistivity too much.

The third effect that we can investigate with the data is that of the resistivity of the country rock. For resistivity measurements, the anomaly decreases as the country rock is made more conducting. The contrast in resistivity between the country rock and the ore zone is all that determines the size of the anomaly for any given geometry. In the case of the induced polarization measurements though, the resistivity of the country rock plays an important role and its effect is difficult to see intuitively. To see what this effect is, I've plotted maps for two cases. In both cases the ore body has the same properties. It has the same D. C. and A. C. resistivities and therefore the same metal factor. I have plotted maps for two cases where the ore body is situated in country rock of different resistivities. Since nothing else is changed the differences in the apparent metal factor maps must be due to the effect of varying the country rock.

The first two of these characteristics of the induced polarization effect can be studied on Figures 62-67. In all of these, the country rock has a resistivity of $\rho/2\pi = 337$ ohm-feet while that of the ore zone for D. C. current $\rho/2\pi = 31.6$ ohm-feet. The figures are grouped in pairs so that the upper one on each page had a metal factor of 3700

in the ore zone and the lower one had a metal factor of 9000 in the ore zone. A ratio of about 2-1/2. We see that in each case, for all three depths, the apparent metal factor anomaly increased by almost this same factor. This is very different from the resistivity anomaly which changes very little when the contrast is doubled.

The apparent metal factors do drop off very quickly as the depth increases. Although there seems to be less decrease from two to three units deep than between one and two. There is no doubt that the anomalies from the horizontal ore body are much larger than from any of the other geometries.

In order to study the last characteristic of induced polarization, we must compare Figures 63, 65 and 67 with Figures 68, 69 and 70. In the former, as we have seen, the D. C. resistivity of the ore body is $\rho/2\pi = 31.6$ and the metal factor is 9000. The country rock has a resistivity of $\rho/2\pi = 337$ ohm-feet. In Figures 68, 69 and 70 an ore body with almost exactly the same D. C. resistivity and metal factor is in country rock where $\rho/2\pi = 750$ ohm-feet. A comparison of the two sets of maps shows that the increase of the country rock resistivity by more than a factor of two actually decreases the apparent metal factor anomaly!! Also, the deeper the ore body is located, the more the decrease in the metal factor anomaly. This property of the induced polarization effect is exactly the opposite

of resistivity anomalies. If an ore body is in quite conducting country rock, the chances of finding it by resistivity measurements is correspondingly reduced from the case where the ore body is in resistive rock. This is another reason why the induced polarization measurements in the southwestern U. S. , discussed in section 5.3, gave such large anomalies. As mentioned previously, the country rocks in that area are quite conductive.

Although the model measurements were for a pole-dipole configuration they can be compared with the dipole-dipole field results from a horizontal ore body which were discussed in section 4.3. If the potentials from the modelling measurements were used to get the dipole-dipole results from the same geometry, we would see that the resulting maps would be symmetrical and that the part for the dipole sender located over the ore body would look very much like the part of the pole-dipole maps that are due to the dipole receiver being over the ore body; i. e. , if we make the right half of our pole-dipole contour maps look like the left halves we would have the shape of the contours for the dipole-dipole measurements.

The induced polarization maps would be symmetric also and the area of small or even negative metal factors under the main positive anomaly would be accentuated even more. The values in this region are measured when the sender and receiver are on opposite sides of

the ore body. This is opposite to what intuition might lead you to expect. It might seem that having the complete ore zone between the sender and receiver, it would give the ore zone a chance to have its maximum effect on the current flow. The measured results are opposite to what this argument would lead you to expect. If the problem is considered by looking at the sources being induced around the outside of the ore body and adding a secondary potential field to that from the applied source, the results seem more logical. Looking at it this way it seems more reasonable that the effect would begin to drop off when the receiver gets past the induced sources around the ore body. As the sender gets near the ore body and induced sources increase in magnitude, the effect should again increase in magnitude.

Figures 9 and 10 which show lines A and C from Fredericktown have this area of low apparent metal factors in the center of the anomaly. As is so often the case, the background noise was high at the most interesting stations and only a few receiver positions could be occupied for each sender along this part of the lines. However, enough values are plotted so that a definite trend in the contours at that part of the anomaly can be seen. The high metal factors are definitely situated on both sides of a central zone of low values. The similarity with the model results for the horizontal ore body is very evident.

6.8 Conclusions

I think that it is obvious that modelling of the kind described above can play an important role in the interpretation of field results. Once the procedure is set up, new geometries or differently placed lines for the geometries already considered can be set up and the measurements taken rather quickly. In this way, a set of contour maps can be collected that give the character and magnitude of the anomalies for varying conditions.

These maps are necessary to take the place of experience in interpretation. Until more field work has been done, there will be no experience available, and the model maps will be the only source of information for the interpreter. At this stage, the model maps are not to be used for "curve matching". Their use is even more fundamental. We have seen that because the measurements made are measurements of differences; that the contour maps vary widely in character. The recognition of the contour maps from several basic geometries will be necessary for anyone trying to use this method of plotting the data.

Besides giving standard maps for comparison, the modelling can be used to get information on the properties of induced polarization and resistivity surface measurements. How the surface measurements will change when the character of the region varies is important in

trying to use experience from one area in interpreting results from somewhere else where the conditions are different.

Finally, the model measurements are important as we shall see because they furnish us with potential values from controlled and known geometries. This exact information is important in trying to develop an approximate method for calculating the potentials for difficult geometries. If the approximation can be shown to be good enough then further work on resistivity interpretation is possible; but, it must first be determined how good the approximation is and also when it gives good results and when it gives poor ones. Modeling is the only way that this exact data can be gotten.

VII. INVESTIGATION OF THE APPROXIMATE CONDUCTION EQUATION

7.1 The Need for the Approximate Solution

We have seen that the number of cases in which a theoretical solution to the equations of electrical conduction can be obtained is limited. Scale modelling, as described in the previous section, can be used as an analogue computer to give exact results in a few more simple cases, but with one exception, no method has been devised to solve the inverse problem. The theoretical and modelling data will only furnish curves or maps to be compared with field results. The inverse problem of determining from the surface data the resistivity of the earth has only been satisfactorily attacked for the horizontal layering case. (Pekeris, 1940; Vozoff, 1956).

Since the solution of the inverse problem furnishes the knowledge that is desired, it is the ultimate aim of resistivity surveys. The methods described by Pekeris and Vozoff for solving the horizontal layering problem use the theoretical solution of the resistivity problem in horizontal layers and give approximate results based upon certain assumptions concerning the geometry. For the case of a general geometry, we can not even derive equations with which to begin. It is obvious that if a method of attacking the inverse problem is to be developed, it must start with an approximation. This approximation was first mentioned by Stevenson (1934) and is developed by K. Vozoff

in Section II, Part Two of his thesis. Most of the following will be a restatement of Vozoff's results, although the presentation will be slightly different. This brief development is included here for completeness.

7.2 The Approximate Solution

The differential equation discussed in section 2.3 can be written in the following way in the case where we are considering a point source of current at the origin of coordinates. The sets of coordinate points $(x, y, z); (x_0, y_0, z_0); (x_1, y_1, z_1)$ are defined and will be identified by using only the (x) coordinate. For instance,

∇_x^2 means that the differentiation is in the (x, y, z) coordinates;

$\delta(x_0)$ is a short way of writing $\delta(x_0, y_0, z_0)$ and $r(x-x_0)$ refers to the distance between the two points (x, y, z) and (x_0, y_0, z_0) .

We can then write;

$$\nabla_x^2 \phi(x) = - \left[q_0 \delta(x) + \nabla_x \ln \sigma(x) \cdot \nabla_x \phi(x) \right]$$

and the solution, as described in section 2.3 is given by;

$$\phi(x) = \frac{q_0}{4\pi\gamma(x)} + \frac{1}{4\pi} \iiint_{V_0} \frac{\nabla_{x_0} \ln \sigma(x_0) \cdot \nabla_{x_0} \phi(x_0)}{\gamma(x-x_0)} dV_0$$

Proceeding in the usual way to get an iterated solution we

let the first approximation take the form.

$$\phi^0(x) = \frac{q_0}{4\pi\gamma(x)}$$

and

$$\phi^1(x) = \phi^0(x) + \frac{1}{4\pi} \iiint_{V_0} \frac{\nabla_{x_0} \ln \sigma(x_0) \cdot \nabla_{x_0} \phi^0(x_0)}{r(x-x_0)} dV_0$$

or

$$\phi^1(x_1) = \frac{q_0}{4\pi r(x_1)} + \frac{1}{4\pi} \iiint_{V_0} \frac{q_1(x_0)}{r(x_1-x_0)} dV_0$$

where

$$q_1(x) = \nabla_x \ln \sigma(x) \cdot \nabla_x \left[\frac{q_0}{4\pi r(x)} \right] \quad \text{defined only in } x_0 \text{ domain!}$$

putting this back into the general expression we get;

$$\begin{aligned} \phi^2(x) = & \frac{q_0}{4\pi r(x)} + \frac{1}{4\pi} \iiint_{V_1} \frac{q_1(x_1)}{r(x-x_1)} dV_1 \\ & + \frac{1}{4\pi} \iiint_{V_1} \frac{\nabla_{x_1} \ln \sigma(x_1) \cdot \nabla_{x_1} \left[\frac{1}{4\pi} \iiint_{V_0} \frac{q_1(x_0)}{r(x_1-x_0)} dV_0 \right]}{r(x-x_1)} dV_1 \end{aligned}$$

This may, of course, be continued indefinitely but an investigation of these two terms is enough to tell us what is happening in the successive terms of the solution.

We have;

$$\phi^2(x) = \frac{q_0}{4\pi r(x)} + \frac{1}{4\pi} \iiint_{V_1} \frac{q_1(x) + q_2(x)}{r(x-x_1)} dV_1$$

where

$$q_1(x_1) = \nabla_{x_1} \ln \sigma(x_1) \cdot \nabla_{x_1} \left[\frac{1}{r(x_1)} \right] \left(\frac{q_0}{4\pi} \right)$$

and

$$q_2(x_1) = \frac{1}{4\pi} \iiint_{V_0} \left[\nabla_{x_1} \ln \sigma(x_1) \cdot \nabla_{x_1} \left[\frac{1}{r(x_1-x_0)} \right] \left\{ \nabla_{x_0} \ln \sigma(x_0) \cdot \nabla_{x_0} \left[\frac{1}{r(x_0)} \right] \left(\frac{q_0}{4\pi} \right) \right\} \right] dV_0$$

The total potential is given by the applied source term which

Repeat

falls off as $(1/r)$ from the origin and potentials from other sources induced at every point where $\sigma(x)$ has a non-constant value. The strength of the induced source at each point is dependent upon several things; a) the strength of the induced sources at every other point in space, b) the magnitude and direction of $\nabla \ln \sigma$ at the point where the induced source is being calculated and c) the magnitude and direction of $\nabla (1/r)$ at the point where the induced source is being calculated, where (r) is distance from all of the other induced sources.

For instance, $q_1(x_1)$ is created by the applied source q_0 at the origin. The strength of $q_1(x_1)$ at every point is determined by the scalar product of the two vectors $\nabla_{x_1} \ln \sigma(x_1)$ and $\nabla_{x_1} \left[\frac{1}{r(x_1)} \right]$ at the point (x_1) where the strength of the induced source is being calculated. The charges $q_2(x_1)$ have a strength at each point that is determined by the size of $q_1(x_0)$ times the scalar product of $\nabla_{x_1} \ln \sigma(x_1)$ and $\nabla_{x_1} \left[\frac{1}{r(x_1-x_0)} \right]$ at the point (x_1) integrated over the (x_0) space. Thus, at each point the induced sources in one cycle are created by the induced sources from the previous cycle. The complete solution to the integral equation is the potential from an infinite series of these sets of induced sources.

The problem as set up here is for a whole space medium. If surface, such as the surface of the earth, is present across which no conduction takes place, the images of each set of induced sources

must be considered in the calculation of the next set. As Vozoff points out this can be simply done by mirroring all of the resistivities below the insulating plane about the plane surface and considering the problem as that of conduction in this whole space.

Vozoff points out that this equation can be considered a solution of the inverse problem in which the potentials are known and the unknown is the conductivity configuration in the ground. This integral equation is non-linear in $\ln \sigma$ as well as singular in limits and kernel. The solution of the general inverse resistivity problem would be the solution of this non-linear integral equation. This formal solution would be exceedingly difficult and present day mathematics can not cope with it.

However, if all of the terms but the first two are neglected, the problem becomes linear in $\ln \sigma$ and we have as the expression for the potential,

$$\phi(x) \approx \frac{\gamma_0}{4\pi r(x)} + \frac{1}{4\pi} \iiint_{V_0} \frac{\nabla_{x_0} \ln \sigma(x_0) \cdot \nabla_{x_0} \left[\frac{1}{r(x_0)} \right] \left(\frac{\gamma_0}{4\pi} \right)}{r(x-x_0)} dV_0$$

7.3 Solving the Inverse Problem

The interpretation of this equation in terms of induced sources is quite simple. If the ground has a continually varying conductivity, these induced sources will be volume sources. If the changes of conductivity occur on surfaces, i. e., if the anomalous

region is of a constant conductivity but different from the country rock, the induced sources will be surface sources on the outside of the anomalous region. Furthermore, since the problem is now linear in $\ln \sigma$ the problem of two regions of different contrast with the country rock can be done by superposition. The potential from the induced sources on each of the regions can be calculated separately and added. If the two regions have a common boundary, the induced sources calculated for each, in the absence of the other, will partially cancel along the common boundary and the resulting source on that surface will be of the correct value. Vozoff shows that if the resistivity variations are assumed to take place within a limited region, the area of the half space in which the variations take place can be divided into a number of blocks each with an assigned conductivity (σ ;). If enough measurements are taken on the surface and all of the geometric factors calculated the problem can be reduced to the solution of a system of linear equations for the variables (σ ;). This is an approximate solution to the inverse problem; i. e. , from the surface data an estimate of the conductivity of the ground can be derived.

This equation is, of course, also linear in changes in σ . If the conductivity of one of the blocks changes by a small amount, the geometric factor for that block, calculated for each sender and receiver position, will predict how much this change $\Delta \sigma$ will

effect the potential readings at any station when the sender is located at any other station. Thus, if the variations in potential $\Delta \phi$ on the surface that occur when the current is changed from D. C. to A. C. are related to the variations in conductivity $\Delta \sigma$ of the blocks through the appropriate geometric factors we can again set up a system of linear equations. This time, the unknowns will be the $\Delta \sigma$'s. From our knowledge of the metal factor we can then say that any block that has a low value of σ and a large contribution to the $\Delta \sigma$ solution will have contributed a great deal to the induced polarization effect measured on the surface. There is therefore the possibility of developing a procedure for interpreting both resistivity and induced polarization surface measurements.

The usefulness of any such method depends, of course, upon the accuracy of this first approximation. If the potential on the surface can be described reasonably well using just the potential from the applied source and the effect of the first induced sources, then there is some hope that this sort of procedure might give good results in the inverse case. Since the effect of each set of induced sources on the neighboring discontinuities of conductivity is decreased each time by a term like $\nabla (1/r)$ the succeeding terms will decrease in size. For a localized roughly equidimensional anomalous region, they will also generally alternate in sign at each point. These facts indicate that the terms might converge and that the first approximation might give

reasonable results but only some calculations will give an estimate of how good it really is.

7.4 The Contrast Factor

For the medium where the only change in σ is gradual the development of the induced charges is straightforward. If, however, the conductivity changes are all discontinuities at definite surfaces, the problem of what $\nabla \ln \sigma$ should be is not obvious. An examination of the equations reveals that a term like $\ln \frac{\sigma_1}{\sigma_0}$ could be used where σ_1 and σ_0 are the conductivities on either side of the boundary. If we suppose then that we have a rectangular ore body such as the one used in the modelling, the first approximation tells us that on the surface we will have induced sources each governed in size by the relationship between the normal to the surface and the grade ($1/r$) where (r) is the distance from the applied source and also $\ln \sigma_1 / \sigma_0$ which is a constant in this case for all of the ore body. The second set of sources would be created by the first set, which exist all over all six surfaces of the rectangle. The image sources because of the surface of the half space must also be considered. Because of the term $\nabla \ln \sigma \cdot \nabla \left(\frac{1}{r} \right)$, which in this case can be written $\left(-\ln \frac{\sigma_1}{\sigma_0} \frac{1}{r^3} \bar{n} \cdot \bar{r} \right)$ since the change in σ is normal to the surface, those induced sources on the same plane as the point being considered will not induce any more sources there, or so it appears. The fact that this isn't the complete answer is suggested by the modelling and theoretical work.

As I've mentioned previously, theory indicates and modeling shows that some sort of saturation takes place; i. e. , that as the resistivity gets larger a change in that contrast will have less effect on the potentials than when the contrast is small. Everything said so far about the first approximation seems to indicate that as the contrast increases the induced sources should continue to increase in size, and therefore, the potentials should continue to change at the same rate. Since this does not agree with experimental results we must investigate the first approximation more thoroughly.

We can begin by delving a little deeper into the exact theory for conduction in a continuous medium. Jeans (1941, Chapter X) and Abraham and Becker (1949, Chapter VI) discuss the fact that when current flows across a boundary between media of different conductivities charge must be maintained at the boundary. They go on to show that this surface charge is responsible for a discontinuity in the normal derivative of the potential at the boundary and that $\left[\left(\frac{\delta \phi}{\delta n} \right)_+ - \left(\frac{\delta \phi}{\delta n} \right)_- \right]$ at the boundary gives the magnitude of the surface charge. This surface charge at the surfaces of discontinuity in conductivity must clearly be the same as the induced charges described by the general equations. The first approximation solution should give very much the same induced charges as the exact solutions if it is to be of any use.

Two rather simple, but non-physical cases can be solved

exactly for purposes of comparison with the approximate results. The cases of a conducting cylinder and a conducting sphere in a uniform field can be solved in a very straightforward way by using harmonic expansions (see Morse and Feshbach). By taking the indicated differences in the normal derivatives of the potential at the surfaces, the charges maintained at these surfaces can be calculated. In the case of the cylinder the charges are given by $2 \frac{\sigma_1 - \sigma_0}{\sigma_1 + \sigma_0} \cos \theta$ where θ is the polar angle. In the case of the sphere where spherical coordinates are used with the uniform field in the (z) direction the sources come out to be $3 \frac{\sigma_1 - \sigma_0}{\sigma_1 + 2\sigma_0} \cos \theta$ where in this case θ is the usual angle of latitude in spherical coordinates.

In both cases, the solution by using the first approximation gives the same angular dependence for the sources but the constant is in σ_1/σ_0 . A plot of what these constants look like for $\sigma_0 = 1$ and various values of σ_1 is shown on Fig. 71. For small contrasts all three have very similar values; however, as the contrasts are increased the (ln) term keeps on increasing while the other two show the saturation we have mentioned previously. The evidence that some sort of saturation takes place is strong. It is not clear yet though what the reason for this discrepancy is. In both of the cases discussed here, the second set of induced sources from the integration of the first set around the cylinder or sphere might have been enough to reduce the value

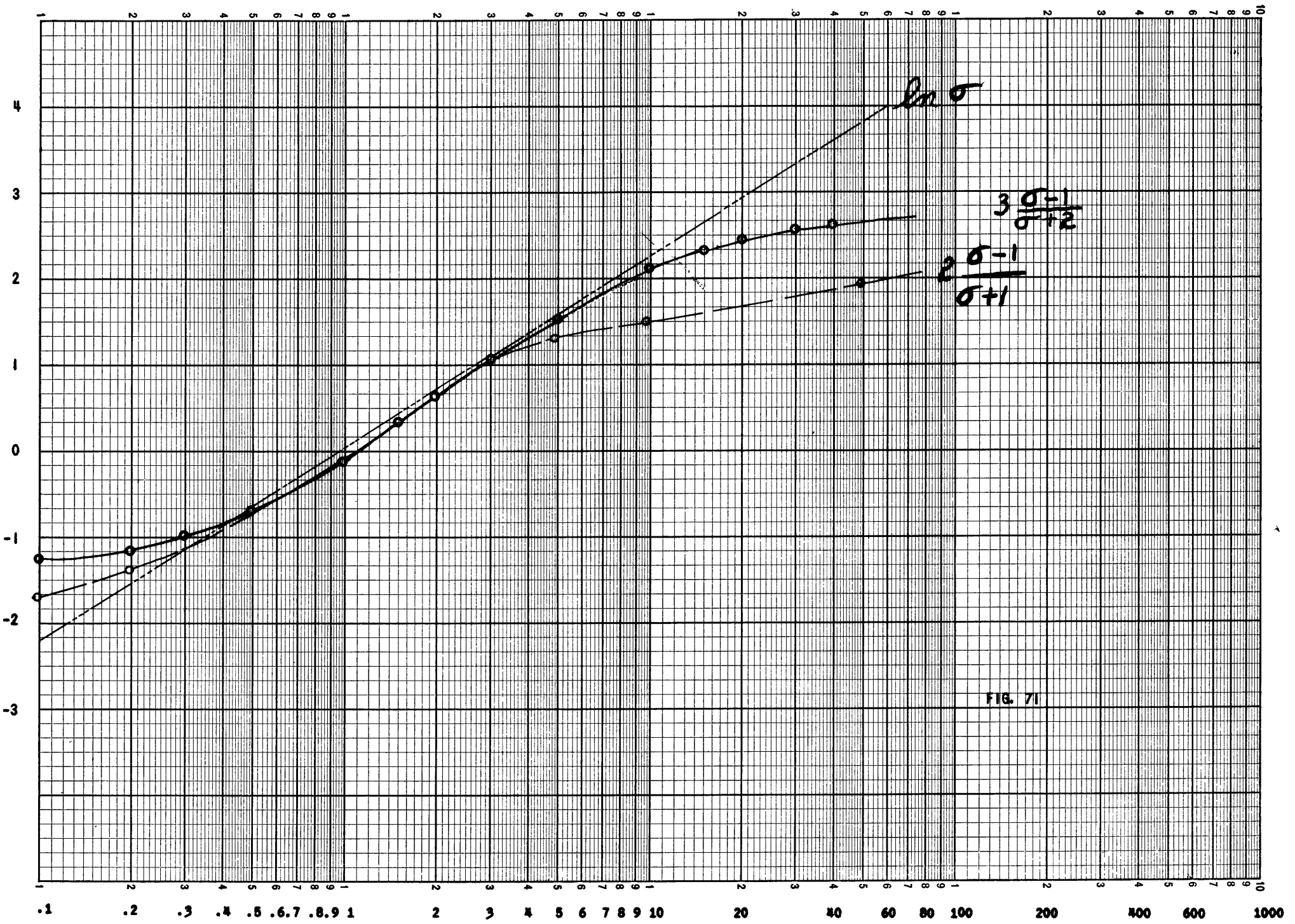


FIG. 71

from the $\left[\ln \sigma_1 / \sigma_0 \right]$ of the first approximation. Since all of the sources vary with the angle though, you might not expect the sources at each point to be reduced in exact proportion to the first set of induced sources at that point.

There is one case though, in which all of the induced sources are on one plane so that the iterated solution would say that there should be no secondary induced sources. That is the case for one vertical interface with a point source of applied current in front of it. The potential expressions for this case were given in section 5.2a. If the charges on the interface are calculated from the normal derivatives they are found to be equal to $2 \frac{\sigma_1 - \sigma_0}{\sigma_1 + \sigma_0} \cos \theta$ where θ is the angle between the normal to the surface through the applied source and the radius vector from the applied source point to the induced source point. Interestingly enough, the constant is the same in this case as for a cylinder in a plane field. The first approximation gives the same dependence on location but the constant term is the usual $\ln \sigma_1 / \sigma_0$. In this case, there is very definitely something wrong with the form of the first approximation since no secondary induced sources are predicted and the first approximation should be exact.

By this time, it is obvious that a better examination must be given the case of a discontinuity in conductivity. We can do this by allowing the conductivity to change linearly across a thickness

(d) and then letting (d) go to zero. The coordinate system to be used is shown on Fig. 72. In this case, we have;

$$\nabla \ln \sigma = \left(\frac{\ln a \sigma - \ln \sigma}{d} \right) \bar{a}_z = \left(\frac{\ln a}{d} \right) \bar{a}_z$$

and

$$q_1(x, y, z) = \left(\frac{\ln a}{d} \right) \bar{a}_z \cdot \nabla \left(\frac{q_0}{4\pi r_0} \right) = q_0/4\pi \frac{\ln a}{d} \bar{a}_z \cdot \nabla \left(\frac{1}{r_0} \right)$$

$$\stackrel{(x_0, y_0, z_0)}{r_0} = q_0/4\pi \frac{\ln a}{d} \frac{\cos(180^\circ - \phi)}{r_0^2} = -q_0/4\pi \frac{\ln a}{d} \frac{z}{r_0^3}$$

In Fig. 73 we have the coordinate system for integrating to get the secondary induced sources. Using the equations from section 7.2 we get;

$$q_2(x, y, z) = \frac{1}{4\pi} \iiint_{V_0} \left[\nabla_x \ln \sigma(x) \cdot \nabla_x \left(\frac{1}{r_1} \right) \left\{ q_1(x_0) \right\} \right] dV_0$$

$$= \frac{1}{4\pi} \iiint_{V_0} \left[\frac{\ln a}{d} \bar{a}_z \cdot \nabla_x \left(\frac{1}{r_1} \right) \right]$$

$$q_2(x, y, z) = q_0/16\pi^2 \left(\frac{\ln a}{d} \right)^2 \int_{z-d}^z \int_{-\infty}^{\infty} \int_{-\infty}^{\infty} \frac{z_0(z-z_0)}{\left\{ \left[(x-x_0)^2 + (y-y_0)^2 + (z-z_0)^2 \right] \left[x_0^2 + y_0^2 + z_0^2 \right] \right\}^{3/2}} dx_0 dy_0 dz_0$$

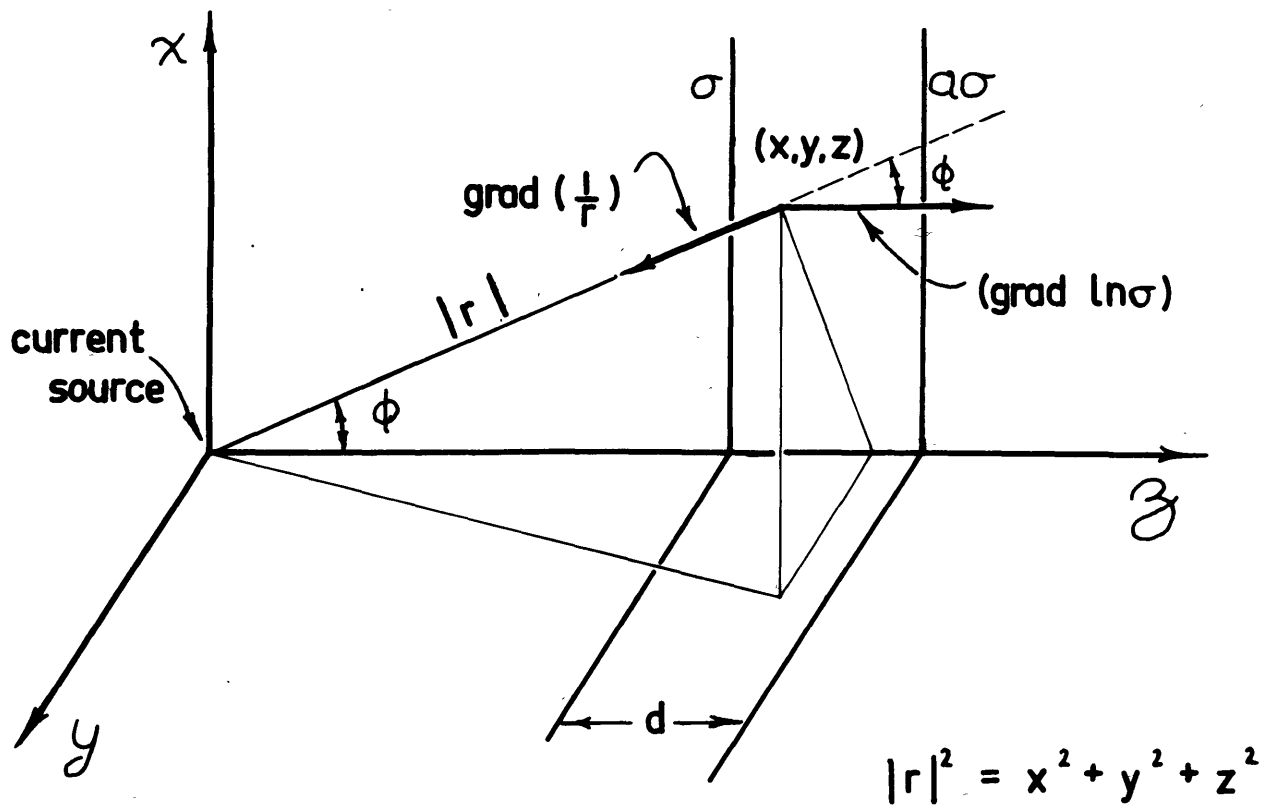


Fig. 72

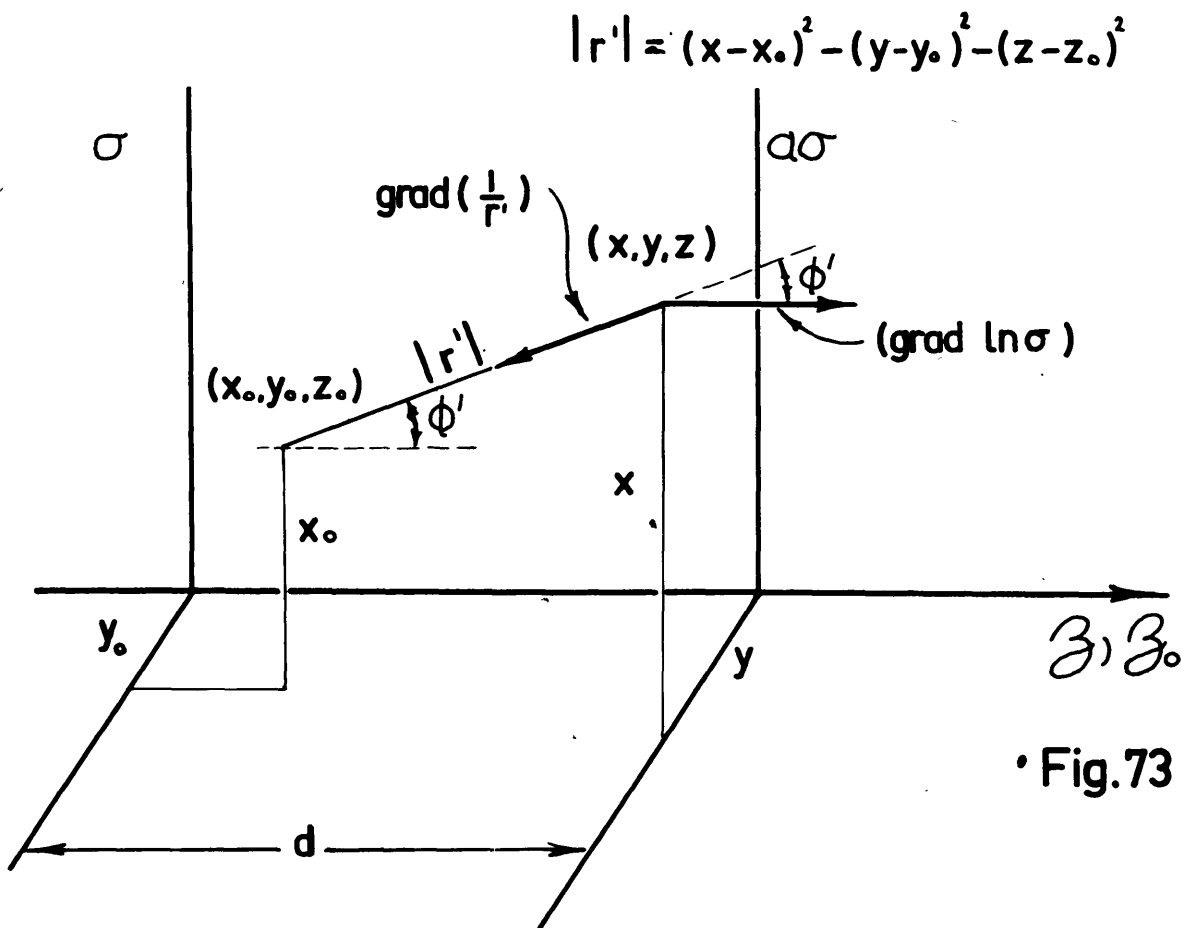


Fig. 73

if the change of variable $z_0 = (z - \epsilon)$ is made the integral becomes,

$$q_z(x, y, z) = \frac{q_0}{16\pi^2} \left(\frac{\ln a}{d} \right)^2 \int_{-\infty}^{\infty} \int_{-\infty}^{\infty} \int_0^d \frac{\epsilon (z - \epsilon) d\epsilon dx_0 dy_0}{\left[(x-x_0)^2 + (y-y_0)^2 + (\epsilon)^2 \right]^{\frac{3}{2}} \left[x_0^2 + y_0^2 + (z-z_0)^2 + \epsilon^2 \right]^{\frac{3}{2}}}$$

Now, in the limit we are going to let $d \rightarrow 0$ so that all terms in ϵ are small. All other terms such as $(x-x_0)$, $(y-y_0)$, x_0 , y_0 will have large values as well as values near zero while z will always be a constant much larger than ϵ . The first integral can then be approximated by;

$$\int_0^d \frac{z \epsilon d\epsilon}{\left[(x-x_0)^2 + (y-y_0)^2 + \epsilon^2 \right]^{\frac{3}{2}} \left[x_0^2 + y_0^2 + z^2 \right]^{\frac{3}{2}}}$$

which may be evaluated to give;

$$\frac{z}{\left[x_0^2 + y_0^2 + z^2 \right]^{\frac{3}{2}}} \left[\frac{1}{\sqrt{(x-x_0)^2 + (y-y_0)^2}} - \frac{1}{\sqrt{(x-x_0)^2 + (y-y_0)^2 + d^2}} \right]$$

If d is very small, the term in brackets is zero unless the point (x_0, y_0) is very near the point (x, y) so that the second integral may be approximated by

$$q_z(x, y, z) = \frac{4z}{\left[x^2 + y^2 + z^2 \right]^{\frac{3}{2}}} \frac{q_0}{16\pi^2} \left(\frac{\ln a}{d} \right)^2 \int_{-\delta}^{\delta} \int_{-\delta}^{\delta} \left[\frac{1}{\sqrt{\epsilon^2 + \gamma^2}} - \frac{1}{\sqrt{\epsilon^2 + \gamma^2 + d^2}} \right] d\epsilon d\gamma$$

where the limits δ must be big enough to take in the major part of the contribution near ϵ and $\nu = 0$. By changing to polar coordinates about the point ϵ and $\nu = 0$ we get;

$$q_2(x, y, z) = \frac{8\pi z}{(x^2 + y^2 + z^2)^{3/2}} \cdot \frac{q_0}{16\pi^2} \left(\frac{\ln a^2}{d} \right) \int_0^{\delta'} \left[1 - \frac{r_0}{\sqrt{r_0^2 + d^2}} \right] dr_0$$

The limit of this integral as $d \rightarrow 0$ is unknown but it is obvious that it has some value and that it isn't zero and therefore that the value of $q_2(x, y, z)$ isn't zero. Therefore, even in the case of one plane the interaction of the induced sources within the infinitesimally thin sheet of charge is important. This is why the theoretical solution is different from the solution given by the first approximation. However, the form of the solution for q_2 shows that only the induced sources very near the point (x, y, z) have any effect in inducing the secondary sources. The third set of induced sources is created only by the secondary sources near the point, and etc. In fact, in the limit as $d \rightarrow 0$ only the charges in an infinitesimally small circle around the point (x, y, z) will contribute to the next induced sources there. They all contribute in such a way as to reduce the apparent source there from $\ln \sigma_1 / \sigma_0$ to $2 \frac{\sigma_1 - \sigma_0}{\sigma_1 + \sigma_0}$. The contributions all come from points so close that the angle factor doesn't enter into it and it is as though all of the contributing sources were of the same value.

Now, if a curved surface had no sharp point on it, any small region could be considered flat and the above argument could be applied to that surface and the source term reduced from $\ln \sigma_1/\sigma_0$ to $2 \frac{\sigma_1 - \sigma_0}{\sigma_1 + \sigma_0}$. In the case of the cylinder this would give the exact answer while for the sphere it would at least give saturation. The sources on the sphere may be further reduced because of the secondary effect of the sources on the rest of the sphere although the exact reason for the difference between the sphere and the cylinder is not clear to me.

For a rectangular ore body as used in the modelling, the above argument is obviously very good on all of the plane faces except possibly at the corners. However, the amount of source on the exact corner will be small compared to the total induced on the ore body. I think that the use of $2 \frac{\sigma_1 - \sigma_0}{\sigma_1 + \sigma_0}$ instead of $\ln \sigma_1/\sigma_0$ in the first approximation will give results nearer the measured values. For small contrasts Fig. 71 shows that they will give the same results but for larger contrasts they will be quite different with the expected saturation occurring for the former.

A quick check, on the variations at least, can be done by using the model results. If the first approximation is correct, the apparent resistivity maps for the same geometry and two different contrasts should vary only by the scale factor. They should vary by the ratio of the contrast factor that is used to give the induced sources in the

two cases. This variation of the surface potentials when the contrast is changed can be checked using the model results shown in Figures 32-70. If the variations from contrast to contrast are checked with the change predicted by $2\frac{\sigma_1 - \sigma_0}{\sigma_1 + \sigma_0}$ and $\ln \sigma_1/\sigma_0$ the algebraic term is found to give better results. In all cases though, it predicts less increase than was measured. The ln term overshoots in each case, particularly for the large contrasts, since it predicts no saturation. Curiously, the algebraic term gives better predictions for the shallow ore bodies than for the deep ones.

The fact that the exact change isn't predicted for each change in the resistivity contrast means, of course, that the first approximation doesn't give exact results. What must be done now is to check and see how good the first approximation really is.

VIII. ACCURACY OF FIRST APPROXIMATION

8.1 Method of Attack

The calculation of the surface potentials around a current source in the neighborhood of a buried, rectangular conducting body would not be practical, even for the first approximation, without the aid of a high speed computer. The high speed digital computer, Whirlwind I, is available at M. I. T. for this sort of computation. In this case, the problem is being worked on by N. Ness of the Department of Geology and Geophysics who is a research assistant under the Institute Computation Center. As a first step he is programming the calculation of the first set of induced sources on the ore body and then the potentials on the surface from these induced sources. He has digitalized the problem by dividing the faces of the ore body into small squares and using the value of the induced sources in the center of the square as an average over the whole square.

With this rather crude method the limited amount of results so far indicate that the first approximation gives potentials and apparent resistivities that agree fairly well with the exact data from the modelling. There is then reason to believe that the approximate solution to the resistivity problem will be of use in calculating expected results from various ground resistivity configurations.

At the present time, Mr. Ness is doing some preliminary work toward taking the next step, that of doing the inverse problem as set forth in Dr. Vozoff's thesis. This involves solving for the resistivity configurations in the ground using the potential data measured on the surface. The results of this work could be very important in the general problem of resistivity prospecting.

IX. SUGGESTIONS FOR FURTHER WORK

Certainly the problem of the interpretation of resistivity and induced polarization data has not been solved and much more work is indicated in many directions. The lack of experience in interpreting the new contour maps can be corrected by more field work as well as more modelling. The field work is being done and probably will continue to be done as long as there is interest in resistivity and induced polarization as methods of prospecting for metallic ores.

Because the size of the induced polarization effect in any one rock depends upon the size and location of the metallic particles as well as the total amount of metal present, much more empirical data are necessary before quantitative interpretations can be possible. Only by measurements in the field can the size of the metal factor for a type of mineralization be determined. As more measurements are made in different areas with different types and grades of mineralization, experience is gained that aids in determining the importance of a measured induced polarization effect in a new area.

The modelling work that has been done has been with one model. More work could be done on the effect of changing the size and/or shape of the ore body. Information is also lacking about the shape of the anomalies when the lines are not placed at right angles to and centered

over the ore body. Off center lines parallel to the strike of the ore body should also be investigated to get some idea how far from an ore body its effects can be measured. This knowledge is useful in planning geophysical exploration when there is some information concerning the expected size and geometry of any mineralized regions.

A great deal of work remains to be done on the study of the first approximation. A systematic survey of the parameters that are important in determining the accuracy of the first approximation is still to be done. Such things as the contrast, depth, attitude and shape of the ore body are all going to determine how accurate the potentials calculated from the first approximation are going to be. Here modeling must be done too to give accurate values with which to compare the approximate information. Along with this there is still much to be studied in the actual mechanics of the calculation. The best size for the squares on the surface of the ore body on which the induced charges are calculated is just one of these problems.

However, as stated before, the end product of this investigation could be a direct and reasonably accurate method for the interpretation of resistivity data. After the accuracy and limitations of the first approximation are established, the reverse problem can be considered in a few simple cases and the use of the direct interpretation evaluated. If a direction interpretation procedure can be worked out, it will be a worthwhile contribution to the science.

APPENDIX A

(a) For the source in region I (Fig. 24)

for $0 < z \leq d_1$

$$U_1(r, z) = Q_1 \int_0^{\infty} [f_1(\lambda) e^{+\lambda z} + e^{-\lambda |z|}] J_0(\lambda r) d\lambda$$

for $d_1 \leq z \leq d_2$

$$U_2(r, z) = Q_1 \int_0^{\infty} [f_2(\lambda) e^{+\lambda z} + g_2(\lambda) e^{-\lambda z}] J_0(\lambda r) d\lambda$$

for $z > d_2$

$$U_3(r, z) = Q_1 \int_0^{\infty} [g_3(\lambda) e^{-\lambda z}] J_0(\lambda r) d\lambda$$

where the exponents have been chosen to assure that the potential stays finite in the layer in which it is defined and the source term has been added into the expression for U_1 .

The boundary conditions to be satisfied are that at

$$z = d_1$$

$$\text{at } z = d_2$$

$$U_1 = U_2$$

$$U_2 = U_3$$

$$\frac{1}{\epsilon_1} \frac{\delta U_1}{\delta z} = \frac{1}{\epsilon_2} \frac{\delta U_2}{\delta z} \quad \frac{1}{\epsilon_2} \frac{\delta U_2}{\delta z} = \frac{1}{\epsilon_3} \frac{\delta U_3}{\delta z}$$

Now the integrals can be made to satisfy the boundary conditions if the kernels do since all of the operations on z can be performed under the integral sign. We can therefore impress the boundary conditions on the kernels.

at $x = d_1$;

$$f_1(\lambda)e^{\lambda d_1} + e^{-\lambda d_1} = f_2(\lambda)e^{\lambda d_1} + g_2(\lambda)e^{-\lambda d_1} \quad a \ 1$$

$$\frac{1}{e_1} f_1(\lambda)e^{\lambda d_1} - \frac{1}{e_1} e^{-\lambda d_1} = \frac{1}{e_2} f_2(\lambda)e^{\lambda d_1} - \frac{1}{e_2} g_2(\lambda)e^{-\lambda d_1} \quad a \ 2$$

at $x = d_2$;

$$f_2(\lambda)e^{\lambda d_2} + g_2(\lambda)e^{-\lambda d_2} = g_3(\lambda)e^{-\lambda d_2} \quad a \ 3$$

$$\frac{1}{e_2} f_2(\lambda)e^{\lambda d_2} - \frac{1}{e_2} g_2(\lambda)e^{-\lambda d_2} = \frac{1}{e_3} g_3(\lambda)e^{-\lambda d_2} \quad a \ 4$$

by multiplication and addition,

$$f_2(\lambda)e^{\lambda d_2} \left[\frac{1}{e_2} + \frac{1}{e_3} \right] + g_2(\lambda)e^{-\lambda d_2} \left[\frac{1}{e_3} - \frac{1}{e_2} \right] = 0 \quad a \ 5$$

$$f_2(\lambda)e^{\lambda d_1} \left[\frac{1}{e_2} - \frac{1}{e_1} \right] - g_2(\lambda)e^{-\lambda d_1} \left[\frac{1}{e_2} + \frac{1}{e_1} \right] = \frac{2}{e_1} e^{-\lambda d_1} \quad a \ 6$$

so,

$$f_2(\lambda) = -g_2(\lambda) \cdot e^{-2\lambda d_2} \left[\frac{e_2 - e_3}{e_2 + e_3} \right]$$

from this we can get by substitution

$$g_2(\lambda) = \frac{2}{e^{-2\lambda \tau} \left[\frac{e_2 - e_3}{e_2 + e_3} \right] \left[\frac{e_1 - e_2}{e_2} \right] + \left[\frac{e_1 + e_2}{e_2} \right]}$$

where

$\tau = (d_2 - d_1)$ is the thickness of the center layer,

and

$$f_2(\lambda) = \frac{-2 e^{-2\lambda d_2} \left[\frac{\rho_2 - \rho_3}{\rho_2 + \rho_3} \right]}{e^{-2\lambda \tau} \left[\frac{\rho_2 - \rho_3}{\rho_2 + \rho_3} \right] \left[\frac{\rho_1 - \rho_2}{\rho_2} \right] + \left[\frac{\rho_1 + \rho_2}{\rho_2} \right]}$$

now, if

$$k_{mn} = \frac{\rho_m - \rho_n}{\rho_m + \rho_n}$$

$$1 - k_{mn} = \frac{2\rho_n}{\rho_m + \rho_n}; \quad 1 + k_{mn} = \frac{2\rho_m}{\rho_m + \rho_n}$$

then

$$g_2(\lambda) = \frac{(1 - k_{12})}{1 + k_{12} k_{23}} e^{-2\lambda \tau}$$

$$f_2(\lambda) = - \frac{(1 - k_{12}) k_{23} e^{-2\lambda d_2}}{1 + k_{12} k_{23}} e^{-2\lambda \tau}$$

from equation (a. 4)

$$g_3(\lambda) = f_2(\lambda) e^{2\lambda d_2} + g_2(\lambda)$$

so that

$$g_3(\lambda) = \frac{(1 - k_{12})(1 - k_{23})}{1 - k_{12} k_{23}} e^{-2\lambda \tau}$$

this function of the resistivities is present in all of the terms so we

may represent it by

$$K(\lambda, \tau) = \frac{(1 - k_{12})(1 - k_{23})}{1 + k_{12} k_{23}} e^{-2\lambda \tau}$$

finally, from equation (a. 1)

$$f_2(\lambda) = f_2(\lambda) + g_2(\lambda) e^{-2\lambda d_1} - e^{-2\lambda d_1}$$

so

$$f_1(\lambda) = - \frac{(1+k_{12})k_{23} e^{-2\lambda d_2}}{1+k_{12}k_{23} e^{-2\lambda \tau}} + \frac{(1-k_{12}) e^{-2\lambda d_1}}{1+k_{12}k_{23} e^{-2\lambda \tau}} - e^{-2\lambda d_1}$$

thus we have for our kernels,

$$f_1(\lambda) = \frac{K(\lambda, \tau) e^{-2\lambda d_1}}{(1-k_{23})} - \frac{k_{23} K(\lambda, \tau) e^{-2\lambda d_2}}{(1-k_{23})} - e^{-2\lambda d_1}$$

$$f_2(\lambda) = - \frac{k_{23} K(\lambda, \tau) e^{-2\lambda d_2}}{(1-k_{23})}$$

$$g_2(\lambda) = - \frac{K(\lambda, \tau)}{(1-k_{23})} ; g_3(\lambda) = K(\lambda, \tau)$$

These expressions are equal but not identical to those derived by Logn. They may be substituted into the original expressions to give the integral form for the three potentials.

(b) For the source in region II (Fig. 25)

In this case, the general expressions may be written

$$U_1(r, z) = Q_2 \int_0^{\infty} f_1(\lambda) e^{\lambda z} J_0(\lambda r) d\lambda \quad \text{for } z \leq -d_1$$

$$U_2(r, z) = Q_2 \int_0^{\infty} f_2(\lambda) e^{\lambda z} + g_2(\lambda) e^{-\lambda z} + e^{-\lambda|z|} J_0(\lambda r) d\lambda \quad \text{for } -d_1 \leq z \leq d_2$$

$$U_3(r, z) = Q_2 \int_0^{\infty} g_3(\lambda) e^{-\lambda z} J_0(\lambda r) d\lambda \quad \text{for } z \geq d_2$$

Here, the boundaries are at $Z = -d_1$ and $+d_2$ the factor from the source term

$$e^{-\lambda|z|} = \begin{cases} e^{\lambda z} & \text{for } z < 0 \\ e^{-\lambda z} & \text{for } z > 0 \end{cases}$$

the boundary conditions are

$$\text{at } z = -d_1$$

$$\text{at } z = +d_2$$

$$U_1 = U_2$$

$$U_2 = U_3$$

$$\frac{1}{\rho_1} \frac{\delta U_1}{\delta z} = \frac{1}{\rho_2} \frac{\delta U_2}{\delta z}$$

$$\frac{1}{\rho_2} \frac{\delta U_2}{\delta z} = \frac{1}{\rho_3} \frac{\delta U_3}{\delta z}$$

these conditions give

$$f_1(\lambda) e^{-\lambda d_1} = f_2(\lambda) e^{-\lambda d_1} + g_2(\lambda) e^{+\lambda d_1} + e^{-\lambda d_1} \quad \text{b.1}$$

$$\frac{1}{\rho_1} f_1(\lambda) e^{-\lambda d_1} = \frac{1}{\rho_2} f_2(\lambda) e^{-\lambda d_1} - \frac{1}{\rho_2} g_2(\lambda) e^{+\lambda d_1} + \frac{1}{\rho_2} e^{-\lambda d_1} \quad \text{b.2}$$

$$f_2(\lambda) e^{\lambda d_2} + g_2(\lambda) e^{-\lambda d_2} + e^{-\lambda d_2} = g_3(\lambda) e^{-\lambda d_2} \quad \text{b.3}$$

$$\frac{1}{\rho_2} f_2(\lambda) e^{\lambda d_2} - \frac{1}{\rho_2} g_2(\lambda) e^{-\lambda d_2} - \frac{1}{\rho_2} e^{-\lambda d_2} = \frac{1}{\rho_3} g_3(\lambda) e^{-\lambda d_2} \quad \text{b.4}$$

by multiplication and addition

$$k_{12} f_2(\lambda) - g_2(\lambda) e^{2\lambda d_1} + k_{12} = 0$$

$$f_2(\lambda) e^{2\lambda d_2} + k_{23} g_2(\lambda) + k_{23} = 0$$

where as before

$$k_{mn} = \frac{\rho_m - \rho_n}{\rho_m + \rho_n}$$

so that

$$g_2(\lambda) = \frac{k_{12} k_{23} e^{-2\lambda\tau} + k_{12} e^{-2\lambda d_1}}{1 + k_{12} k_{23} e^{-2\lambda\tau}}$$

where $\tau = (d_1 + d_2)$

also,

$$f_2(\lambda) = \frac{1}{k_{12}} \left[g_2(\lambda) e^{2\lambda d_1} - k_{12} \right]$$

so that

$$f_2(\lambda) = - \frac{k_{12} k_{23} e^{-2\lambda\tau} + k_{23} e^{-2\lambda d_2}}{1 + k_{12} k_{23} e^{-2\lambda\tau}}$$

from (b. 1)

$$f_1(\lambda) = f_2(\lambda) + g_2(\lambda) e^{2\lambda d_1} + 1$$

so,

$$f_1(\lambda) = 1 + \frac{k_{12} - k_{23} (1 + k_{12}) e^{-2\lambda d_2} - k_{12} k_{23} e^{-2\lambda\tau}}{1 + k_{12} k_{23} e^{-2\lambda\tau}}$$

from (b. 3)

$$g_3(\lambda) = f_2(\lambda) e^{2\lambda d_2} + g_2(\lambda) + 1$$

so

$$g_3(\lambda) = 1 + \frac{-k_{23} + k_{12} (1 - k_{23}) e^{-2\lambda d_1} - k_{12} k_{23} e^{-2\lambda\tau}}{1 + k_{12} k_{23} e^{-2\lambda\tau}}$$

So, our kernels may be written

$$f_1(\lambda) = 1 + \frac{k_{12}}{(1 - k_{12})} \frac{1}{(1 - k_{12})} K(\lambda, \tau) - \frac{(1 + k_{12})}{(1 - k_{12})} \frac{k_{23}}{(1 - k_{23})} K(\lambda, \tau) e^{-2\lambda d_2} - \frac{k_{12}}{(1 - k_{12})} \frac{k_{23}}{(1 - k_{23})} K(\lambda, \tau) e^{-2\lambda\tau}$$

$$f_2(\lambda) = \frac{k_{23}}{(1-k_{23})} \frac{-1}{(1-k_{12})} K(\lambda\tau) e^{-2\lambda d_2} - \frac{k_{12}}{(1-k_{12})} \frac{k_{23}}{(1-k_{23})} K(\lambda\tau) e^{-2\lambda\tau}$$

$$g_2(\lambda) = \frac{1}{(1-k_{23})} = \frac{1}{(1-k_{23})} \frac{k_{12}}{(1-k_{12})} K(\lambda\tau) e^{-2\lambda d_1} - \frac{k_{12}}{(1-k_{12})} \frac{k_{23}}{(1-k_{23})} K(\lambda\tau) e^{-2\lambda\tau}$$

$$g_3(\lambda) = 1 + \frac{k_{12}}{(1-k_{12})} K(\lambda\tau) e^{-2\lambda d_1} - \frac{1}{(1-k_{12})} \frac{k_{23}}{(1-k_{23})} K(\lambda\tau) e^{-2\lambda\tau}$$

These expressions may now be put into the original expressions

to obtain the integral form for the potentials when the current source is in region II.

(c) When the source is in region III.

In this case, the potentials are symmetric with the case when the source is in region I (Fig. 25).

for $z \leq -d_1$

$$U_1(r, z) = Q_3 \int_0^{\infty} [f_1(\lambda) e^{+\lambda z}] J_0(\lambda r) d\lambda$$

for $-d_1 \leq z \leq -d_2$

$$U_2(r, z) = Q_3 \int_0^{\infty} [f_2(\lambda) e^{\lambda z} + g_2(\lambda) e^{-\lambda z}] J_0(\lambda r) d\lambda$$

for $z \geq -d_2$

$$U_3(r, z) = Q_3 \int_0^{\infty} [e^{-\lambda|z|} + g_3(\lambda) e^{-\lambda z}] J_0(\lambda r) d\lambda$$

Here, as in the other two cases, d_1 is the distance from the source to the boundary between regions I and II and d_2 is the distance to the boundary between regions II and III.

The boundary conditions are;

at $z = -d_1$

$$U_1 = U_2$$

$$\frac{1}{\rho_1} \frac{\delta U_1}{\delta z} = \frac{1}{\rho_2} \frac{\delta U_2}{\delta z}$$

at $z = -d_2$

$$U_2 = U_3$$

$$\frac{1}{\rho_2} \frac{\delta U_2}{\delta z} = \frac{1}{\rho_3} \frac{\delta U_3}{\delta z}$$

by forcing the kernels to satisfy these conditions we get

at $z = -d_1$

$$f_1(\lambda) e^{-\lambda d_1} = f_2(\lambda) e^{-\lambda d_1} + g_2(\lambda) e^{\lambda d_1} \quad c 1$$

$$\frac{1}{\rho_1} f_1(\lambda) e^{-\lambda d_1} = \frac{1}{\rho_2} f_2(\lambda) e^{-\lambda d_1} - \frac{1}{\rho_2} g_2(\lambda) e^{\lambda d_1} \quad c 2$$

at $z = -d_2$

$$f_2(\lambda) e^{-\lambda d_2} + g_2(\lambda) e^{\lambda d_2} = e^{-\lambda d_2} + g_3(\lambda) e^{\lambda d_2} \quad c 3$$

$$\frac{1}{\rho_2} f_2(\lambda) e^{-\lambda d_2} - \frac{1}{\rho_2} g_2(\lambda) e^{\lambda d_2} = \frac{1}{\rho_3} e^{-\lambda d_2} - \frac{1}{\rho_3} g_3(\lambda) e^{\lambda d_2} \quad c 4$$

by multiplication and subtraction

$$\left[\frac{1}{\rho_2} - \frac{1}{\rho_1} \right] f_2(\lambda) - \left[\frac{1}{\rho_2} + \frac{1}{\rho_1} \right] g_2(\lambda) e^{2\lambda d_1} = 0 \quad c 5$$

$$\left[\frac{1}{\rho_3} + \frac{1}{\rho_2} \right] f_2(\lambda) + \left[\frac{1}{\rho_3} - \frac{1}{\rho_2} \right] g_2(\lambda) e^{2\lambda d_2} = \frac{2}{\rho_3} \quad c 6$$

so that

$$f_2(\lambda) = \frac{g_2(\lambda) e^{2\lambda d_1}}{k_{12}}$$

and

$$f_2(\lambda) + k_{23} g_2(\lambda) e^{2\lambda d_2} = (1+k_{23})$$

therefore

$$g_2(\lambda) = \frac{k_{12} (1+k_{23}) e^{-2\lambda d_1}}{1+k_{12} k_{23} e^{-2\lambda \tau}} = \frac{k_{12}}{(1-k_{12})} \frac{(1+k_{23})}{(1-k_{23})} K(\lambda \tau) e^{-\lambda d_1}$$

where

$$\tau = (d_1 - d_2)$$

and

$$f_2(\lambda) = \frac{1}{(1-k_{12})} \frac{(1+k_{23})}{(1-k_{23})} K(\lambda \tau)$$

from c. 1,

$$f_1(\lambda) = f_2(\lambda) + g_2(\lambda) e^{2\lambda d_1}$$

$$f_1(\lambda) = \frac{(1+k_{12})}{(1-k_{12})} \frac{(1+k_{23})}{(1-k_{23})} K(\lambda \tau)$$

from c. 3

$$g_3(\lambda) = g_2(\lambda) + f_2(\lambda) e^{-2\lambda d_2} - e^{-2\lambda d_2}$$

$$g_3(\lambda) = \frac{1}{(1-k_{12})} \frac{(1+k_{23})}{(1-k_{23})} K(\lambda \tau) e^{-2\lambda d_2} + \frac{k_{12}}{(1-k_{12})} \frac{(1+k_{23})}{(1-k_{23})} K(\lambda \tau) e^{-2\lambda d_1} - e^{-2\lambda d_2}$$

These kernels may be substituted into the original integrals

and then we will have the desired integral expressions for the potentials.

APPENDIX B

Two tabulations of the value of the integral function

$$G(D; a) = \int_0^1 \frac{dy}{D - y^2} \quad \text{are}$$

contained in Tables I and II in the following pages. To keep the tables completely general, the value tabulated is only that of D. Nothing is said about the values of resistivity that give rise to this value of D.

Therefore, the following list of the value of ρ_2/ρ_0 and the corresponding value of D for the case where $\rho_1 = \rho_3 = \rho_0$ will be needed in calculating potentials for the vertical dike.

One interesting thing to be noticed is that the factor for D

$$D = \left[\frac{1 + \rho_2/\rho_0}{1 - \rho_2/\rho_0} \right]^2 \quad \text{has the same value if}$$

the resistivity contrast is inverted, i. e. ,

$$\text{if } \sqrt{D} = \frac{1 + x/4}{1 - x/4} ; \quad \text{then } -\sqrt{D} = \frac{1 + 4/x}{1 - 4/x} \quad \text{and}$$

D has the same value in both cases. In the expressions for the potentials the \sqrt{D} refers to the positive factor.

D	e_2/e_0 or	e_0/e_2	D	e_2/e_0 or	e_0/e_2
∞	1	1	1.1427	.03333	30.0
9	.5	2	1.1211	.02857	35.0
4.0	.333	3	1.10519	.02500	40.0
3.0	.2683	3.732	1.1000	.0244	41.0
2.7778	.2500	4.00	1.0930	.02222	45.0
2.25	.200	5.0	1.08330	.0200	50.0
2.00	.173	5.83	1.07545	.01818	55.0
1.96	.16667	6.00	1.06895	.016667	60.0
1.7778	.1429	7.00	1.06348	.01538	65.0
1.6531	.1250	8.00	1.05881	.014286	70.0
1.5625	.1111	9.00	1.05478	.013333	75.0
1.50	.1031	9.70	1.051274	.012500	80.0
1.4938	.1000	10.0	1.0500	.01236	81.0
1.3061	.06667	15.0	1.04819	.011765	85.0
1.250	.0560	17.67	1.04545	.011111	90.0
1.2216	.0500	20.00	1.04301	.010526	95.0
1.1736	.0400	25.00			

TABLE I

$$\int_0^1 \frac{dx}{D - x^a}$$

<u>D</u>	<u>9.0</u>	<u>3.0</u>	<u>2.0</u>	<u>1.5</u>	<u>1.25</u>	<u>1.10</u>	<u>1.05</u>
a = 2.0	.122	.380	.623	.926	1.296	1.820	2.32
1.0	.1225	.405	.694	1.10	1.612	2.41	3.12
.50	.1230	.432	.777	1.296	2.028	3.29	4.32
.20	.1233	.462	.864	1.560	2.628	4.77	6.94
.10	.1237	.476	.914	1.714	3.048	6.02	9.32
.050	.1240	.485	.945	1.820	3.380	7.21	12.0
.020	.1240	.4903	.967	1.902	3.656	8.40	15.06

TABLE II

$$\int_0^1 \frac{dx}{D-x^a}$$

D	9.0	4.0	2.778	2.250	1.960	1.778	1.653	1.562	1.494
a = .01	.1244	.3296	.5531	.7829	1.015	1.248	1.481	1.714	1.947
.02	.1243	.3287	.5506	.7778	1.007	1.235	1.463	1.690	1.916
.05	.1239	.3262	.5434	.7636	.9830	1.200	1.414	1.626	1.834
.10	.1233	.3222	.5327	.7429	.9492	1.151	1.347	1.538	1.725
.20	.1223	.3155	.5149	.7093	.8961	1.075	1.246	1.410	1.567
.50	.1201	.3013	.4790	.6445	.7973	.9385	1.070	1.192	1.306
1.0	.1178	.2877	.4463	.5878	.7138	.8267	.9287	1.022	1.107
2.0	.1155	.2747	.4159	.5365	.6400	.7298	.8088	.8791	.9424
5.0	.1133	.2622	.3874	.4893	.5732	.6436	.7037	.7558	.8016
10.0	.1123	.2567	.3752	.4695	.5457	.6087	.6618	.7074	.7472
D	1.306	1.222	1.174	1.143	1.121	1.105	1.093	1.083	1.075
a = .01	3.098	4.230	5.341	6.432	7.503	8.556	9.591	10.610	11.609
.02	3.022	4.090	5.123	6.123	7.092	8.033	8.946	9.835	10.700
.05	2.829	3.754	4.619	5.432	6.201	6.929	7.623	8.284	8.918
.10	2.588	3.359	4.055	4.692	5.280	5.826	6.337	6.817	7.270
.20	2.269	2.864	3.383	3.843	4.258	4.635	4.982	5.304	5.604
.50	1.788	2.169	2.484	2.753	2.989	3.199	3.388	3.561	3.720
1.0	1.451	1.708	1.913	2.085	2.233	2.363	2.480	2.587	2.685
2.0	1.187	1.360	1.496	1.608	1.704	1.790	1.868	1.941	2.008
5.0	.9717	1.089	1.180	1.256	1.324	1.386	1.444	1.499	1.551
10.0	.8933	.9935	1.073	1.140	1.201	1.257	1.310	1.361	1.411

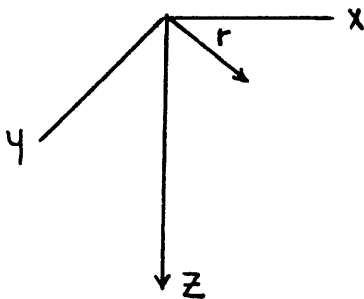
TABLE II (Cont'd)

$$\int_0^1 \frac{dx}{D-x^a}$$

D	1.069	1.063	1.059	1.055	1.051	1.048	1.045	1.043
a = .01	12.594	13.564	14.519	15.459	16.386	17.300	18.201	19.090
.02	11.543	12.366	13.168	13.953	14.720	15.470	16.205	16.924
.05	9.525	10.109	10.672	11.214	11.738	12.245	12.737	13.213
.10	7.699	8.107	8.496	8.868	9.224	9.566	9.894	10.210
.20	5.884	6.148	6.397	6.634	6.859	7.073	7.278	7.474
.50	3.867	4.005	4.134	4.256	4.372	4.482	4.587	4.688
1.0	2.777	2.863	2.945	3.022	3.096	3.167	3.236	3.302
2.0	2.072	2.134	2.192	2.249	2.304	2.358	2.411	2.463
5.0	1.602	1.652	1.700	1.748	1.795	1.841	1.887	1.933
10.0	1.459	1.506	1.553	1.598	1.644	1.689	1.733	1.777

APPENDIX C

The solution for transversely anisotropic layered media is best found in cylindrical coordinates also. We assume a cylindrical system in which conduction is better in the (r) direction than in the (z) direction. We assume, $\sigma_r = a \sigma_z = a \sigma$



For any small source free region in the material, the usual equation for continuity of current results in the expression;

$$\nabla \cdot \bar{J} = 0 \quad \text{where } \bar{J} = J_z \bar{a}_z + J_r \bar{a}_r$$

if we have

$$\bar{E} = E_z \bar{a}_z + E_r \bar{a}_r$$

we have for the general anisotropic

case that

$$\bar{J} = \overleftrightarrow{\sigma} \bar{E}$$

where $\overleftrightarrow{\sigma}$ is the dyadic that

transforms the vector \bar{E} into the vector \bar{J} . In this case $\overleftrightarrow{\sigma}$ is diagonal and we have that

$$\bar{J} = \sigma_r E_r \bar{a}_r + \sigma_z E_z \bar{a}_z$$

so that

$$\nabla \cdot \bar{J} = \sigma_r \frac{\delta E_r}{\delta r} + \frac{\sigma_r}{r} E_r + \sigma_z \frac{\delta E_z}{\delta z} = 0$$

and if $\bar{E} = \text{grad } U$

$$\sigma_r \frac{\delta^2 U}{\delta r^2} + \frac{\sigma_r}{r} \frac{\delta U}{\delta r} + \sigma_z \frac{\delta^2 U}{\delta z^2} = 0$$

if now, $z = \alpha z'$ and $\frac{dz}{dz'} = \alpha$

$$\frac{\delta U}{\delta z'} = \frac{\delta U}{\delta z} \left(\frac{dz}{dz'} \right) = \alpha \frac{\delta U}{\delta z} ; \frac{\delta^2 U}{\delta z'^2} = \frac{\delta}{\delta z} \left[\frac{\delta U}{\delta z'} \right] \left(\frac{dz}{dz'} \right) = \alpha^2 \frac{\delta^2 U}{\delta z^2}$$

so, by substitution

$$\sigma_r \frac{\delta^2 U}{\delta r^2} + \frac{\sigma_r}{r} \frac{\delta U}{\delta r} + \frac{\sigma_z}{\alpha^2} \frac{\delta^2 U}{\delta z'^2} = 0$$

if

$$\frac{\sigma_z}{\alpha^2} = \sigma_r \quad \text{or} \quad \alpha = \sqrt{\frac{\sigma_z}{\sigma_r}} = \frac{1}{\sqrt{\omega}}$$

we can write

$$\sigma_r = \alpha \sigma_z$$

$$\sigma_r \left[\frac{\delta^2 U}{\delta r^2} + \frac{1}{r} \frac{\delta U}{\delta r} + \frac{\delta^2 U}{\delta z'^2} \right] = 0$$

as the equation

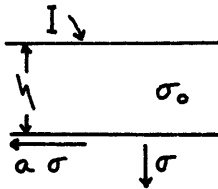
which governs current flow in our system; the usual general solution is gotten by separation of variables.

$$J_0(\lambda r) e^{\pm \lambda z'} \quad \text{or} \quad J_0(\lambda r) e^{\pm \lambda \sqrt{\alpha} z}$$

This is the usual change of scale that everyone talks about when discussing anisotropic conduction. As we shall see, in any but a homogeneous anisotropic earth the introduction of boundary conditions will make the problem more complicated. These boundary conditions

are that no current flows across the earth surface, that the potentials and current flow are continuous across the boundaries. Since these boundaries are all normal to the (z) direction this last condition is that $\sigma_z \frac{\delta U}{\delta z}$ be continuous.

What we don't know yet, is what form the source term takes when the current is being applied in the anisotropic medium. It will probably be something like $\frac{I}{2\pi\sigma R}$ but to intuitively guess its exact form is difficult. One way to get it is to solve the problem for a homogeneous, isotropic layer on top of an anisotropic half space and then let the thickness of the layer go to zero.



In the top layer we use $2I$ for the current and in the usual way get

$$Q = \frac{\rho_0 I}{2\pi}$$

The equations for the potentials are

$$U_1 = Q \int_0^\infty J_0(\lambda r) e^{-\lambda|z|} d\lambda + Q \int_0^\infty [f_1(\lambda) e^{-\lambda z} + g_1(\lambda) e^{\lambda z}] J_0(\lambda r) d\lambda \quad C1$$

$$U_2 = Q \int_0^\infty f_2(\lambda) J_0(\lambda r) e^{-\lambda\sqrt{\alpha} z} d\lambda \quad C2$$

The boundary conditions are that the secondary part of U_1 contribute no current to flow across the surface and the usual conditions at $z = h$

$$\frac{\delta U}{\delta z} = 0 \text{ at } z = 0 \text{ for part of } U_1 \text{ not from source}$$

$$\sigma_0 \frac{\delta U_1}{\delta z} = \sigma \frac{\delta U_2}{\delta z} \text{ at } z = h$$

these give,

$$\text{at } z=0 \quad -f_1(\lambda)e^{-\lambda z} + g_1(\lambda)e^{+\lambda z} = 0 \quad \text{or } f_1(\lambda) = g_1(\lambda)$$

$$\text{at } z=h \quad e^{-\lambda h} + f_1(\lambda)(e^{-\lambda h} + e^{+\lambda h}) = f_2(\lambda)e^{-\lambda\sqrt{a}h}$$

$$-\sigma_0 e^{-\lambda h} + \sigma_0 f_1(\lambda)(-e^{-\lambda h} + e^{+\lambda h}) = -\sqrt{a} \sigma f_2(\lambda)e^{-\sqrt{a}\lambda h}$$

these give,

$$f_1(\lambda) = g_1(\lambda) = \frac{e^{-2\lambda h}}{\frac{\sigma_0 + \sqrt{a}\sigma}{\sigma_0 - \sqrt{a}\sigma} - e^{-2\lambda h}} \quad \text{C 3}$$

$$f_2(\lambda) = \frac{\frac{2\sigma_0}{\sigma_0 - \sqrt{a}\sigma} e^{-\lambda h(1-\sqrt{a})}}{\frac{\sigma_0 + \sqrt{a}\sigma}{\sigma_0 - \sqrt{a}\sigma} - e^{-2\lambda h}} \quad \text{C 4}$$

Comparison of equation (C. 3) with equation 2. 37 of Sunde

(1949) reveals that this case gives the same potential U_1 as an isotropic two layer case if we give the bottom layer of the isotropic case a resistivity of

The expression for U_2 is quite different though, and can be

written as

$$U_2(r, z) = \frac{I}{2\pi\sigma_0} \int_0^{\infty} \frac{\frac{2\sigma_0}{\sigma_0 - \sqrt{a}\sigma} e^{-\lambda h(1-\sqrt{a})}}{\frac{\sigma_0 + \sqrt{a}\sigma}{\sigma_0 - \sqrt{a}\sigma} - e^{-2\lambda h}} J_0(\lambda r) e^{-\lambda\sqrt{a}z} d\lambda$$

If now, we let $h \rightarrow 0$ we will have the potential for when

the current is applied to the surface of a half space that is anisotropic

$$U(r, z) = \frac{I}{2\pi\sqrt{a}\sigma} \int_0^{\infty} J_0(\lambda r) e^{-\lambda\sqrt{a}z} d\lambda \quad \text{C 5}$$

If by analogy we write the exponent as $-\lambda |\sqrt{a} z|$ we can write this as

$$U(r, z) = \frac{I}{2\pi\sqrt{a}\sigma} \frac{1}{\sqrt{r^2 + a z^2}}$$

Thus, the potential looks like that in an isotropic medium in which the conductivity is $(\sqrt{a} \sigma)$ and with z axis scaled so that $z' = \sqrt{a} z$

For the case of an anisotropic layer on top of an isotropic one we get for the potentials

$$U_1'(r, z) = Q' \int_0^\infty J_0(\lambda r) e^{-\lambda |\sqrt{a} z|} d\lambda + Q' \int_0^\infty \left[f_1(\lambda) e^{-\lambda \sqrt{a} z} + g_1(\lambda) e^{+\lambda \sqrt{a} z} \right] J_0(\lambda r) d\lambda$$

$$U_2'(r, z) = Q' \int_0^\infty f_2(\lambda) e^{-\lambda z} J_0(\lambda r) d\lambda$$

if σ_2 is the conductivity of the bottom and $\sigma_r = a \sigma_z = a \sigma$ we have as boundary condition

$$\frac{\partial U_1'}{\partial z} = 0 \text{ at } z = 0$$

where only the non-source part of U_1 is used

$$U_1' = U_2'; \sigma \frac{\partial U_1'}{\partial z} = \sigma_2 \frac{\partial U_2'}{\partial z} \text{ at } z = h$$

these require,

at $z = 0$

$$-\lambda \sqrt{a} f_1(\lambda) e^{-\lambda \sqrt{a} z} + \lambda \sqrt{a} g_1(\lambda) e^{+\lambda \sqrt{a} z} = 0$$

$$\text{or } f_1(\lambda) = g_1(\lambda)$$

at $z = h$

$$e^{-\lambda\sqrt{a}h} + f_1(\lambda) \left[e^{\lambda\sqrt{a}h} + e^{-\lambda\sqrt{a}h} \right] = f_2(\lambda) e^{-\lambda h}$$

$$-\sqrt{a}\sigma e^{-\lambda\sqrt{a}h} + \sqrt{a}\sigma f_1(\lambda) \left[e^{\lambda\sqrt{a}h} - e^{-\lambda\sqrt{a}h} \right] = -\sigma_2 f_2(\lambda) e^{-\lambda h}$$

which give

$$f_1(\lambda) = g_1(\lambda) = \frac{e^{-2\lambda\sqrt{a}h}}{\left(\frac{\sqrt{a}\sigma + \sigma_2}{\sqrt{a}\sigma - \sigma_2}\right) - e^{-2\lambda\sqrt{a}h}} \quad \text{c 6}$$

$$f_2(\lambda) = \frac{\frac{2\sqrt{a}\sigma}{\sqrt{a}\sigma - \sigma_2} e^{-\lambda h \sqrt{a} - 1}}{\left(\frac{\sqrt{a}\sigma + \sigma_2}{\sqrt{a}\sigma - \sigma_2}\right) - e^{-2\lambda\sqrt{a}h}} \quad \text{c 7}$$

Another comparison of the complete form for $U_1'(r, z)$

with the expression for the homogeneous two layer problem reveals that the potentials on the surface are altered in two ways for this case. First, the resistivity of the surface layer appears to be $\sqrt{a}\sigma$ and also, all measurements in the z direction are increased by \sqrt{a} . Including, the depth to the interface which now appears to be at $\sqrt{a}h$.

Thus we see, that when we have only one interface between isotropic and anisotropic regions that the effect on the potentials on the surface can be very simple related to a geometric mean of the two resistivities in the anisotropic layer and in some cases a change of scale in the z direction by the magnitude of \sqrt{a} . However, if we were to add to the complexity by introducing another interface

and studying the effect of a finite layer of anisotropic material in an other-wise isotropic half space, we would find that the potential expressions, even for the top layer, are no longer changed in any uniform way. They are still of the same form as for the isotropic case but the factor \sqrt{a} appears in many places in the expressions.

As an example of how the expressions now become altered, I'll outline below the determination of the potentials for a vertical dike of anisotropic material that conducts better along the strike than it does across the strike. The problem is set up in exactly the same way as the problem in Appendix A except that the same changes are made as were made in the development above for the horizontal layers.

For the current source on the left of the dike and with d_1 and d_2 defined as in Fig. 24. We can write the potentials as before for $0 \leq z \leq d_1$

$$U'_{a_1}(r, z) = \frac{\rho_0 I}{2\pi} \int_0^{\infty} \left[f_1(\lambda) e^{+\lambda z} + e^{-\lambda|z|} \right] J_0(\lambda r) d\lambda$$

for $d_1 \leq z \leq d_2$

$$U'_{a_2}(r, z) = \frac{\rho_0 I}{2\pi} \int_0^{\infty} \left[f_2(\lambda) e^{+\lambda\sqrt{a}z} + g_2(\lambda) e^{-\lambda\sqrt{a}z} \right] J_0(\lambda r) d\lambda$$

for $z \geq d_2$

$$U'_{a_3}(r, z) = \frac{\rho_0 I}{2\pi} \int_0^{\infty} \left[g_3(\lambda) e^{-\lambda z} \right] J_0(\lambda r) d\lambda$$

where α is the degree of anisotropy in the dike and the coordinate system is as before. By satisfying the boundary conditions we get

$$f_1(\lambda) = \sqrt{D'}(\sqrt{D'}-1) \frac{e^{-\lambda d_1}}{D'-e^{-2\lambda\sqrt{\alpha}\tau}} + (\sqrt{D'}-1) \frac{e^{-2\lambda[\sqrt{\alpha}d_2-(\sqrt{\alpha}-1)d_1]}}{D'-e^{-2\lambda\sqrt{\alpha}\tau}} - e^{-2\lambda d_1}$$

$$f_2(\lambda) = (\sqrt{D'}-1) \frac{e^{-\lambda[2\lambda\sqrt{\alpha}d_2-(\sqrt{\alpha}-1)d_1]}}{D'-e^{-2\lambda\sqrt{\alpha}\tau}}; \quad g_2(\lambda) = \frac{\sqrt{D'}(\sqrt{D'}-1)e^{-\lambda(1-\sqrt{\alpha})d_1}}{D'-e^{-2\lambda\sqrt{\alpha}\tau}}$$

$$g_3(\lambda) = \frac{(D'-1)e^{-\lambda(\sqrt{\alpha}-1)\tau}}{D'-e^{-2\lambda\sqrt{\alpha}\tau}}$$

where as before $\tau = (d_2-d_1)$ is the thickness of the dike and

$$D' = \frac{1+\rho'/\rho_0}{1-\rho'/\rho_0} \quad \text{and} \quad \rho' = \frac{1}{\sigma'} = \frac{1}{\sqrt{\alpha}\sigma} = \frac{\rho}{\sqrt{\alpha}}$$

and $\sigma_r = \alpha\sigma_z$. $[D']$ is the same factor as for the isotropic case when geometric mean of the conductivities in the anisotropic dike is used.

For the current source in the vertical dike, we can follow the notation of Fig. 25 and use the following potentials $Q' = \frac{I}{2\pi\sqrt{\alpha}\sigma}$

for $z \leq -d_1$

$$U'_{b_1} = Q' \int_0^{\infty} f_1(\lambda) e^{\lambda z} J_0(\lambda) d\lambda$$

for $-d_1 \leq z \leq d_2$

$$U_{b_2} = Q' \int_0^{\infty} \left[f_2(\lambda) e^{\lambda\sqrt{\alpha}z} + g_2(\lambda) e^{-\lambda|\sqrt{\alpha}z|} \right] J_0(\lambda\tau) d\lambda$$

for $z \geq +d_2$

$$U_{b_3} = Q' \int_0^{\infty} g_3(\lambda) e^{-\lambda z} J_0(\lambda\tau) d\tau$$

Applying the boundary conditions we get

$$f_1(\lambda) = e^{-\lambda d_1(\sqrt{a}-1)} + \frac{\sqrt{D_1'} e^{-\lambda(\sqrt{a}-1)d_1}}{D_1' - e^{-2\lambda\sqrt{a}\tau}}$$

$$+ \frac{e^{-\lambda[2\sqrt{a}\tau + (\sqrt{a}-1)d_1]} + \sqrt{D_1'} e^{-\lambda[2\sqrt{a}d_2 + (\sqrt{a}-1)d_1]} + e^{\lambda[-2\sqrt{a}\tau + (\sqrt{a}+1)d_1]}}{D_1' - e^{-2\lambda\sqrt{a}\tau}}$$

$$f_2(\lambda) = \frac{\sqrt{D_1'} e^{-2\lambda\sqrt{a}d_2} + e^{-2\lambda\sqrt{a}\tau}}{D_1' - e^{-2\lambda\sqrt{a}\tau}}; \quad g_2(\lambda) = \frac{\sqrt{D_1'} e^{-2\lambda\sqrt{a}d_1} + e^{-2\lambda\sqrt{a}\tau}}{D_1' - e^{-2\lambda\sqrt{a}\tau}}$$

$$g_3(\lambda) = e^{-\lambda d_2(\sqrt{a}-1)} + \frac{\sqrt{D_1'} e^{-\lambda d_2(\sqrt{a}-1)}}{D_1' - e^{-2\lambda\sqrt{a}\tau}}$$

$$+ \frac{e^{-\lambda[2\sqrt{a}\tau - d_2(\sqrt{a}+1)]} + \sqrt{D_1'} e^{-\lambda[2\sqrt{a}d_1 + d_2(\sqrt{a}-1)]} + e^{-\lambda[2\sqrt{a}\tau + d_2(\sqrt{a}-1)]}}{D_1' - e^{-2\lambda\sqrt{a}\tau}}$$

These potentials, of course, reduce to those in Appendix A when $a = 1$ but they are much more complicated. The factors containing the resistivities are altered in a regular way, as in the previous cases. The geometric mean of the conductivities $\sqrt{a} \sigma$ appears in the expressions in exactly the same manner that the conductivity of the dike appeared in the expressions for an isotropic dike.

The distance factors are changed in many different ways. The factors \sqrt{a} and $(\sqrt{a} - 1)$ enter into the formulas in various places completely changing the distance dependence in the expressions. No simple change of scale can be used to describe these changes, the effects are too jumbled. The same thing happens in the three layer case for horizontal layers. If the boundary conditions must be satisfied at more than one interface between an isotropic and an anisotropic medium, the potentials are very different from the corresponding isotropic case.

ACKNOWLEDGEMENTS

It gives me great pleasure to acknowledge at this time the help and encouragement of Mr. T. R. Madden throughout the work described in this thesis. Many of the ideas developed in the thesis, including the method of plotting the data, originated with Mr. Madden. He and Dr. Vozoff also helped with the taking of all the field data used as examples and in many other ways.

Most of the staff of the Department of Geology and Geophysics and a larger number of the graduate students in geophysics have also helped with their advice and counsel which at all times was freely given. Norman Ness did all of the programming for the computers and all of the calculations discussed in Chapters V and VIII are the results of his work.

The gathering of the field data would not have been possible without the cooperation of the companies and people involved. These include the management and staff of, the Mindamar Metals Corporation Limited, National Lead Company, and Bear Creek Mining Company. Their willingness to help by providing test areas for the field experiments is greatly appreciated.

The two years of investigation during the 1954-55 and 1955-56 school years were made possible by a graduate school Fellowship from the National Science Foundation.

BIBLIOGRAPHY

- Abraham, M. , and Becker, R. , 1949
Electricity and Magnetism - chapter VI
- Carpenter, E. W. , 1955
"Some Notes Concerning the Wenner Configuration"
Geophysical Prospecting, Vol. 3, pp. 388-402
- Carpenter, E. W. , and Habberjam, G. M. , 1956
"A Tri-potential Method of Resistivity Prospecting"
Geophysics, Vol. XXI, No. 2
- Clark, A. R. , 1956
"Delineation of Conducting Ore Bodies"
Geophysics, Vol. XXI, No. 2
- Cook, K. L. , and Van Nostrand, R. G. , 1954
"Interpretation of Resistivity Data over Filled Sinks"
Geophysics, Vol. XIX, No. 4
- Crumrine, K. C. , 1950
"A Method of Electrical Profiling"
Geophysics, Vol. XV, No. 3
- Hummel, J. N. , 1932
"A Theoretical Study of in Surface Potential Methods"
A. I. M. E. Geophysical Prospecting, pp. 392-422
- James, J. A. , 1949
"Geologic Relationships of Ore Deposits in the Fredericktown,
Mo. Area"
Missouri Geological Survey R. I. , No. 8
- Jeans, Sir James, 1951
The Mathematical Theory of Electricity and Magnetism
Cambridge University Press, chapter X
- Langer, R. , 1936
"On the Determination of Earth Conductivity from Surface
Potentials"
Bull. Amer. Math. Sec. Series 2, No. 42, pp. 747-754
- Logn. , O, 1954
"Mapping Nearly Vertical Discontinuities by Earth Resistivities"
Geophysics, Vol. XIX, No. 4

- Madden, T. R.
"Investigation of Inter-electrode Polarization and its Effects
on Conduction in Metal Bearing Rock"
M. I. T. , Ph.D. Thesis, not completed

(1956) Personal Communication
- Maeda, Katsuro, 1955
"Apparent Resistivity for Dipping Beds"
Geophysics, Vol. XX, No. 1
- Maillet, R. , 1947
"The Fundamental Equations of Electric Prospecting"
Geophysics, Vol. 12, p. 529
- Mooney, H. M. , 1954
"Depth Determinations by Electrical Resistivity"
Trans. A. I. M. E. , Vol. 199, p. 915
"Effect of a Variable Surface Layer ρ_a Data"
Trans. A. I. M. E. , Vol. 199, p. 1210
- Mooney, H. M. , and Wetzel, W. W. , 1955
"Potentials About a Point Electrode and ρ_a Curves for a
Four Layer Earth"
Univ. of Minnesota Press
- Morse, P. M. , and Feshbach, H. , 1953
"Methods of Theoretical Physics"
2 volumes, McGraw-Hill Book Co.
- Ness, Norman, 1955
Development of Equipment Used in the Induced Polarization
Method
M. I. T. Dept. of Geol. and Geophy. Bachelor Thesis
- Pekeris, C. L. , 1940
"Direct Method of Interpretation in Resistivity Prospecting"
Geophysics, Vol. V, No. 1
- Pirson, S. J. , 1935
"Effect of Anisotropy on Apparent Resistivity Curves"
Bull. of the A. A. P. G. , Vol. 19, p. 35
- Pirson, S. J. , Review, 1950
"Importance of the Phenomena of Anisotropy in the Problem
of Interpreting the Results of Electrical Surveys" by L. Cagnoid
Geophysics, Vol. XV, No. 1

- Powers, H. , Scharon, L. , and Tolman, C. , 1953
"Geophysical Case History, Fredericktown Lead District,
Missouri"
Trans. A. I. M. E. , Vol. 196, p. 317
- Pritchett, W. C. , 1955
"A Low Frequency Electrical Earth Model"
Geophysics, Vol. XX, No. 4
- Richardson, P. W. , 1953
"Geology of the Mindamar Metals Corporation Property,
Stirling, Nova Scotia"
Proceedings of Geological Association of Canada
- Seigel, H. O. , 1952
"Ore Body Size Determination in Electrical Prospecting"
Geophysics XVII, No. 4
- Stefanescu, S. , Schlumberger, C. , and Schlumberger, M. , 1930
"Sur la Distribution Electrique Potentielle Autor d'une
Prise de Terre Ponctuelle dans au Terrain a'couches
Horizontales, Homogenes et Isotropes"
Jour. Physique et Rodium, Tome I, pp. 132-140
- Stevenson, A. F. , 1934
"On the Theoretical Determination of Earth Resistivities
from Surface Potential Measurements"
Physics, Vol. 5, p. 114
- Stratton, J. A. , 1941
"Electromagnetic Theory"
McGraw-Hill Book Company
- Sunde, E. D. , 1949
"Earth Conduction Effects in Transmission Systems"
D. Van Nostrand Company
- Tagg, G. F. , 1930
"The Earth Resistivity Method of Geophysical Prospecting.
Some Theoretical Considerations"
Mining Magazine, Vol. 43, pp. 150-158
- Unz, M. , 1953
"Apparent Resistivity Curves for Dipping Beds"
Geophysics, Vol. 18, p. 116

Van Nostrand, R. G. , 1953

**"Limitations on Resistivity Methods as Inferred from the
Buried Sphere Problem"
Geophysics, Vol. XVIII, No. 2**

Vozoff, K. , 1956

**"Quantitative Interpretation of Resistivity Data"
M. I. T. Ph. D. Thesis, Dept. of Geology and Geophysics**

BIOGRAPHY OF AUTHOR

The author, Philip George Hallof, was born on March 20, 1931 in St. Louis, Missouri. His parents are Mr. and Mrs. P. Hallof Jr., of Kirkwood, Missouri. He attended the public primary and secondary schools of Kirkwood graduating from Kirkwood High School in 1948.

He entered the Massachusetts Institute of Technology in the fall of 1948 and in his sophomore year transferred into the Department of Geology and Geophysics. Having received an S. B. degree in Geophysics in June, 1952, he began his graduate training at M. I. T. in the fall of 1952.